Karlova Univerzita v Praze

Přírodovědecká fakulta

Studijní program: Biologie

Studijní obor: Buněčná a vývojová biologie - fyziologie buňky

Bc. Lea Marie Beranová

Úloha sulfhydryl oxidázy 1 v karcinogenezi
Role of sulfhydryl oxidase 1 in cancerogenesis

Diplomová práce

Školitel: Mgr. Jaroslav Truksa, Ph.D.

Praha 2019

Prohlášení: Prohlašuji, že jsem závěrečnou práci zpracoval/a samostatně, a že jsem uvedl/a všechny použité informační zdroje a literaturu. Tato práce, ani její podstatná část, nebyla předložena k získání jiného nebo stejného akademického titulu.

V ..... dne ..... podpis .....

Acknowledgements:

I would like express the deepest appreciation to my supervisor Mgr. Jaroslav Truksa, PhD. as well as Msc. Cristian Sandoval Acuña, PhD. for their valuable insights and advice that helped me shape this thesis to its present form.

My thanks also go to every member of the Laboratory of Tumor Resistance AV ČR team in Vestec for their support throughout my Master's studies.

I am also grateful for all the love and understanding from my beloved fiancé Mgr. Michal Outrata who always lifted my spirits whenever I was feeling down.

And last but not least I would like to thank my parents for the lifelong encouragement to pursue my dreams.

Abstrakt: Cysteinové můstky hrají významnou roli při sbalování proteinů do nativní konformace, stejně jako v regulaci enzymové aktivity a účastní se tak mnoha intracelulárních, avšak i extracelulárních, dějů.

Sulfhydryl oxidáza QSOX1 pomáhá tyto můstky *de novo* vytvářet čímž ovlivňuje aktivitu svých substrátů a přímo či nepřímo tím reguluje životně důležité procesy v buňce. Cílem této práce bylo prozkoumat roli QSOX1 v karcinogenzi a to především u buněk nádorů prsu (MCF7, MDA-MB-231) a slinivky břišní (Panc-1) a zároveň objasnit možnou spojitost mezi koncentrací kyslíku v rámci nádorového mikroprostředí a hladinou QSOX1 na proteinové i mRNA úrovni.

Vytvořením dvou typů geneticky modifikovaných linií (*QSOX1*-overexprimující a *QSOX1*-knockout linie) byl pozorován pozitivní vliv QSOX1 na proliferaci trojnásobně negativních nádorových buněk MDA-MB-231. Buňky nevytvářející QSOX1 projevují nižší tendenci k proliferaci, zatímco nadbytek tohoto proteinu na tempo růstu vliv zdá se nemá. Nedostatek QSOX1 má také za následek viditelnou změnu v morfologii buňky, kdy dochází ke smrštění do kulovitějších útvarů s méně znatelnými lamelipodii, či jejich naprostou absencí, což je v souladu s teorií důležitosti QSOX1 nejen pro proliferaci ale také pro migraci a invazivitu nádorových buněk.

Zároveň byl sledován efekt hypoxického prostředí o různé koncentraci kyslíku na čtyři buněčné linie (MCF10A, MCF7, MDA-MB-231 a Panc-1). Podle dostupné literatury je QSOX1, obsahující hypoxia-responsive elements ve své DNA, indukován sníženým obsahem kyslíku v atmosféře. V naší práci jsme ukázali, že hypoxie mírně zvyšuje expresi *QSOX1*, zvýšení hladiny proteinu QSOX1 v buňkách byl minimální, ale docházelo k výrazné sekreci QSOX1 do média.

Na základě těchto výsledků se QSOX1 jeví jako eventuální cíl nádorových terapií a léčiv a hraje důležitou roli při karcinogenezi.

Klíčová slova: QSOX1, rakovina, sulfhydryl oxidáza, proliferace, hypoxie

Abstract: Disulfide bridges play a significant role in protein-folding as well as enzyme activity and thus regulate many intra- and extracellular processes.

Sulfhydryl oxidase QSOX1 forms S-S bridges *de novo*, modulating the activity of its substrates and thus directly or indirectly influences vital cellular processes. The first part of this thesis focuses on characterization of the role of QSOX1 in cancerogenesis, using breast cancer cell lines (MCF7, MDA-MB-231) and pancreatic cancer cell line (Panc-1), while the second part emphasizes the regulation of *QSOX1* expression by different oxygen concentrations.

To study the effect of QSOX1 on proliferation of triple-negative cancer cells MDA-MB-231, two genetically modified cell lines – *QSOX1*-overexpressing and *QSOX1* knockout cell lines – were constructed. While increased QSOX1 protein levels do not have a significant effect, the absence of QSOX1 leads to a decreased cellular growth. Lack of *QSOX1* also results in visible change in cellular morphology. *QSOX1* knockout cells can be mostly characterized as more round-shaped with less noticeable or completely missing lamellipodia. This finding is with agreement with to-date literature suggesting that QSOX1 is important not only for cellular proliferation but also for migration and invasiveness.

While authenticating the theory of QSOX1 being regulated by atmospheric oxygen concentration via hypoxia-responsive elements included in *QSOX1* promoter, we found that tested cells responded to hypoxia by an increase at the level of *QSOX1* mRNA, there was almost no change on the protein level within the cells, yet, the hypoxic conditions led to a significant secretion of QSOX1 into the media.

These findings support the QSOX1 as a putative target for development of anti-neoplastic drugs and confirms its important role in cancerogenesis.

Keywords: QSOX1, cancer, sulfhydryl oxidase, proliferation, hypoxia

Contents

List of abbreviations

CA9	Carbonic Anhydrase
HMOX1	Heme Oxygenase 1
AA	Amino Acid
ALR	Augmenter of Liver Regeneration
AP-1	Activator Protein 1
APS	Ammonium Persulphate
ASK1	Apoptosis Signaling-regulating Kinase 1
BAN	4-bromoanisol
BCA	Bicinchoninic Acid
BSA	Bovine Serum Albumine
CDKI	Cyclin-dependent Kinase Inhibitor
cDNA	Complementary DNA
CHOP	CCAAT-enhancer-binding Protein Homologous Protein
CSCs	Cancer Stem-like Cells
DMEM	Dulbecco's Modified Eagle Medium
Drp1	Dynamin-related Protein 1
ECM	Extracellular Matrix
EMT	Epithelial-mesenchymal Transition
ER	Endoplasmic Reticulum
ERAD	ER-associated Degradation
ERO1	Endoplasmic Reticulum Oxidoreductin 1
Ero1-L	Endoplasmic Reticulum Oxidoreductin-like Protein 1
ERp44	Endoplasmic Reticulum Resident Protein 44
ESR	Estrogen Receptor
ETC	Electron Transport Chain
FAD	Flavin Adenine Dinucleotide
FBS	Fetal Bovine Serum
FMN	Flavin Mononucleotide
GA	Golgi Apparatus
gDNA	Genomic DNA

GFER	Growth Factor Erv-1 Like
GPx7/8	Glutathione Peroxidase 7/8
GSH	Reduced Glutathione
GSSG	Oxidized Glutathione
HCC	Hepatic Cancer Cell
HDR	Homology Directed Repair
HER2	Human Epidermal Growth Factor Receptor 2
HIF1	Hypoxia Inducible Factor 1
HIF2	Hypoxia Inducible Factor 2
HPO	Hepatopoietin
HRE	Hypoxia Response Elements
HRP	Horseradish Peroxidase
HS	Horse Serum
HSC	Hematopoietic Stem Cells
HSS	Hepatic Stimulatory Substance
HUVEC	Human Umbilical Vein Endothelial Cells
IgM	Immunoglobulin M
IHC	Immunohistochemistry
IMS	Intermembrane Space
JAB1	Jun Activation Domain-binding Protein 1
KO	Knockout
MAPK	Mitogen-Activated Protein Kinase
MMPs	Metalloproteinases
Mr	Molecular Weight
NAD(P)H	Nicotinamide Adenine Dinucleotide (Phosphate)
NCDs	Noncommunicable Diseases
NHEJ	Non-homology End Joining
PAF	Paraformaldehyde
PBS	Phosphate Buffer Saline
PCR	Polymerase Chain Reaction
PDI	Protein Disulfide Isomerase
PHD	Prolyl Hydroxylase

PR	Progesterone Receptor
Prx4	Peroxiredoxin 4
PVDF	Polyvinylidene Difluoride
QSCN6/Q6	Quiescin 6
QSOX family	Quiescent Sulfhydryl Oxidase Family
QSOX1	Quiescent Sulfhydryl Oxidase 1/Quiescin 6
QSOX1v1/QSOX1-L/QSOX1A	QSOX1 Longer Variant
QSOX1v2/QSOX1-S/QSOX1B	QSOX1 Shorter Variant
Ref1	Redox Factor 1
ROS	Reactive Oxygen Species
RTCA	Real Time Cell Analysis
SDS-PAGE	Sodium Dodecyl Sulfate - Polyacrylamide Gel Electrophoresis
SLB	Sample Loading Buffer
SOX	Sulfhydryl Oxidase
SOX-2	Sulfhydryl Oxidase from Rat Seminal Vesicles
TAE	Tris-acetate-EDTA Buffer
TBS	Tris Buffer Saline
TNP	Triple Negative Phenotypic Tumor
TOM	Translocase of the Outer Membrane
TRX	Thioredoxin
TRXR	Thioredoxin Reductase
TXNIP	Thiredoxin-interacting Protein
UPR	Unfolded Protein Response
VEGF	Vascular Endothelial Growth Factor
WB	Western Blot

1. Introduction

1.1 Cancer

Cancer is the second leading cause of death worldwide (see Figure 1.1) - in total it is responsible for approximately 1 in 6 deaths [World Health Organisation, 2018]. It has become one of the most globally studied diseases and at the same time one of the most complex, due to its variablity, distinct behavior and therefore different treatment responses.

Because of the overwhelming number of people affected by cancer and its major economic impact (the total annual cost of cancer in 2010 was estimated at approximately US$ 1.16 trillion [Stewart et al., 2014]), it is very important to continue in the fundamental research that could help in finding and developing novel anti-cancer treatments.

1.1.1 Breast cancer

As a leading cause of cancer-caused death in women [Global Cancer Observatory, 2018], breast cancer has been studied extensively over the past decades [Cailleau et al., 1974, Simstein et al., 2003, Griffiths and Olin, 2012]. Since it is not a single disease with one major cause, it was very important to create an accurate grouping system of breast cancers according to their immunohistochemical (IHC) markers such as estrogen receptor (ESR), progesterone receptor (PR), human epidermal growth factor receptor 2 (HER2) as well as the proliferative marker Ki67 [Vallejos et al., 2010]. Based on the expression of these markers, we can define three classes (see Figure 1.2) - (1) luminal, (2) HER2 overexpressing and (3) triple negative phenotypic (TNP) tumors [Dai et al., 2015].

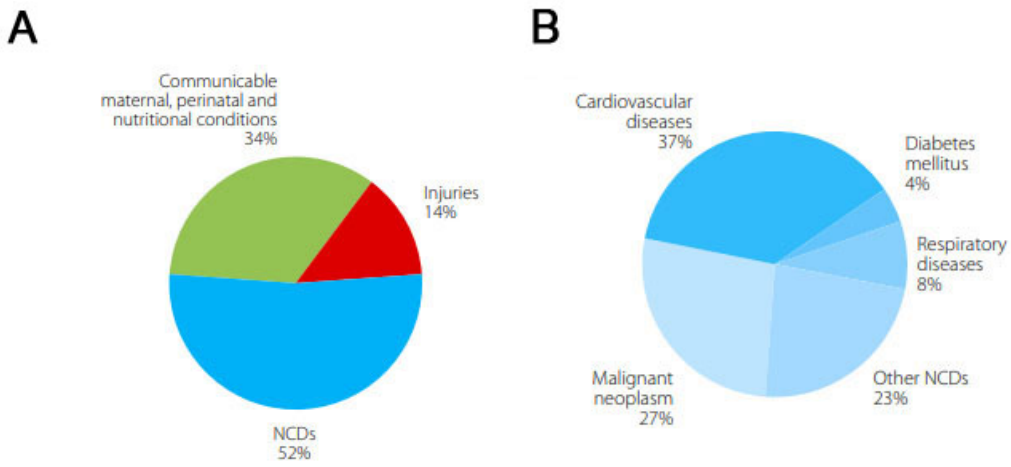

Figure 1.1: **Statistics from Global status report on noncommunicable diseases in 2012 A** Statistics of all death causes; **B** Statistics of deaths due to noncommunicable diseases (NCDs) (reproduced from [Organization et al., 2014])

In general, luminal subtypes make up the majority of breast cancer cases [Dai et al., 2015] and carry a good prognosis for the patients [Sørlie et al., 2003] while HER2 positive and basal tumors are associated with higher tumor grade and poor outcome [Brenton et al., 2005].

Intrinsic subtype	IHC status	Grade	Outcome	Prevalence
Luminal A	[ER+|PR+] HER2-KI67-	1|2	Good	23.7% [p1]
Luminal B	[ER+|PR+] HER2-KI67+	2|3	Intermediate	38.8% [p1]
	[ER+|PR+] HER2+KI67+		|Poor	14% [p1]
HER2 over-expression	[ER-PR-] HER2+	2|3	Poor	11.2% [p1]
Basal	[ER-PR-] HER2-, basal marker+	3	Poor	12.3% [p1]
Normal-like	[ER+|PR+] HER2-KI67-	1|2|3	Intermediate	7.8% [p2]

Figure 1.2: **Summary of the breast cancer molecular subtypes** Luminal A and luminal B subclasses falls into the luminal class whereas basal subclass is a part of TNP class. Normal-like is a unique group of tumors with normal breast tissue profiling and similar IHC status with the luminal A subtype (reproduced from [Dai et al., 2015])

During the treatment and therapy, patients are divided into distinct clinical groups according to the expression of the IHC markers within the tumor - (1) ER+/HER2-, (2) ER+/HER2+, (3) ER-/HER2+ and (4) ER-/HER2- [Prat and Perou, 2011]. These groups differ in distribution of patients from the intrinsic subtypes. Therefore, the ability to precisely and accurately identify the breast cancer subtype and clinical group of the patient could lead to improvement in treatment and better prognosis for the patient.

1.1.2 Pancreatic cancer

Another type of cancer with predicted poor outcome is pancreatic cancer. Even though the incidence of pancreatic cancer is significantly lower compared to breast cancer, the parallel between the incidence and mortality is very close making the pancreatic cancer highly lethal [Siegel et al., 2014] - the five-year survival in patients with pancreatic cancer is as low as 6% in the USA [Gillen et al., 2010]. This is generally attributed to the early recurrence, high grade of metastasis and resistance to chemotherapy and radiotherapy [Kamisawa et al., 1995]. At the same time, a very severe problem is the difficulty of early diagnosis of the disease leading to late stage diagnoses and poorly treatable complications. Most of the patients do not manifest any symptoms until the advanced stage of the disease [Gillen et al., 2010].

1.1.3 Molecular mechanisms of cancer

In 2000, Hanahan and Weinberg proposed six hallmarks of cancer (see Figure 1.3) that are being recognized by the academic society ever since [Hanahan and Weinberg, 2000] (also see an updated version [Hanahan and Weinberg, 2011]). To briefly summarize this comprehensive work, the next few paragraphs will focus on the journey of normal cells becoming malignant and creating neoplastic formations.

Cancer differs from non-malignant tissues predominantly in its enhanced capability of proliferation and growth. While normal cells encounter many obstacles during their cell cycle, malignant cells have come to ways of evading such control mechanisms and can proliferate without restraints. To be able to do that, cancer cells must primarily sustain the proliferative signaling. While in normal cells, excess of growth-promoting signals can be fatal and promote cell senescence, cancerous cells learned to exploit this feature to their benefit by deregulation of the receptor levels displayed on the cell surface or modulation of the receptors themselves [Witsch et al., 2010].

Whereas the mitogenic signaling promotes cell division and proliferation, growth suppressors have the very opposite purpose. Under normal circumstances, pathways involved in growth

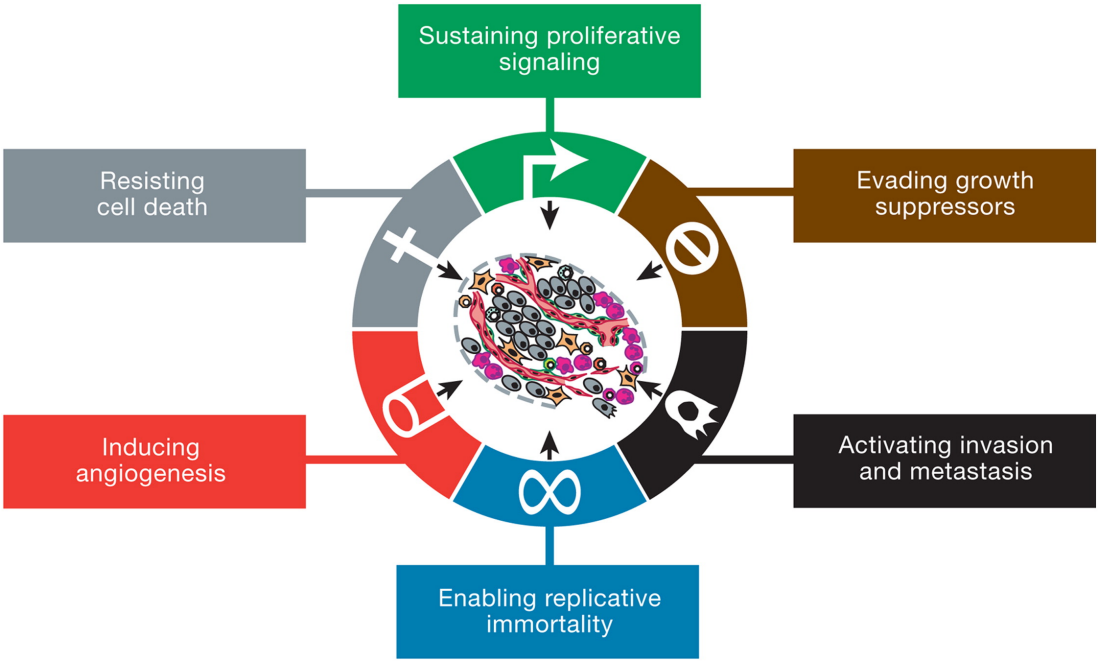

Figure 1.3: **The hallmarks of cancer.** Schematic representation of the six hallmarks of cancer originally proposed by Hanahan and Weinberg in 2000 (reproduced from [Hanahan and Weinberg, 2011])

suppression control cellular stress levels caused by either DNA damage, growth-promoting signals, glucose concentration as well as contact inhibition by neighbouring cells or other limiting factors, and are capable of inducing cell cycle arrest or guiding cell to apoptosis. In case of cancerous cells, one or more of these pathways can be defective, leading to dissemination of this condition [Sherr and McCormick, 2002].

The apoptosis - a programmed cell death - is an indispensable tool in development of organisms and their tissues as well as a control mechanism securing safe removal of defective cellular units. The balance of anti-apoptotic and pro-apoptotic factors is disrupted in tumor cells, favoring the pro-survival pathways thus evading cellular death and overcoming the imaginary "barrier to cancer" [Evan and Littlewood, 1998]. A very different stress-response that is, unlike apoptosis, upregulated in cancerous cells is autophagy. Since the excessive proliferation is a very costly process, cancerous cells often struggle with nutrient deficiency. To replenish the intrinsic stocks of building material, tumor cells resort to breaking down their own cellular organelles, recycling the catabolites for biosynthesis and energy metabolism [Levine and Kroemer, 2008]. This interesting approach is recorded to be cytoprotective for cancer cells dealing with stress in favorable way.

When normal healthy cells proliferate, they are capable of only a limited number of successive cell growth-and-division cycles. However, this is not true for the tumor cells that are known to have unlimited replicative potential. This transition to immortalization is linked to induced expression of a specialized DNA polymerase termed telomerase. During the genome replication in S phase of cell cycle, within each round, the telomeric hexanucleotide repeats located at the end of chromosomal DNA shorten progressively in the non-immortalized cells. When telomerase is present, it can actively renew the DNA ends thus preventing the shortening and loss of important information and therefore overturn the otherwise inevitable senescence or apoptosis [Blasco, 2005].

Besides the multiple ways of escaping death, tumor cells are also equipped with the indispensable ability to induce formation of neovasculature. This new vascular system helps

supplying the newly formed tumor masses with nutrients and oxygen and also functions as a waste shaft for the metabolic waste and carbon dioxide. Similarly to apoptosis, neoangiogenesis is triggered by a disruption of a balance between pro- and anti-angiogenic factors [Hanahan and Folkman, 1996]. These newly-formed vessels are known to be extremely leaky, form microhemorrhages and display abnormal levels of endothelial cell proliferation and apoptosis [Baluk et al., 2005] while enabling the tumor tissue to grow and prosper.

The last hallmark of cancer is also the most responsible one for the lethal nature of cancer. Once the primary tumor is formed, a percentage of cancer cells frequently enter epithelial-mesenchymal transition (EMT) which allows them to vanquish the barrier of basal lamina surrounding the tumor and initiate the process of invasion and metastasis. When the cells invade beyond the basal lamina and intravasate into the vascular and/or lymphatic system, the invasion-metastatic cascade continues with extravasation in a suitable niche where it forms a micrometastatic lesions growing into macroscopic tumors. The colonization of distant organs usually leads to their failure and therefore might be fatal [Fidler, 2003].

In order to escape the primary locations, cancer cells have to be able to modify the extracellular space as well as its own morphology. There are various pathways involved in these processes and some of the available literature suggests that disulfide bonds-forming enzymes such as thioredoxins and sulfhydryl oxidases may play an important role [Arner and Holmgren, 2006, Cao et al., 2009, Moenner et al., 2007, Lake and Faigel, 2014] either in oxidative (modification of ECM components) or degradative (activation of MMPs in ECM) manner. This way, TRXs and SOXs presumably influence the invasiveness and metastatic potential of cancer.

1.2 Thioredoxin

Thioredoxin (TRX) is a well-studied protein present in multiple forms and variants across the organisms. However, the following section will focus mainly on the TRX1 found in human tissues that shares a significant portion of its DNA sequence with QSOX1 sulfhydryl oxidase [Coppock et al., 1998].

This ubiquitously expressed enzyme has multiple functions that differ based on its subcellular localization [Mahmood et al., 2013]. Even though its main working site is cytosol, under certain circumstances it can be either secreted to the extracellular matrix (ECM) and act as a chemokine [Bertini et al., 1999]) or it is transfered in a karyopherin-α-dependent manner into the nucleus [Schroeder et al., 2007] in response to oxidative stress [Hirota et al., 1999] and/or other unknown stimuli. Inside the nucleus, thioredoxin can bind to transcription factors, modulating their activity using the redox active cysteines [Schroeder et al., 2007]. For example, the nuclearly localized bifunctional protein Ref1 (redox factor 1) is reduced by TRX1 which results in activation of hypoxia inducible factor 1 (HIF1) [Ema et al., 1999], p53 [Ueno et al., 1999], ESR [Hayashi et al., 1997] and others [Go and Jones, 2010, Mahmood et al., 2013].

TRX is an important element of the thioredoxin system consisting of the TRX, TRXR (thioredoxin reductase), NADPH reducing equivalent and TRX inhibitor TXNIP (thioredoxin-interacting protein).

The ancient fold of thioredoxin (see Figure 1.4), including a CxxC redox active motif, is conserved over the last four billion years [Ingles-Prieto et al., 2013]. A small moiety of 100 AAs constitutes a 12 kDa protein in cytosolic form (TRX1) and a slightly larger mitochondrial form (TRX2, containing the mitochondrial transit signal peptide at the N-terminus) [Choi, 2012]. There is also a less known TRX3 (also called SpTRX) playing an important role in a newly formed spermatozoa [Miranda-Vizuete et al., 2001].

A truncated version of TRX, the so-called TRX-80, was found in the plasma of patients

with severe schistosomiasis [Dessein et al., 1984]. From the previous research it seems that metalloproteinases ADAM10 and ADAM17 are responsible for the formation of this 10 kDa peptide in the brain where it forms 30kDa aggregates [Gil-Bea et al., 2012]. It was found to have a special function in activation of monocytes [Lemarechal et al., 2007] and in the release of pro-inflamatory cytokines [Bertini et al., 1999] suggesting a role in immunity defense system.

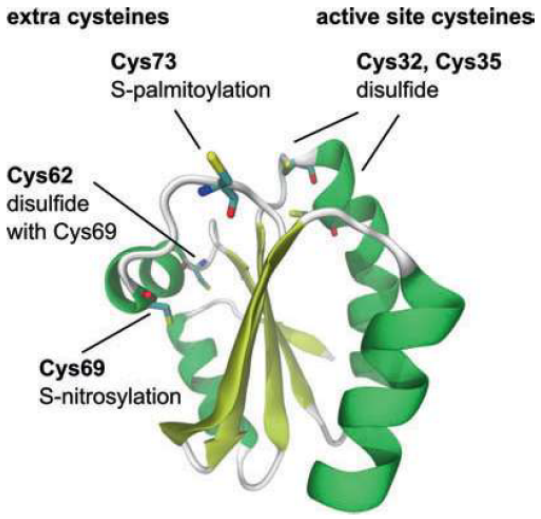

Figure 1.4: **Thioredoxin fold.** Active site cysteines (Cys32 and Cys35) and extra cysteines (Cys62, Cys69, Cys73) are highlighted on a crystal structure representation of reduced human TRX1, with their respective posttranslational modifications mentioned (reproduced from [Choi, 2012])

The cytosolic TRX1 mostly contributes to the cellular redox balance and cellular antioxidant defense by removing reversible thiol modifications from proteins [Hanschmann et al., 2013] and therefore changing their properties and functions. After the attack by a cysteine in the active site to the disulfide bond, a mixed disulfide intermediate is formed for a brief moment, followed by an oxidation of TRX and a reduction of the substrate. In order to be active, TRX is reduced again by the flavoenzyme TRXR and NADPH (see Figure 1.5). By doing so, TRX indirectly contributes to the maintenance of cellular redox balance as it reduces oxidized peroxiredoxins, therefore reactivates them to scavenge the reactive oxygen species (ROS) [Chae et al., 1994]. Importantly, this process can be reversed and TRX can function as an oxidase - oxidizing the substrate proteins while using H_2O_2 as an electron acceptor [Choi, 2012].

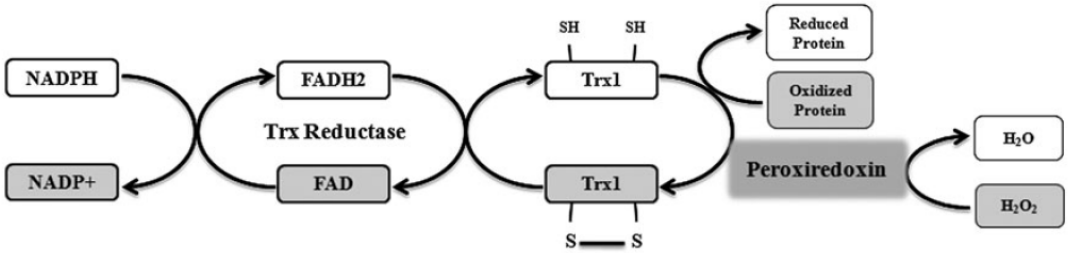

Figure 1.5: **Schematic representation of TRX system.** Oxidized Trx is reduced by electrons from NADPH *via* thioredoxin reductase. Reduced TRX in turn reduces proteins with disulfide bonds. The scheme also shows that TRX can indirectly scavenge free radicals by reduction of peroxiredoxin which is one of the TRX substrates (reproduced from [Mahmood et al., 2013]).

Another relevant aspect is the antiapoptotic property of TRX. Importantly, the redox

status of caspase-3 is controlled by TRX [Mitchell and Marletta, 2005]. Furthermore, the apoptosis signaling-regulating kinase 1 (ASK1), a major player in mitogen-activated protein kinase pathway (MAPK), is a substrate of TRX. When the TRX is bound to the ASK1, it inhibits its apoptotic activity [Saitoh et al., 1998].

Despite the vast literature on TRX, its role in cancer is still controversial. The TRX1 has been unanimously reported to be elevated in most cancer cells but one part of the scientific community attributes this to the result of significantly increased oxidative stress in the tumor cells [Mahmood et al., 2013] and mentions the increased TXNIP expression in several cancers (breast carcinoma [Cha et al., 2009], colorectal cancer [Raffel et al., 2003] and others). Meanwhile, different evidence points out to a role of TRX in the stimulation of cancer cell growth and to enhancement of the sensitivity to other growth factors. It also plays a role in inhibition of spontaneous apoptosis and decreased sensitivity to drug-induced apotosis [Skogastierna et al., 2012] as well as to induction of HIF1, therefore the vascular endothelial growth factor (VEGF). This can lead to tumor angiogenesis and drug resistance [Welsh et al., 2002]. Importantly, TRX1-overexpressing transgenic mice did not show any increase in malignancies [Mitsui et al., 2002].

1.3 Oxidases

In contrast to well-known oxygenases and dehydrogenases, oxidases require only molecular oxygen as an electron acceptor, usually using tightly, but not covalently bound cofactors to facilitate the process of electron transfer. These cofactors are either copper or iron ions in different molecular configurations or flavin adenin dinucleotides (FAD)/flavin mononucleotides (FMN) moieties. Only few examples of cofactor independent oxidases have been described, commonly interpreted as a consequence of a very poor ability of amino acids (AAs) to mediate redox reactions [Fetzner and Steiner, 2010].

Oxygenases and dehydrogenases, in order to be functional, need reducing equivalents (e.g. nicotinamide adenine dinucletotide (phosphate) (NAD(P)H)) together with molecular oxygen, and organic coenzymes (e.g. quinons or NAD^+) as a final electron acceptor, respectively. Since oxidases directly oxidize molecular oxygen, producing water, hydrogen peroxide, or even more harmful O_2^- superoxide as a byproduct, they contribute to ROS formation [Dijkman et al., 2013].

This superfamily of enzymes participates in a wide variety of processes in living cells - from maturation of proteins [Sevier and Kaiser, 2002] through metabolism of glucose [Dijkman et al., 2013] to maintaining functional electron transport chain (ETC) [Ridge et al., 2008]. The member of this superfamily that will be discussed in this work belongs to the family of sulfhydryl oxidases (SOXs) that introduces disulfide bonds into small molecules and proteins while producing H_2O_2 [Kiermeier and Petz, 1967].

1.4 Sulfhydryl oxidases

Disulfides in proteins can be a result of either air oxidation [Anfinsen, 1973], a catalysis of intercellular processes by thiol-disulfide-interchange-small-molecules (such as glutathione (GSH/GSSG)) [Ahmed et al., 1975], enzymatic catalysis of thiol-disulfide interchange [Larsson et al., 1983] or enzymatic catalysis by sulfhydryl oxidases. Nevertheless, air oxidation is, under physiological conditions, rather unlikely to occur, since the rate of this reaction is strongly inhibited above 25°C [Anfinsen, 1973]. Glutathione or protein disulfide-isomerase (PDI) can act

in physiological environments but are unable to form disulfides *de novo*, differentiating oxidases from the rest of these oxidizing elements.

The reaction catalyzed by this particular group of enzymes is as follows:

$$2\mathrm{RSH} + \mathrm{O_2} \longrightarrow \mathrm{RSSR} + \mathrm{H_2O_2}$$

where R is either a cysteine residue of denatured globular proteins or a small monothiol/dithiol molecule [Janolino and Swaisgood, 1975].

Sulfhydryl activity was reported in bovine, caprine, porcine, human and rat milk, as well as in lactating rat mammary gland, kidney and pancreas. At the same time, it was not detected in heart, liver, lung, spleen and thymus [Clare et al., 1984]. These discoveries lead in their time to a suggestion that SOXs can play a role in intestinal tract of newborns [Isaacs et al., 1984].

The first mammalian sulfhydryl oxidase ever studied was discovered in 1975 by Janolino and Swaisgood [Janolino and Swaisgood, 1975]. It is an iron-dependent sulfhydryl oxidase from bovine milk, later found also in membrane vesicles of bovine kidney [Schmelzer et al., 1982] and bovine pancreas [Clare et al., 1988].

Other metal-dependent sulfhydryl oxidases were found to be cuproproteins containing one atom of copper per subunit of enzyme. These Cu-dependent proteins were isolated mainly from rats (rat skin [Goldsmith, 1987], rat kidney [Ormstad et al., 1979], small-intestinal epithelium [Lash and Jones, 1983]) or pigs [Lash and Jones, 1986]. There are only two hypotheses to this date of their role in mammals. One is their possible function in assembly of immunoglobulin M (IgM) pentamer in mice [Roth and Koshland, 1981] and the second one is regulation of metabolites transport in and out of kidney or similar organs by altering the membrane thiol-disulfide status. Since there is a difference between the thiol:disulfide ratio of intracellular and extracellular proteins (the former are usually active in more reduced forms while the latter favor more oxidized forms), the effect of sulfhydryl oxidases is likely to be different in various proteins [Lash and Jones, 1986]. These metalloenzymes still remain poorly understood even though they may play some role in mammalian disulfide bond generation. They will not be further discussed in this work.

The last group in this family are flavoprotein sulfhydryl oxidases. Their research started with sulfhydryl oxidase from chicken egg white, isolated for the first time in 1996 by Thorpe's laboratory [Hoober et al., 1996]. They stated that this homodimeric oxidase contains 1 FAD molecule, two disulfide bridges and 1 free sulfhydryl group (which is noninteractive in native oxidized enzyme) per subunit [Hoober et al., 1996].The first study of proteins as sulfhydryl oxidase substrates (small monothiol and dithiol substrates were used before) was carried out by the same group only three years later, testing several different proteins (see Figure 1.6) for kinetic studies of chicken egg white sulfhydryl oxidase activity [Hoober et al., 1999b]. They concluded that there seems to be no obvious restrictions as to molecular weight (Mr) or isoelectric point for the substrates tested - all unfolded cytoplasmic proteins without native disulfide bridges can be oxidized. It was also suggested that in order to help proteins to fold into their native conformation properly, SOXs are likely to cooperate with PDI in the endoplasmic reticulum (ER) [Hoober et al., 1999b].

The chicken egg white SOX is not the sole member of the newly formed quiescent sulfhydryl oxidases family (QSOX). It contains also rat seminal vesicles SOX (SOX-2) [Ostrowski and Kistler, 1980], bone-derived growth factor [Heckler et al., 2008], cell growth inhibitory factor [Coppock and Thorpe, 2006], placental-derived prostate growth factor [Heckler et al., 2008], SOX-3 [Musard et al., 2001] and quiescin 6 (QSOX1/QSCN6/Q6) [Coppock et al., 1993].

Kinetic parameters were determined as described under "Experimental Procedures."

Protein	M_r	pI	-SH[a] initial	-SH[b] final	TN_{max}[c]	K_m[d]	TN_{max}/K_m[e]
					min^{-1}	μM	$M^{-1}\ s^{-1}$
RNase	13,700	7.8	0	8	610	115 (14)	8.8×10^4
Lysozyme	14,300	10.7	0	8	860	110 (14)	1.3×10^5
Riboflavin-binding protein	34,000	4.2	0	18	1100	230 (13)	8.0×10^4
Ovalbumin	45,000	4.5	4	6	565	330 (55)	2.9×10^4
Aldolase	40,200	6.1	8	8	200	160 (20)	2.1×10^4
Pyruvate kinase[f]	59,250	6.6	9	9	475	1,250 (140)	6.3×10^3
Insulin A chain	2,340	3.8	0	4	1000	215 (55)	7.8×10^4
Insulin B chain[f]	3,400	6.9	0	2	700	300 (150)	3.9×10^4
N-acetyl-EAQCGTS	740	4.0	1	1	1420	1,720	1.4×10^4
GSH[g]	300	2.8	1	1	1385	20,000	1.2×10^3

[a] Number of thiols before reduction.
[b] Total thiols after reduction of any disulfide bonds.
[c] TN_{max} values are disulfide bonds formed/minute.
[d] K_m values are expressed both on a per thiol basis and per substrate molecule (shown in parentheses).
[e] TN_{max}/K_m uses thiol (not protein) concentrations.
[f] In 3 M urea to maintain solubility at higher substrate concentrations.

Figure 1.6: Comparison of several substrates for the egg white sulfhydryl oxidase (reproduced from [Hoober et al., 1999b])

All QSOX family members share the basic features of having one or more thioredoxin domains and one flavin-binding domain called Erv/ALR which is an evolutionary outcome of fusion of still existent Erv/ALR sulfhydryl oxidase and thioredoxin [Coppock et al., 1998].

This "ancient" enzyme of augmenter of liver regeneration (ALR) is together with yeast Erv1p, Erv2p, Ero1p and SOXs from fungal sources like *Aspergillus niger* [De La Motte and Wagner, 1987] and *Penicillium* species [Kusakabe et al., 1982] the remaining member of FAD-dependent sulfhydryl oxidases family.

1.4.1 ALR/ERV1

Augmenter of liver regeneration (ALR), also known as hepatic stimulatory substance (HSS), hepatopoietin (HPO) or growth factor Erv-1 like (GFER), is a protein known for its specific ability to stimulate liver regeneration [Gupta and Venugopal, 2018].

It is a FAD-linked sulfhydryl oxidase that is highly homologous to the yeast Erv family of proteins involved in respiration and vegetative growth [Lisowsky, 1992] and therefore essential for life of yeast. Its reduced form was reported to be 21 and 23 kDa (205 AAs) in size for the longer variant and 15 kDa (125 AAs) for the shorter, secreted one. These two variants differ only in an N-terminal leader sequence that is missing in the shorter protein. Under non-reducing conditions however, available data suggests that ALR forms homodimers and heterodimers within the different splicing variants, resulting in existence of various ALR complexes in human liver tissue [Li et al., 2002].

ALR expression is ubiquitous throughout the human body, although it is highly increased in liver and testis [Giorda et al., 1996] and most of the existing research focus on tissues of this origin. On the cellular level, shorter ALR was found to be localized in nucleus and cytoplasm, as well as secreted to the extracellular matrix while the longer form is restricted to the mitochondrial intermembrane space (IMS) [Tury et al., 2005]. The soluble, shorter ALR version, was reported to have its affiliated receptor that is highly specific for its ligand [Wang et al., 1999] and plays an important role in the liver regeneration process [LaBrecque and Pesch, 1975].

Apart from this function, ERV1 is known to participate in cysteine-rich protein import into mitochondrial IMS in cooperation with Mia40 [Grumbt et al., 2007], but also in protein folding and electron transport system in mitochondria *via* its sulfhydryl oxidase activity (see Figure 1.7) [Daithankar et al., 2009].

Any defect in ERv1-Mia40 system leads to mitochondrial iron overload [Rouault, 2016] presumably due to its involvement in Fe-S cluster biogenesis and repair [Ferecatu et al., 2014].

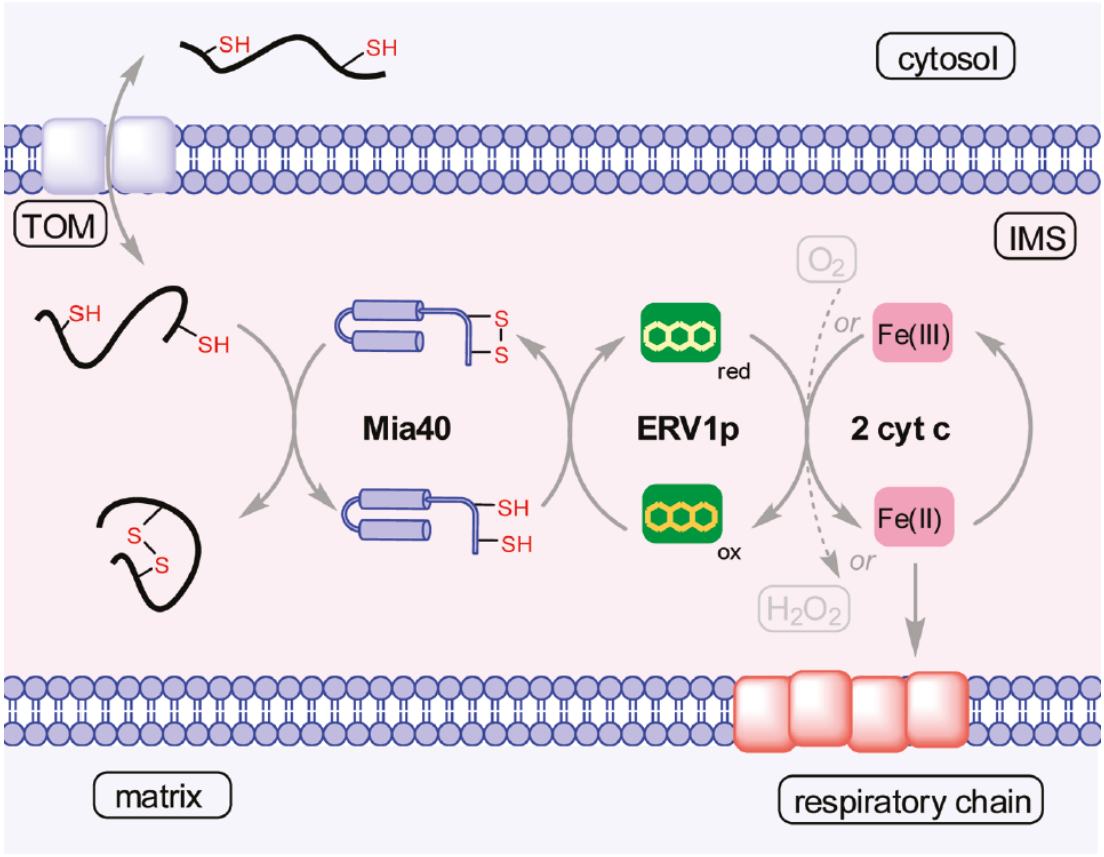

Figure 1.7: **Schematic representation of the Mia40-Erv1 mitochondrial intermembrane assembly system.** Unfolded protein is transported by translocase of the outer membrane (TOM) into IMS where it is sequestered by Mia40 and folded in its native conformation by introduction of disulfide bonds. Mia40 is then reoxidized and therefore reactivated by Erv1. The electrons are further transferred to cytochrome c and to mitochondrial respiratory chain. In an alternative pathway, marked by a gray dotted arrow, hydrogen peroxide generated by oxidase activity serves as a net oxidant for cytochrome c peroxidase (reproduced from [Daithankar et al., 2009])

Most interestingly, ALR was found to be upregulated in hematopoietic stem cells (HSC) where it was reported to maintain quiescence *via* the JAB1/p27^{kip1} (see Figure 1.8) [Teng et al., 2011] and CaMKIV-CREB-CBP pathways [Sankar and Means, 2011], as well as in murine embryonic stem cells, sustaining pluripotency by downregulation of dynamin-related protein 1 (Drp1) mediated mitochondrial fission and therefore keeping mitochondria in primitive state. However, this phenomenon is inherent to this very specific cell type since depletion of ALR in more differentiated cells has not affected mitochondrial function and/or cell viability whatsoever [Todd et al., 2010].

Upregulation of ALR was also reported in several malignant cell lines where it was associated with protective effect on the cancer cell survival [Nguyen et al., 2017]. In hepatic cancer cells (HCC), - which are the most frequently studied cells in this particular field - ALR is suggested to be connected with cancerogenesis. It was established that HepG2 and QGY cell lines are stimulated by ALR in a dose-dependent manner while, no significant impact on primary hepatocytes was found. This specific effect is suggested to be due to the presence of different ALR receptors on hepatocytes and hepatocarcinoma cells [Liu et al., 2004]. In some of the conducted studies, ALR suppression resulted in significant decrease of the carcinoma

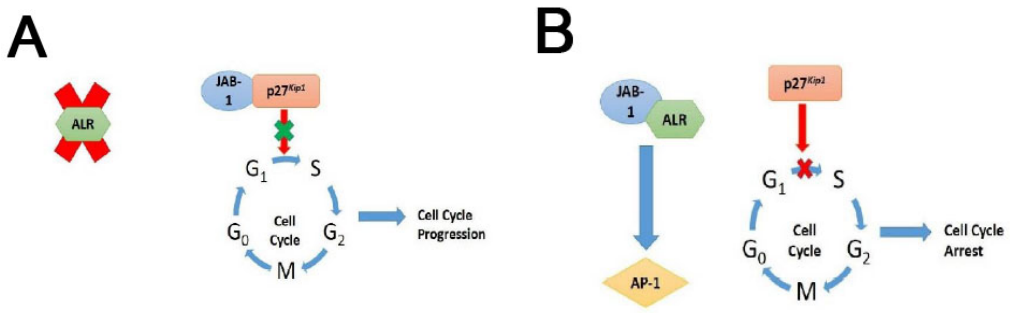

Figure 1.8: **Schematic representation of proteasomal pathway regulation by ALR in HSC in nucleus. A** Jun activation domain-binding protein-1 (JAB1) binds to $p27^{kip1}$ and inhibits nuclear export, ubiquitination and increased turnover of this cyclin-dependent kinase inhibitor (CDKI) [Sankar and Means, 2011] by proteasomal degradation which leads to overcoming of G1 arrest and transition into S-phase of cell cycle. **B** ALR sequesters JAB1 and interacts with activator protein 1 (AP-1) transcription factor resulting in cell cycle arrest in G1 phase (reproduced from [Gupta and Venugopal, 2018])

growth [Tang et al., 2009]. This could be explained by its "protection" of mitochondria and reduction of cytochrome c release when under stress [Cao et al., 2009]. On the other hand, depletion of JAB1 that is sequestered by ALR, was documented as inhibitory for cellular growth and proliferation [Fukumoto et al., 2006]. It is clear, that additional studies to fully understand the connection of ALR and cancer are required.

1.4.2 ERO1

Another known participant of ER disulfide relay is ER oxidoreductin 1 (ERO1), also named ER oxidoreductin-like protein 1 (Ero1-L).

Similarly to ALR, ERO1 is a FAD-linked sulfhydryl oxidase with only one variant in yeast (Ero1p) but two variants in higher eukaryotes - ERO1α and ERO1β [Pagani et al., 2000]. These two isoforms are 468 and 467 AAs in length, respectively, resulting in molecular weight of about 54 kDa [UniProt, 2019]. They can form homodimers and heterodimers, and interact with PDI in a redox-dependent manner [Dias-Gunasekara et al., 2005]. Even though their sequences are very similar which suggests a possible evolutionary conservation in their function the proteins are encoded by different genes [Pagani et al., 2000].

On the tissue expression level however, the similarity ends. ERO1α was reported to be expressed ubiquitously throughout the body [Cabibbo et al., 2000], whereas the ERO1β is predominantly enriched in highly secretory cells like pancreatic β cells [Dias-Gunasekara et al., 2005] or antibody producing lymphocytes [Zito, 2015].

Even though ERO1 is missing the KDEL (PDI) or RDEL (ERp44) C-terminal sequence, it is maintained exclusively in the ER [Pagani et al., 2000]. The general notion here is that ERO1 could be using a thiol-dependent association with either PDI [Otsu et al., 2006], endoplasmic reticulum resident protein 44 (ERp44) [Anelli et al., 2003] or both, exploiting their localization sequences for transportation into the ER. In yeast, Ero1p was reported to be a membrane-associated protein [Pagani et al., 2001]. The human ERO1, however, lacks the C-terminal tail that interacts with the membrane, rendering its position within the ER yet unknown so far [Otsu et al., 2006].

Since the lumen of the ER is a highly oxidative environment in comparison to cytosol (the ratio of reduced and oxidized glutathione is 5:1 [Dixon et al., 2008], while in the cytosol it ranges from 30:1 to 100:1 [Hwang et al., 1992]), it represents a perfect compartment for ERO1 activity: the formation of disulfide bonds. Similarly to ALR, ERO1 uses molecular oxygen as a terminal acceptor of electrons [Gross et al., 2006] in order to introduce disulfides into miscellaneous substrates. One of those is the above mentioned PDI which relies on ERO1 for its reoxidation [Frand and Kaiser, 1999] after transferring disulfides to nascent polypeptides (see Figure 1.9).

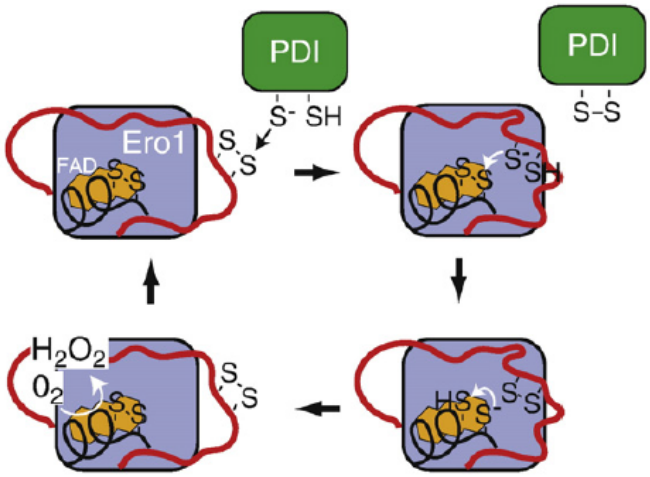

Figure 1.9: **Schematic representation of catalytic mechanism of ERO1 electron transfer after PDI reoxidation**. ERO1 reoxidizes PDI, transfers the electrons from shuttle cysteines (red) to active-site cysteines (black) and from there to the FAD cofactor (yellow). Molecular oxygen serves as a terminal electron acceptor, creating molecule of H_2O_2 (reproduced from [Sevier and Kaiser, 2007])

Upon PDI reactivation, reduced ERO1 is capable of intramolecular electron transfer *via* the shuttle cysteines, towards the active site cysteines and afterwards to the FAD moiety. This enables for *de novo* disulfide formation - a transfer of electrons without another thiol-disulfide exchange [Tu et al., 2000].

Again, H_2O_2 is created as a byproduct of this catalytic activity. For each disulfide bond, one molecule of H_2O_2 is formed during the protein folding [Tu and Weissman, 2004]. To avoid hyperoxidation of ER, there are some putative hydrogen peroxide detoxification pathways [Tavender et al., 2008] but pathways regulating the activity of ERO1 also exist and function as a prevention to excessive oxidative stress.

As expected, in higher eukaryotes, the ERO1 ER stress defense system is redundant. While in yeast ERO1 is essential [Pollard et al., 1998], it is compensated for in mammals with Ero1-independent pathways, involving Prx4 (Peroxiredoxin 4) [Zito et al., 2010], GPx7/8 (Glutathione peroxidase 7/8) [Bulleid and Ellgaard, 2011] or the already mentioned ALR.

The posttranslational regulatory mechanism of Ero1 activity seems to be tightly tethered to its two noncatalytic regulatory cysteine pairs and their isomerization or reduction [Sevier et al., 2007]. When needed, ERO1 is activated by PDI itself, which leads to alteration of the redox balance of its local environment and afterwards to reoxidation of its regulatory disulfides and inactivation in a negative feedback manner (see Figure 1.10) [Tavender and Bulleid, 2010].

Any pharmacological or physiological disruptions of ER folding events that lead to accumulation of unfolded proteins in the ER lumen and ER stress, induce unfolded protein response (UPR) [Ron and Walter, 2007]. Such activation entails an increase of the ER folding capacity,

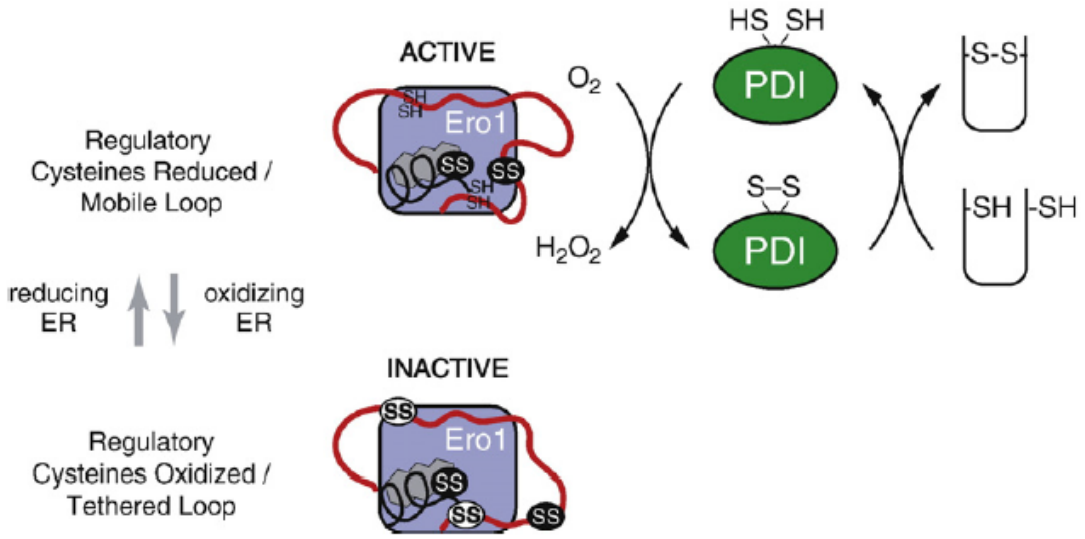

Figure 1.10: **Schematic representation of ERO1 regulation on protein level.** Catalytic cysteines are depicted in black ovals while regulatory cysteines in white ovals. When regulatory cysteins are oxidized, non-helical loop of ERO1 containing shuttle cysteines is tethered to the protein core and blocks mobility of shuttle cysteines, resulting in inactive protein. When regulatory cysteines are reduced however, the non-helical loop is mobile and ERO1 is active (reproduced from [Sevier and Kaiser, 2007])

augmentation of the complement of folding chaperones and modifying enzymes, and enhancement of removal of irreparably misfolded proteins from the lumen by ER-associated degradation process (ERAD). Any further defects that would cause the UPR to be ineffective direct the cell towards apoptosis [Sevier and Kaiser, 2007].

To be able to regulate the process thoroughly, one of the transcription targets of UPR-activated transcription factor CHOP (CCAAT-enhancer-binding protein homologous protein) is ERO1α [Marciniak et al., 2004], while expression of ERO1β is also induced under UPR [Pagani et al., 2000] only with a different, yet unknown, pathway [Tavender and Bulleid, 2010]. Interestingly, Ero1α was found to be upregulated also by hypoxia. The CpG islands in its promoter region contain two copies of the most common active HIF1 binding consensus sequence ACGTG [Gess et al., 2003].

In cancer, upregulation of ERO1 is associated with poor prognosis [Endoh et al., 2004]. Since some tumor cells are capable of survival, even proliferation, under hypoxic conditions, which was reported to lead to increase of ERO1 expression, it is possible that Ero1 may play a role in the cell viability. The exact mechanism is still to be elucidated but one study suggests that ERO1 is involved in increased VEGF secretion and therefore better vascular supplementation to the tumor [May et al., 2005].

1.4.3 QSOX1

QSOX1, also called quiescin 6 (Q6/QSCN6) is another member of the sulfhydryl oxidase family and is the main focus of this diploma thesis. Its name refers to the first discovery of this protein by Coppock et al. [Coppock et al., 1993], upregulated in quiescent human embryonic lung fibroblasts (WI38). Its putative human paralog QSOX2 (previously called SOXN) is expressed at much lower levels in human tissues [Thorpe et al., 2002] and is not a main focus

in this study.

According to Coppock et al., two proteins - ALR/Erv1 and TRX - underwent a gene fusion event during metazoan evolution, resulting in a single gene *QSOX1* [Coppock et al., 1998]. The dedicated protein, QSOX1, contains two thioredoxin domains (TRX1, TRX2) with one CxxC motif in the N-terminal and one Erv1/ALR domain with two CxxC motifs in the C-terminal end. This latter domain also holds an ADP-binding motif interacting with the FAD prosthetic group important for its function. This domain structure is more or less conserved in higher and lower animals as well as in plants (see Figure 1.11).

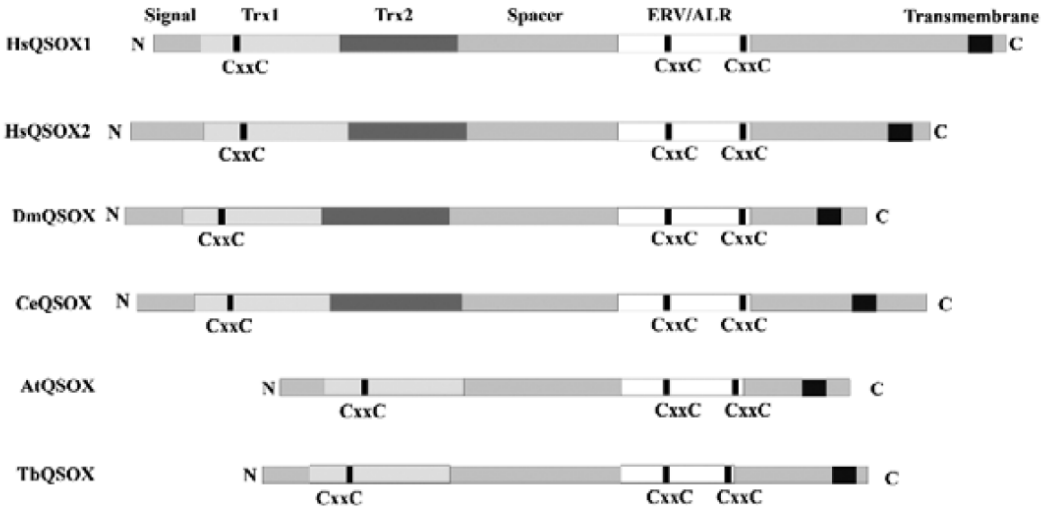

Figure 1.11: **Schematic representation of QSOX1 primary protein structure in different models.** Two human QSOXs with following structure: from N-terminal end - a signal sequence for ER-retention (not shown); first thioredoxin domain (TRX1) with redox-active CxxC motif; second, weaker thioredoxin domain (TRX2) with no CxxC motif; spacer; Erv1/ALR domain with two CxxC motifs - catalytic site, and FAD-binding domain; spacer; NEQEQPLGQWHLS peptide (not shown); spacer; transmembrane domain. The figure also depicts one QSOX1 of four from *Drosophila melanogaster*, one of three from *Caenorhabditis elegans*, one of two from *Arabidopsis thaliana* and a single QSOX1 from *Trypanosoma brucei* (reproduced from [Coppock and Thorpe, 2006])

Similarily to ALR, QSOX1 has two protein isoforms - longer (QSOX1v1/QSOX1-L/QSOX1A) and shorter (QSOX1v2/QSOX1-S/QSOX1B). These two versions are sequentially almost identical (except for two AAs - L603 and I604) only QSOX1v2 is missing the C-terminal tail of 104 AAs with the transmembrane region. Prior research suggests that this truncation is generated by alternative splicing [Benayoun et al., 2001] resulting in transmembrane and soluble proteins that are capable of interacting with each other to form heterodimers [Rudolf et al., 2013] and probably also homodimers, as would be expected from homology with other QSOX oxidases [Coppock and Thorpe, 2006].

QSOX1 expression varies throughout the tissues of human body [Coppock and Thorpe, 2006], being upregulated generally in tissues involved in apocrine secretion such as plasma cells, pituitary, prostate [Turi et al., 2001] or islets of Langerhans, parotid gland and apocrine glands of the skin [Thorpe et al., 2002].

On the intracellular level, QSOX1v1 can be found predominantly bound to the membrane of rough ER [Thorpe et al., 2002] or in the Golgi apparatus (GA) [Rudolf et al., 2013], while the shorter version, QSOX1v2, is secreted out of the cell. Interestingly, the longer variant can

undergo a proteolytic cleavage, leading to its release from the membrane and following secretion to the ECM as well [Rudolf et al., 2013]. Both versions of QSOX1 can be therefore present in the extracellular millieu.

Secreted QSOX1 probably has a very similar function to the one inside the cell. As it works as a sulfhydryl oxidase by introducing disulfide bonds into native proteins, helping in oxidative protein folding at the expense of molecular oxygen and forming H_2O_2 as a byproduct [Hoober et al., 1999a], outside the cell it can play an important role in ECM remodeling and formation [Ilani et al., 2013]. In the ER, QSOX1 cooperates very closely with PDI to fold a wide range of proteins - surprisingly, PDI is not a substrate of QSOX1 but at the same time, neither of the two are efficient in folding proteins independent of each other [Rancy and Thorpe, 2008].

The mechanism of QSOX1 catalysis is probably analogous to the one of ALR - the first TRX domain (TRX1) oxidizes a dithiol substrate and transfers the reducing equivalents to the active site C-terminal CxxC motif in Erv1/ALR domain. The electrons would then be shuttled from one subunit of the QSOX1 dimer to another (from C-terminal CxxC motif to the central one) and reduce the flavin. The last step of this disulfide relay is the reduction of molecular oxygen and formation of H_2O_2 [Coppock and Thorpe, 2006].

To prevent hyperoxidation of the cell compartments, QSOX1 catalytic activity should be tightly regulated. While Shi *et al.* suggest that *QSOX1* expression is induced by HIF1 *via* its hypoxia-response element (HRE) [Shi et al., 2013] in a similar way as Ero1 [Gess et al., 2003], Tury et al. described regulation by estrogen in rats [Tury et al., 2004] similarly to the SOX-3 oxidase [Musard et al., 2001]. Another possible regulation of QSOX1 could be managed by proteolytic cleavage of membrane-bound QSOX1v1. In this scheme, QSOX1v1 is inactive by tethering to the membrane which does not allow for the necessary conformational changes in the protein. Once it is cleaved, it becomes soluble and active. At the same time, while QSOX1v1 is bound to the membrane, it is thought to associate with a free QSOX1v2 and thus sequester it [Rudolf et al., 2013].

Even though the role of QSOX1 is probably cell type dependent, it is safe to say that it plays a role in tumorigenesis. It is highly overexpressed in tumor cells but not in adjacent normal tissue [Katchman et al., 2011] even compared to the highly secretory cells such as islet cells in the pancreas [Lake and Faigel, 2014]. In regards to its function in this thoroughly examined process, the literature is contradictory. Pernodet et al. has reported that increased expression of QSOX1 reduces the tumor formation rate and contributes to better prognosis for breast cancer patients [Pernodet et al., 2012]. However, this study was found to be inadequate by various sources [Das et al., 2013, Lake and Faigel, 2014] and subsequent studies were carried out with completely opposite results [Ilani et al., 2013, Soloviev et al., 2013, Katchman et al., 2013].

Katchman *et al.* has shown that increased QSOX1 expression in pancreatic [Katchman et al., 2011] and breast [Katchman et al., 2013] cancer cells is associated with higher invasive and metastatic phenotype as well as enhanced proliferation. This could be due to its putative posttranslational activation of metalloproteinases (MMPs) MMP-2 and MMP-9 inside or outside the cells *via* a yet unknown mechanisms [Katchman et al., 2011]. These highly functional gelatinases are secreted into the ECM in their inactive form where they can be activated through an oxidation or isomerization, thus the QSOX1 seems a possible interacting partner whether outside or inside the cell [Köhrmann et al., 2009]. Nonetheless, BT474 cells that do not secrete detectable levels of MMP-2 or MMP-9 responded to QSOX1 deprivation with decreased invasivness [Katchman et al., 2013] suggesting that there is more than one pathway

involved. Another possible explanation was proposed by Ilani et al. when this group reported that QSOX1 plays a role in extracellular laminin incorporation into the ECM and overall cell attachment to surfaces [Ilani et al., 2013]. As a suggestion for higher proliferation with upregulated QSOX1, Morel et al. published a study about its protective effects against H_2O_2-induced stress and apoptosis [Morel et al., 2007] and since QSOX1 is one of the producers of H_2O_2 in the ER, the mechanism of cell protection would probably involve some kind of negative feedback loop response.

In the light of these findings, QSOX1 seems as a promising antineoplastic target, meanwhile it can be also considered a biomarker for cancer grade due to its correlation with poor prognosis [Katchman et al., 2013] and a fact that a 16 AAs long peptide NEQEQPLGQWHLS, that can be traced back to the longer variant of QSOX1, was found in plasma of 70% of pancreatic cancer patients while it was missing in the plasma of all healthy patients [Antwi et al., 2009].

Over the past few years, our laboratory has studied on the differences in iron metabolism of the so-called cancer stem-likes cells (CSCs) that represent the distinct population of cancer cells that is resistant to commonly used chemotherapeutic drugs and very likely participates on cancer relapse and secondary tumor formation [Rychtarcikova et al., 2017]. While working on this project, a differential iron metabolism-related gene signature was identified, and, importantly *QSOX1* was significantly upregulated in these cells at the mRNA as well as protein level. Therefore, we decided to study the role of QSOX1 in cancerogenesis aiming to understand its benefits for cancer cells.

2. Aims

This thesis was focused on the role of QSOX1 in cancerogenesis and molecular mechanisms of its regulation, and comprised several particular aims that are listed below:

- To compare the protein level of QSOX1 between non-malignant and malignant cells.
- To test the effect of *QSOX1* overexpression on proliferation of cancer cells by using inducible TetON3G system.
- To generate an experimental model that lacks *QSOX1 via* the CRISPR methodology and test the effect of QSOX1 knockout on cell proliferation.
- To determine whether QSOX1 responds to hypoxia at the level of mRNA, protein and secretion.

3. Materials and methods

3.1 Cell culture

Under normal conditions, cells were cultivated at 37 °C and in atmosphere of 21% O_2 and 5% CO_2 in humidified incubator. Two different media were used for growth of the cells (see Table 3.1 for media and cell lines specifications) - complete medium containing:

- Dulbecco's Modified Eagle Media (DMEM) (LONZA)
- Streptomycin (100 µg/ml)
- Penicillin (100 U/ml)
- L-glutamine (2mM)
- HEPES, pH 7.2 (10mM)
- Fetal bovine serum (FBS)

or MCF10A medium containing:

- DMEM (LONZA)
- Streptomycin (100 µg/ml)
- Penicillin (100 U/ml)
- HEPES, pH 7.2 (10mM)
- Horse serum (HS)
- rhEGF (20 ng/ml)
- Hydrocortisone (0.5 µg/ml)
- Cholera toxin (0.1 µg/ml)
- Insulin (10 µg/ml)

Under hypoxic conditions, cells were cultivated at 37 °C and in atmosphere of 0%, 0.1%, 0.5%, 1%, 2% or 5% O_2 and 5% CO_2 in humidified hypoxic chamber (McCoy) with the same medium as specified before.

3.2 TetON3G-inducible system

MDA-MB-231 cells containing pTRE3G-BI-mCherry vector (see Fig 3.1) producing both protein variants QSOX1v1 (Cl12, Cl14) and QSOX1v2 (Cl41, Cl47) were supplied by my supervisor Mgr. Jaroslav Truksa, PhD. The variants were cloned with restriction endonucleases BamHI and NotI and verified by sequencing.

3.2.1 Fluorescent microscopy

Fluorescent images were taken on fluorescent microscope (Nikon) using Leica400 software.

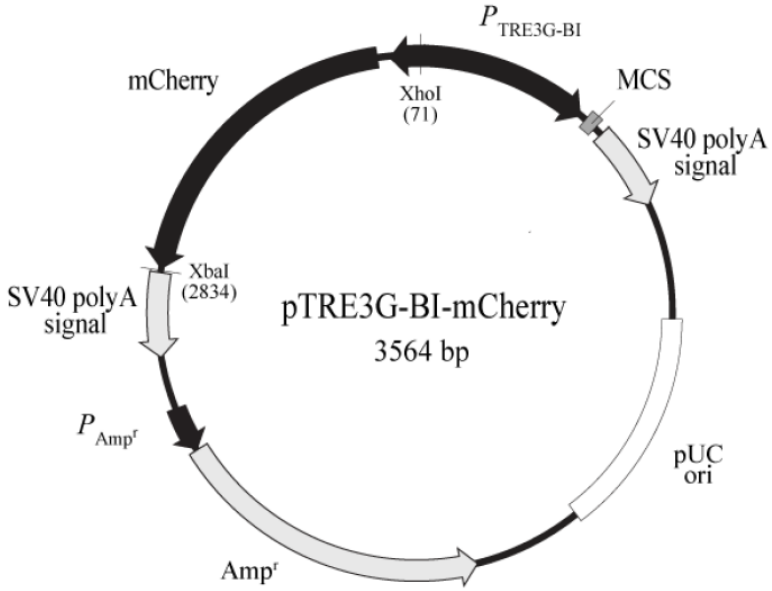

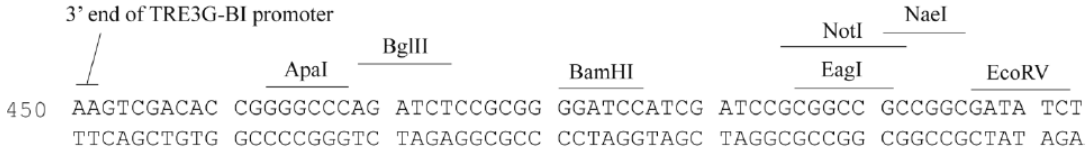

Figure 3.1: **Vector map of pTRE3G-BI-mCherry vector (Clontech) and the multiple clonning site.**

Cells	Medium	Additives
BJ	complete	none
BT474	complete	none
MCF10A	MCF10A	none
MCF7	complete	none
MDA-MB-231	complete	none
MDA-MB-231 Cl5	complete	none
MDA-MB-231 Cl16	complete	none
MDA-MB-231 Cl17	complete	none
MDA-MB-231 Cl29	complete	none
MDA-MB-231 Cl33	complete	none
MDA-MB-231 CRISPR/Cas9 Cl16 1A4	complete	none
MDA-MB-231 CRISPR/Cas9 Cl16 1C9	complete	none
MDA-MB-231 CRISPR/Cas9 Cl16 1F4	complete	none
MDA-MB-231 CRISPR/Cas9 Cl16 2C8	complete	none
MDA-MB-231 CRISPR/Cas9 Cl16 2D10	complete	none
MDA-MB-231 CRISPR/Cas9 Cl7 1E2	complete	none
MDA-MB-231 CRISPR/Cas9 Cl7 2D1	complete	none
MDA-MB-231 CRISPR/Cas9 Cl7 2D8	complete	none
MDA-MB-231 CRISPR/Cas9 Cl7 2E4	complete	none
MDA-MB-231 CRISPR/Cas9 Cl7 2E9	complete	none
MDA-MB-231 CRISPR/Cas9 Cl7 2F12	complete	none
MDA-MB-231 CRISPR/Cas9 C33 1B4	complete	none
MDA-MB-231 CRISPR/Cas9 C33 1D1	complete	none
MDA-MB-231 CRISPR/Cas9 C33 1E11	complete	none
MDA-MB-231 CRISPR/Cas9 C33 1E4	complete	none
MDA-MB-231 CRISPR/Cas9 C33 1G11	complete	none
MDA-MB-231 TetON 3G BI-mCherry EV5	complete	puromycine, geneticine
MDA-MB-231 TetON 3G BI-mCherry Cl12	complete	puromycine, geneticine
MDA-MB-231 TetON 3G BI-mCherry Cl14	complete	puromycine, geneticine
MDA-MB-231 TetON 3G BI-mCherry Cl41	complete	puromycine, geneticine
MDA-MB-231 TetON 3G BI-mCherry Cl47	complete	puromycine, geneticine
Panc-1	complete	none
PaTu-892	complete	none
T47D	complete	none

Table 3.1: List of cell lines, their derivatives and appropriate medium and additives used

3.3 CRISPR/Cas9 system

CRISPR/Cas9 vector plasmid (see Figure 3.2) with cloned sgRNA targeting *QSOX1* exon 6 was a kind gift from my colleague Mgr. Sandra Lettlová, PhD. The primers used for sgRNA assembly are listed in Table 3.2. These primers were annealed and cloned into the LentiCRISPR vector (pXPR_ 001) cut with BcmBI restriction enzyme, leading to insertion of the following sequence 5'-CAGAGCCATTCCGGAACAGC-3'.

Gene	Manufacturer	Primer
QSOX1 seq	Generi Biotech	F 5'-CACCGCAGAGCCATTCCGGAACAGC-3'
		R 5'-AAACGCTGTTCCGGAATGGCTCTGC-3'

Table 3.2: List of primers for sgRNA assembly.

This system was used to knockout (KO) the gene completely, using one double-stranded nick in the recipient DNA resulting in altered DNA, ideally leading to non-functional mRNA or protein resulting in lack of expression of the normal, active protein.

Cells were transfected two times - for the first time, only heterozygotes with one altered allele were obtained (Cl5, Cl16, Cl17, Cl29 and Cl33). These KO cells were afterwards transfected once again using the same protocol as before and full knockouts were obtained and sequenced.

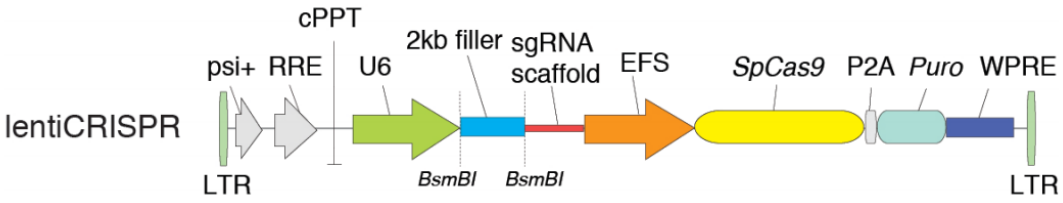

Figure 3.2: **Vector map of LentiCRISPR vector (GeCKO)**

3.3.1 Lipofectamine transfection

MDA-MB-231 cells were transfected using Lipofectamine™ 3000 Reagent (Invitrogen).

Cells were plated in 6-well plates (Thermo Scientific) so they would reach 70-90% confluence on the day of transfection.

Lipofectamine™ LTX was diluted in Opti-MEM™ medium (serum-free without antibiotics) in two different concentrations (3% and 6%). 5 µg of DNA was diluted in 250 µl of the same medium in another tube and 10 µl of P3000™ Reagent was added and the mixture was vortexed thoroughly.

125 µl of the DNA solution was added to each of the Lipofectamine™ 3000 tubes and incubated for 15 minutes at room temperature.

250 µl of two differently concentrated DNA-lipid complex solutions was added to different wells in 6-well plate.

One day after transfection, puromycine was added to cells and they were incubated for another 3 days at 37 °C.

3.4 Flow cytometry

Flow cytometry was used for single-cell sorting in order to obtain clones for knockout and overexpressing cells, originating from one cell. The procedure was carried out by Imaging Methods Core Facility in Biocev, Vestec.

3.5 Harvesting medium

Medium was harvested from cells right before the cells were lysed for protein or RNA isolation. The tubes with medium were spun for 5 minutes at 300 xg, supernatant was aspirated and transferred to new tubes.

Medium was stored at -80 °C.

3.6 Whole cell protein lysate preparation

3.6.1 Normal conditions

Medium was aspirated and cells washed twice with 1xPBS. Remaining PBS was removed carefully so the samples were diluted as little as possible and the cells were lysed by lysis buffer containing following (final concentration indicated in brackets):

- NaCl (150mM)
- Tris pH=8 (50mM)

- NP-40 substitute (1%)
- SDS (0.1%)
- EDTA (1mM)
- Na-Deoxycholate (0.5%)
- H_2O

Samples were transferred on ice and incubated for 15 minutes, then scraped with cell scraper, collected into cold tubes and incubated for another 20 minutes while vortexing after 10 minutes.

Samples were spun down at 15000 xg for 5 minutes, 4 °C and supernatant transferred to new tubes.

Protein samples were stored at -80 °C.

3.6.2 Hypoxic conditions

Medium was aspirated and cells washed twice with 1xPBS stored in the hypoxic chamber. Remaining PBS was removed carefully so the samples were diluted as little as possible and the cells were immediately transferred on dry ice where the same lysis buffer, described in previous section, was added. Afterwards, the procedure was the same as in the previous section.

3.7 Protein concentration measurement

Protein concentration of samples was measured using Pierce™ bicinchoninic acid (BCA) protein assay kit (ThermoFisher Scientific), measuring the total protein concentration, using serial dilution of bovine serum albumine (BSA) as a calibration standard curve.

The samples were prepared according to the manufacturer's instructions. After 30 minutes of incubation at 37 °C, the absorbance at wavelenght of 562 nm was measured using $\text{Infinite}_{\text{M200}}$ TECAN and the concentration was calculated in Excel, using the BSA standard curve as a reference.

Note: medium samples were not measured for protein concentration.

3.8 Sodium dodecyl sulfate - polyacrylamide gel electrophoresis (SDS-PAGE)

3.8.1 Gel preparation

All gels were prepared manually according to the following protocol (giving final concentrations of the constituents in brackets):

Separation gel

- TRIS-HCl, pH 8.8 (375mM)
- SDS (0.1%)
- Acrylamide/bisacrylamide (4%)
- TEMED (0.1%)

- APS (0.05%)
- dH_2O

Stacking gel

- TRIS-HCl, pH 6.8 (125mM)
- SDS (0.1%)
- Acrylamide/bisacrylamide (4%)
- TEMED (0.1%)
- Ammonium persulfate (APS) (0.05%)
- dH_2O

For all SDS-PAGE experiments, 8% acrylamide gels were used. For hypoxia samples, the thicker gels (1.5 mm) were used, the thinner gels (1mm) for the rest.

3.8.2 SDS-PAGE

Samples were mixed with lysis buffer to obtain the desired protein concentration (different volumes of protein were used since we have tried to load as much protein as possible with variously diluted samples) and 4x sample loading buffer (4xSLB), containing following:

- Glycerol (100%)
- TRIS-HCl. pH 6.8 (1M)
- SDS (0.27M)
- 2-mercaptoethanol (1M)
- Blue bromphenol (1.5mM)
- dH_2O

Note: medium samples were mixed only with 4xSLB in following order - 15 µl of medium and 5 µl of 4xSLB.

All samples were boiled for 5 minutes at 95°C to ensure denaturation and afterwards, together with 5 µl of protein ladder (Spectra™ Multicolor Broad Range protein ladder), loaded onto the SDS-PAGE gel with 1x running buffer containing following:

- TRIS (25mM)
- Glycine (192mM)
- SDS (1%)
- dH_2O

The gels were run at room temperature on the following program:

- 80 V 15 minutes
- 120 V until the end

3.9 Western blot (WB)

Sponges and membranes were submerged for approximately 30 minutes before using them, in 1x transfer buffer, containing following:

- TRIS (25mM)
- Glycine (192mM)
- Methanol (100%)
- dH_2O

Polyvinylidene difluoride (PVDF) membranes, that were used for blots with more than two visualized proteins, or when stripping of the membranes was necessary, were activated by methanol prior to use. After SDS-PAGE, gels were transferred onto the sponge with thick paper on it, covered with membrane, thin paper and another sponge and locked into the blotting apparatus (all wet with transfer buffer). The side chambers of the blotting apparatus were filled with ice and ice-cold water and the WB was run at 4 °C either for 2 hours using the Mini blot module (Thermo Scientific):

- 200 mA/gel (max)
- 30 V (constant)
- 25 W

or overnight:

- 100 mA/gel (max)
- 20 V (constant)
- 25 W

Membranes were stained with 0.05% ponceau S in 5% acetic acid directly after blotting, and scanned for future reference. Afterwards, the membranes were washed for 10 minutes with 1x tris buffer saline (TBS)/Tween, containing following:

- TRIS (20mM)
- NaCl (150mM)
- Tween 20 (0.05%)
- dH_2O

After washing away the remaining ponceau S, membranes were blocked with 5ml of 5% skim milk (SERVA) for 1 hour at RT. Membranes were washed again with 1xTBS/Tween buffer three times for 10 minutes and incubated with primary antibody, diluted (according to the antibody's manufacturer's instructions, see Table 3.3) in 5% BSA (Sigma) overnight.

The following day, membranes were washed three times with 1xTBS/Tween for 10 minutes and incubated with secondary antibody diluted 1:10000 in 1% skim milk for 1 hour.

The membranes were washed three times for 10 minutes with 1xTBS/Tween afterwards and proteins were visualized by using chemiluminescent substrates WesternBright™ Sirius (Advansta) or Clarity™ western ECL (BIO-RAD). The chemiluminescent signal was detected by Azure c600 (Azure Biosystems).

Antibody	Manufacturer	Catalogue #	Host	Dilution	Note
CA9	Thermo Scientific	PA1-16592	rabbit	1:2500	polyclonal
CA9	Santa Cruz Biotechnology	sc-365900	mouse	1:2500	monoclonal
HIF1α	SIGMA	PLA0081	rabbit	1:2500	affinity purified
HIF2α	Santa Cruz Biotechnology	sc-46691	mouse	1:1000	monoclonal
mCherry					
DsRed	Santa Cruz Biotechnology	sc-390909	mouse	1:1000	monoclonal
QSOX1	Thermo Scientific	PA5-66006	rabbit	1:2500	polyclonal
β-Actin	Santa Cruz Biotechnology	sc-47778 HRP	mouse	1:10000	monoclonal, HRP-conjugated
α-Tubulin	abcam	ab40742	mouse	1:10000	monoclonal, HRP-conjugated
anti-mouse	Invitrogen	31439	goat	1:10000	polyclonal, HRP-conjugated
anti-rabbit	MERCK/SIGMA	AP132P	goat	1:10000	polyclonal, HRP-conjugated

Table 3.3: List of antibodies.

3.10 RNA isolation

Medium was aspirated and cells were washed twice with 1xPBS. Appropriate volume of RNazol® (Molecular Research Center, Inc.) was added (1ml per 10^7 cells) and cells were resuspended several times in a 1000 µl tip to ensure proper homogenization of the sample. 200 μl of sterile RNase-free water per 500 µl of RNazol® was added and samples were votexed for 15 seconds, then incubated for 10 minutes at room temperature and spun for 15 minutes at 12500 xg, room temperature.

Supernatant was aspirated and transferred to new tubes with 2 µl of glycogen (10mg/ml, SERVA) and 3 µl of 4-bromoanisol (BAN, Molecular Research Center, Inc.). Samples were vortexed for 10 seconds and incubated at room temperature for 5 minutes at 12500 xg, room temperature.

Supernatant was aspirated and transferred to new tubes and mixed with 600 µl of ice-cold isopropanol (SERVA). The samples were incubated for 1-24 hours at -20 °C to precipitate the RNA.

The samples were spun for 15 minutes at 14000 xg, 4 °C. Supernatant was aspirated and discarded, the pellet was washed twice with ice-cold 80% ethanol and dried at 55 °C on a heated block for 1-2 minutes until the pellet was completely dry. Then it was dissolved in 10 - 35 µl of sterile RNase-free water and incubated at 55 °C for 10 minutes. Subsequently it was vortexed, spun quickly and incubated for another 10 minutes at room temperature.

The concentration of total RNA was measured at 260 nm, using absorbance reader $\text{Infinite}_{\text{M200}}$ (TECAN).

RNA was stored at -80 °C.

3.11 Reverse transcription

The First Strand cDNA Synthesis Kit (ThermoScientific) was used. 1 µl of random hexamer primers (50µM) was mixed with 750 ng of total RNA and nuclease-free water was added to a final volume of 6 µl. To ensure disruption of secondary structures on RNA strands, samples were incubated at 65 °C for 5 minutes and subsequently cooled down to 4 °C.

4 µl of mastermix, containing 0.525 µl of RevertAid Reverse Transcriptase (200 U/µl), 0.525 µl of RiboLock RNase inhibitor (20 U/µl), 2.1 µl of 5x reaction buffer (250mM Tris-HCl, pH 8.3; 250mM KCl; 20mM $MgCl_2$; 50mM DTT) and 1.05 µl of 10mM dNTP mix, was added and the samples were incubated in T100™ Thermal Cycler (BIO-RAD) or Biometra TAdvanced (Analytik Jena), using the following program:

- 45 °C 60 minutes

- 75 °C 5 minutes
- 10 °C indefinitely

The complementary DNA (cDNA) was stored at -20 °C and diluted with 177,5 µl of nuclease-free water to final concentration of 4ng/µl before use.

3.12 qPCR

5x HOT FIREPol® EvaGreen® qPCR Mix (Solis BioDyne) was used with specific primers (see Table 3.4) and nuclease-free water according to manufacturer's instructions. 5 µl of mastermix were pipetted into 48- or 384-well plates (Illumina or BIO-RAD, respectively), the plates were spun quickly and 2.5 µl of cDNA (4ng/µl) was added. Plates were spun quickly again, sealed with Microseal® PCR plate sealing film optical tape, mixed by inverting up and down and spun again quickly.

Samples were incubated in qPCR Eco Real-Time PCR system (Illumina, 48-well plates) or CFX384 Touch™ Real-Time PCR detection system (BIO-RAD, 384-well plate), using the following program:

- 95 °C 12 minutes (initial denaturation)

  38x
- 95 °C 10 seconds (denaturation)
- 60 °C 20 seconds (annealing)
- 72 °C 20 seconds (extension and measurement in the SYBR/FAM channel)

The results were analyzed using Excel and GenEx software.

Gene	Manufacturer	Primer
CA9	Sigma	F 5'-CCTTTGCCAGAGTTGACGAG-3'
		R 5'-TTCTTCCAAGCGAGACAGCA-3'
HMOX1	Metabion	F 5'-AGGAGGTGCACACCCAGGCA-3'
		R 5'-ACAGGGGCGAAGACTGGGCT-3'
QSOX1	Invitrogen	F 5'-AGTCCCATCATGACACGTGGC-3'
		R 5'-GCCAGGTACTCTTCGTTATTTCTCGC-3'
18S	Metabion	F 5'-GTAACCCGTTGAACCCCATT-3'
		R 5'-CCATCCAATCGGTAGTAGCG-3'
IPO8	Invitrogen	F 5'-GGCTGAGAGGGTCAAAAGAAA-3'
		R 5'-CGAAGTAAACTGGGGGCAAAA-3'
RPLP0	Invitrogen	F 5'-ATCACAGAGGAAACTCTGCATTCTCG-3'
		R 5'-GATAGAATGGGGTACTGATGCAACAGTT-3'

Table 3.4: List of primers for qPCR.

3.13 genomic DNA (gDNA) isolation

Cells were trypsinized, resuspended in medium and spun down for 5 minutes at 300 xg. Supernatant was aspirated and discarded, pellets were resuspended with 1xPBS, spun for 5 minutes at 300 xg and supernatant was discarded (this step was repeated twice).

Pellets containing the cells were resuspended in 1 ml of DNazol® (Molecular Research Center) and left at 4 °C for 1-2 days to allow degradation of contaminating RNA.

500 µl of absolute ethanol were added and the tubes with samples were placed on a rotating platform for 30 minutes and spun afterwards for 10 minutes at 10000 xg.

Supernatant was discarded and the precipitate was washed twice with 70% ethanol. The precipitate was left to dry at 55 °C for several minutes and dissolved in 100-200 µl of 8mM NaOH and left to incubate for 15 minutes at 55 °C with occasional mixing and vortexing.

Concentration of gDNA was measured at 260 nm, using absorbance reader $\text{Infinite}_{\text{M200}}$ (TECAN).

gDNA was stored at 4 °C.

3.14 Polymerase chain reaction (PCR)

DNA was mixed with 5x HOT FIREPol® Blend Master Mix Ready to Load (Solis BioDyne) and appropriate primers (see Table 3.5) to gain 1x Master Mix with the template and primers and subsequently amplified by following PCR reaction:

Gene	Manufacturer	Primer
QSOX1 seq	Generi Biotech	F 5'-TCACAGGTCACCGAGCTGGGACC-3' R 5'-AGACAGCAGACTGCAGCTTCTCC-3'

Table 3.5: List of primers for PCR and sequencing.

- 98 °C 2 minutes
- 95 °C 12 minutes

35x

- 98 °C 2 seconds
- 60 °C 30 seconds
- 72 °C 1 minutes

- 72 °C 5 minutes
- 10 °C indefinitely

3.15 Agarose gel electrophoresis

For DNA agarose gel electrophoresis, 2% agarose gel with Gel Red dye was used - agarose (Sigma) dissolved in 1x tris-acetate-EDTA (1xTAE), containing:

- 40mM Tris free base (2.2mM)
- 1mM Disodium EDTA (55mM)
- 20mM Glacial acetic acid (2.3mM)
- dH_2O

As a molecular weight ladder, following solution was used:

- 2-log DNA ladder (30µg/ml, New England BioLabs)

- 50x TAE
- 10x Fast digest buffer (Thermo Scientific)
- 6x DNA loading dye (New England BioLabs)
- dH_2O

The gel was run as long as needed on constant voltage of 80 V. Bands were visualized using CCD camera.

3.16 Sequencing

3.16.1 DNA isolation from an agarose gel

DNA was isolated from agarose gel using NucleoSpin®Gel and PCR Clean-up kit.

Bands were extracted from agarose gel using UV lamp and a gel cutting tool.

Gel pieces were weighed, appropriate volume of NTI buffer was added (400 µl of NTI buffer per each 100 mg of gel) and the mixture was incubated for 10 minutes at 50 °C while vortexing every 2 minutes.

Samples were loaded onto Clean-up Columns and spun down for 30 seconds at 11000 xg, room temperature (this step was repeated in case of larger volume of the solution). The silica membrane in Clean-up Columns was washed two times by addition of 700 µl of NT3 buffer and spinning down for 30 seconds at 11000 xg, room temperature.

Columns were dried completely by one additional spinning for 1 minute at 11000 xg and the DNA was eluted using NE buffer and incubation for 1 minute at room temperature. Afterwards, the samples were spun down for 1 minute at 11000 xg and collected.

DNA concentration was measured using $\text{Infinite}_{\text{M200}}$ (TECAN) and the samples were stored at 4 °C.

3.16.2 Sequencing

The purified PCR product (5 µl of 80ng/µl sample) was mixed with appropriate primers (5 µl of 5 pmol/µl of primers, see Table 3.5) and sent for sequencing to GATC Biotech company.

3.17 Crystal violet staining

This experiment was carried out using 96-well plates (Thermo Scientific) during 5 days (where day 1 is the day of seeding cells and day 5 is the day of staining them).

Medium was aspirated and discarded and cells were fixed with 100 µl of 4% paraformaldehyde (4%PAF) for 30 minutes at room temperature.

Plates were washed with 1xPBS three times and after the last wash, they were placed on 37 °C heated block for 5 - 10 minutes to dry completely.

50 µl of crystal violet (Sigma) was added and the samples were incubated for 1-2 hours at room temperature or overnight at 4 °C.

Plates were washed again three times with 1xPBS and dried completely, followed by addition of 100 µl of 1% SDS and incubated for 1 hour on a rocking platform until the suspension reached complete homogeneity.

Absorbance was measured at 595 nm, using absorbance reader $\text{Infinite}_{\text{M200}}$ (TECAN) and data were analysed in Excel.

3.18 Proliferation assays

3.18.1 Ju-Li Live Cell Analysis

Cells were seeded one day prior to the experiment in order to allow the cells attach completely.

$6 \cdot 10^4$ cells/60mm petri dish was seeded and let attach to the surface. Doxycycline was added directly before the experiment was started.

Experiments were carried out on JuLi™ Live cell analyser (NanoEnTek), capturing bright-field and fluorescent images of growing cell culture.

Data were analysed using affiliated JuLi™ software and Excel.

3.18.2 xCelligence Real Time Cell Analysis

Cells were seeded one day prior to the experiment in order to allow the cells attach completely.

The instrument was blanked before usage by measurement of plates with medium without cells.

10^3 cells/well in the xCelligence plate was seeded and let attach to the surface. If any compound was added, it was done so by diluting it in medium and adding such medium to the wells directly before the experiment was started.

The whole experiment was carried out on xCelligence Real Time Cell Analysis Instrument (RTCA, ACEA Biosciences, Inc.), kindly lent to us by Laboratory of Cancer Cell Invasion and data were analysed using affiliated software and GraphPad Prism software.

3.18.3 IncuCyte Live Cell Analysis

Cells were seeded one day prior to the experiment in order to allow the cells attach completely.

10^3 cells/well in the 96-well plate (TPP) was seeded and let attach to the surface. If any compound was added, it was done so by diluting it in medium and adding such medium to the wells directly before the experiment was started.

The whole experiment was carried out on IncuCyte® automated live-cell imaging instrument (Sartorius) in cooperation with group of prof. MUDr. Karel Smetana, DrSc. (Charles University).

Obtained data were analysed using GraphPad Prism software.

3.18.4 Statistics

Statistical significance was assessed by means of GraphPad PRISM software using different statistical tests (t-test, one-way ANOVA or two-way ANOVA). The minimal significance refers to p value lower or equal to 0.05. No sign/Ns: $p > 0.05$, *: ≤ 0.05, **: ≤ 0.01, *** ≤ 0.001 and **** < 0.0001.

4. Results

4.1 Basal expression of QSOX1

We have assessed the basal QSOX1 protein expression and secretion out of the cell in various cell lines ranging from non-malignant MCF10A breast cells through breast cancer cell lines such as MCF7, MDA-MB-231, T47D and BT474 to pancreatic cancer cell lines Panc-1 and Patu-8902 and healthy fibroblast cell line BJ (see Figure 4.1).

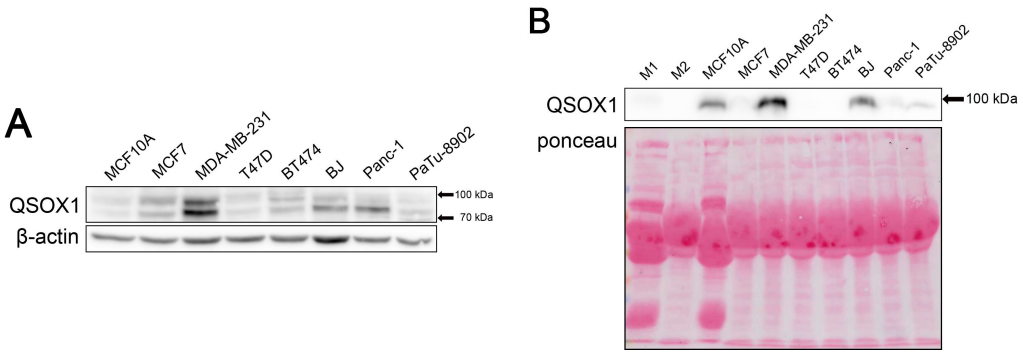

Figure 4.1: **A** 60 µg of total protein from cell lysate was separated by reducing SDS-PAGE followed by Western blotting, β-actin was used as a loading control; **B** 20 µl of centrifuged cell medium was separated by reducing SDS-PAGE followed by Western blotting, ponceau S was used as a loading control. **M1** refers to MCF10A medium without cells, **M2** refers to complete medium without cells.

The QSOX1 expression was the highest in the triple negative MDA-MB-231 breast cancer cells, referred to as highly proliferative and aggressive cell line, while in T47D, BT474 or PaTu-8902, the level of QSOX1 was significantly lower. MDA-MB-231 also showed the highest secretion of QSOX1 into the medium. Interestingly, even though the intrinsic expression of QSOX1 in MCF10A is not significantly higher, the secretion seems to be increased when compared to other cell lines. Similar effect can be seen in the healthy fibroblasts where it was originally found and characterized by Coppock and his group [Coppock et al., 1993].

4.2 Proliferation

4.2.1 QSOX1 overexpression

For better understanding of QSOX1 function we have prepared QSOX1 overexpressing clones with TetON3G inducible system and mCherry fluorescent control using the triple negative breast cancer cell line MDA-MB-231.

The cells were transfected with the pTRE3G-BI-mCherry vector plasmid with cloned *QSOX1v1* or *QSOX1v2* DNA with pTREG promoter, by electroporation performed by my colleagues. After 24 hour incubation with DOX, the surviving cells were sorted *via* single cell sorting with flow cytometer and obtained clones tested for *QSOX1v1/QSOX1v2* and mCherry mRNA expression (see Figure 4.2) as well as by visualization of mCherry fluorescent protein representing the overexpression of *QSOX1* (see Figure 4.4).

Clones with the highest mRNA induction (Cl12, Cl14, Cl41, Cl47) were selected and tested for the intracellular QSOX1 protein levels in the cell lysate (see Figure 4.3A) and the secreted QSOX1 in the medium (see Figure 4.3B). The QSOX1 protein induction in all selected clones was very high, rendering the basal expression of clones not incubated with DOX, as well as controls, undetectable. The phenotype of the cells and mCherry fluorescence is depicted in Figure 4.4.

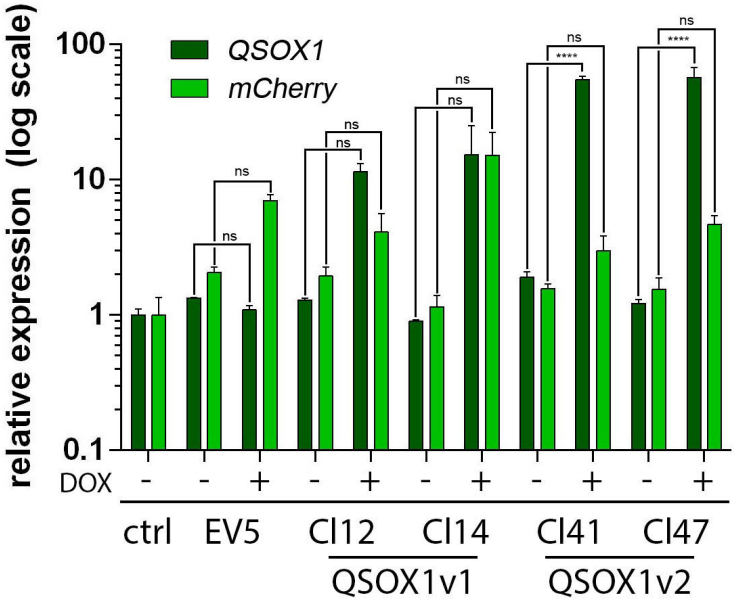

Figure 4.2: **Relative mRNA expression of *QSOX1*-overexpressing clones after 24-hour incubation with 250ng/µl DOX.** *QSOX1* expression was normalized *via* GenEx software to *IPO8* and *RPLP0*. Statistical significance was assessed by two-way ANOVA test by means of GraphPad PRISM software. Ns: $p > 0.05$, *: ≤ 0.05, **: ≤ 0.01, *** ≤ 0.001 and **** < 0.0001. Data are shown as geomean ± SEM (n=3). Only selected clones are shown. Cells were incubated with 250 ng/ul of DOX for 24 hours.

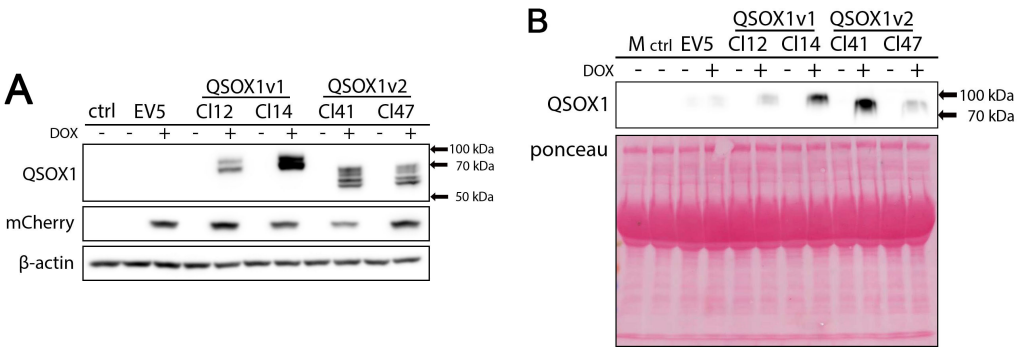

Figure 4.3: **QSOX1 protein level in *QSOX1*-overexpressing clones. A** 23 µg of total protein from cell lysate was separated by reducing SDS-PAGE followed by Western blotting, β-actin was used as a loading control; **B** 20 µl of centrifuged cell medium was separated by reducing SDS-PAGE followed by Western blotting, ponceau S was used as a loading control. Cells treated with DOX were incubated with 250 ng/ul of DOX for 24 hours; **Ctrl** refers to not treated MDA-MB-231 cells, **M** refers to free complete medium without cells.

To determine the extent of the QSOX1 induction by doxycycline with time, we performed a time-dependent experiment with all four selected clones.

The cells were seeded in equal number on seven separate petri dishes dedicated to specific time-points. DOX was added retrospectively (120 hours before harvest in dish labeled 120H and 2 hours before harvest in dish 2H) into appropriate dishes which were afterwards all screened and harvested at the same time after 120 hours of incubation, ensuring similar confluence of the cells.

The induction begins to manifest already after 6 hours of incubation with DOX (see Figure 4.5). However, full induction is not visible until the 24-hour time-point and reaches the peak at 96 hours. Since the half-life of doxycycline is 24 hours, it is only logical that its effect will decline in time - after 96 hours in the case of Cl12 (see Figure 4.5D) and Cl47 (Figure S3) and after 120 hours with Cl14 (Figure S1) and Cl41 (Figure S2).

Since all of the experiments had very similar outcomes, we show here only the data for Cl12 - the rest of the data is accessible in supplementary material (Figures S1-S3).

To assess the effect of *QSOX1* induction and the effect of doxycycline alone on the cellular proliferation, we performed a crystal violet viability assay (see Figure 4.6). Cells were cultivated with 250 ng/µl DOX that was added at the beginning of the experiment. Control cells were incubated completely without DOX.

Neither DOX alone nor the *QSOX1* induction resulted in a significant change in the number of viable cells, showing that high level of QSOX1 does not influence cellular viability and proliferation.

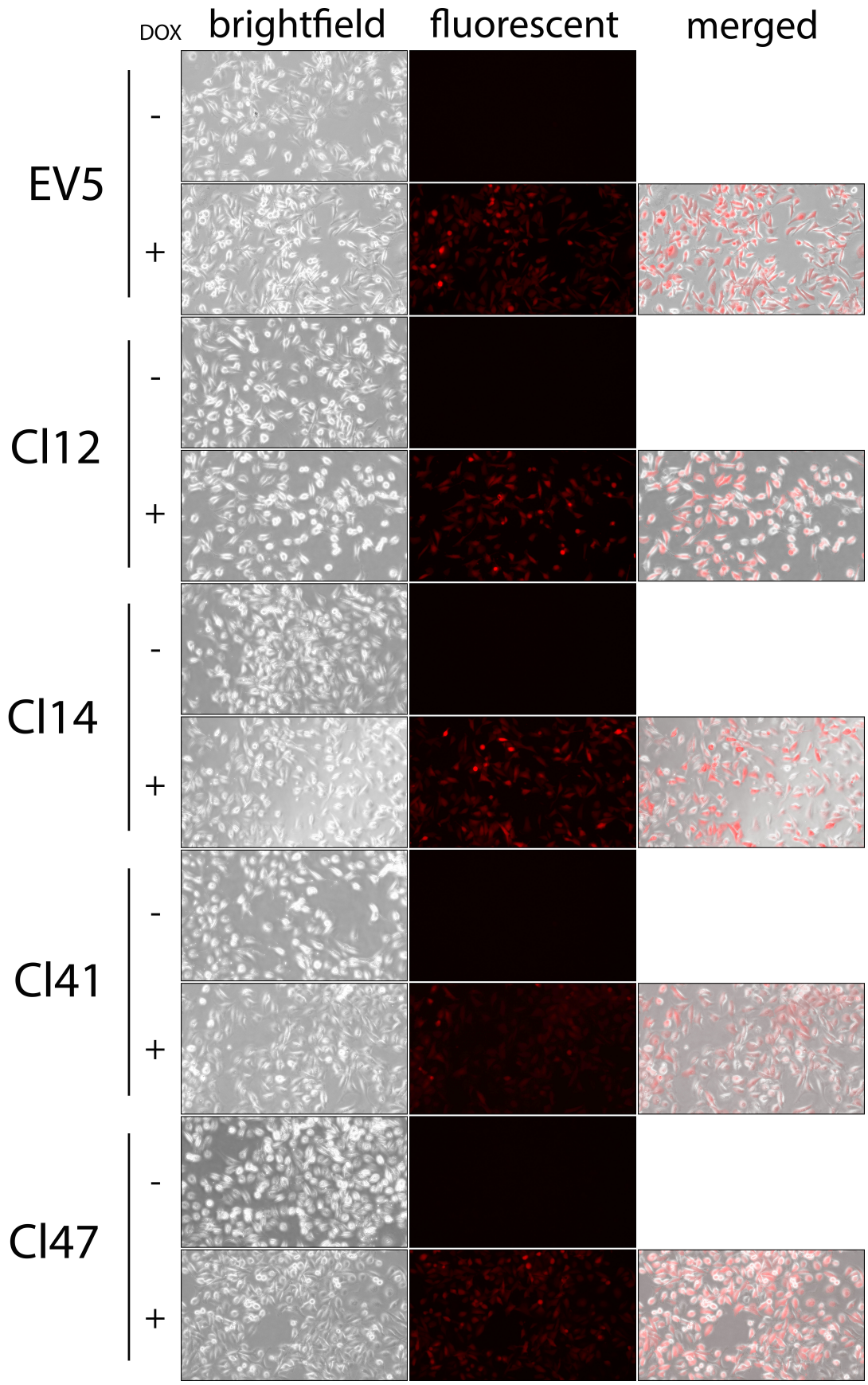

Figure 4.4: **Fluorescent control of mCherry protein induction as a substitute for QSOX1 protein induction.** Pictures were taken with fluorescent microscope Leica400 after 24 hours of incubation with or without 250 ng/ml of DOX and modified in Photoshop software.

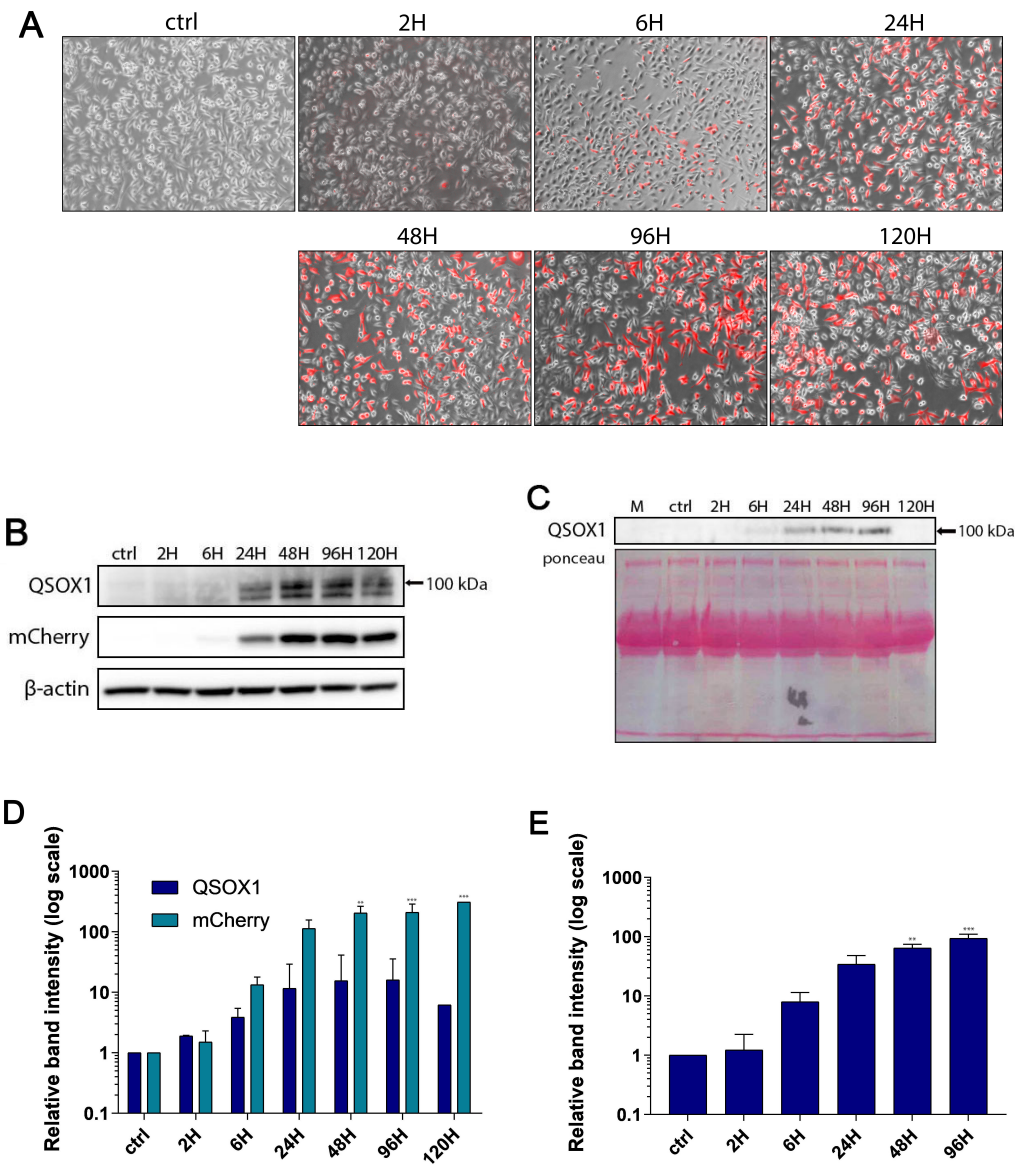

Figure 4.5: **QSOX1 induction in QSOX1-overexpressing clone Cl12. A** Merged images of fluorescent and brightfield pictures of mCherry expression in different time-points during DOX incubation as a substitute for QSOX1 protein induction. Pictures were taken with fluorescent microscope Leica400 after 120 hours of incubation with (2H-120H) or without (ctrl) 250 ng/ml of DOX, and modified in Photoshop software; **B** QSOX1 protein induction after DOX addition in cell lysate. 50 µg of total protein from cell lysate was separated by reducing SDS-PAGE followed by Western blotting, β-actin was used as a loading control; **C** QSOX1 protein induction after DOX addition in conditioned medium. 20 µl of centrifuged cell medium was separated by reducing SDS-PAGE followed by Western blotting, ponceau S was used as a loading control; **D** densitometry of QSOX1 and mCherry protein induction after DOX addition in cell lysate; **E** densitometry of QSOX1 and mCherry protein induction after DOX addition in conditioned medium.
Cells were seeded with the same starting confluence ($3.33 \cdot 10^3$ cells/cm^2) on petri dishes and 250 ng/ml of DOX was added in appropriate time-points to appropriate dishes. *ctrl* refers to not treated MDA-MB-231 cells, *M* refers to free complete medium without cells. Statistical significance in d) and e) was assessed by two-way ANOVA test by means of GraphPad PRISM software. Ns: $p > 0.05$, *: ≤ 0.05, **: ≤ 0.01, *** ≤ 0.001 and **** < 0.0001. Data are shown as geomean $\pm$ SEM (n=3 for all samples except for 120 hours where n=1).

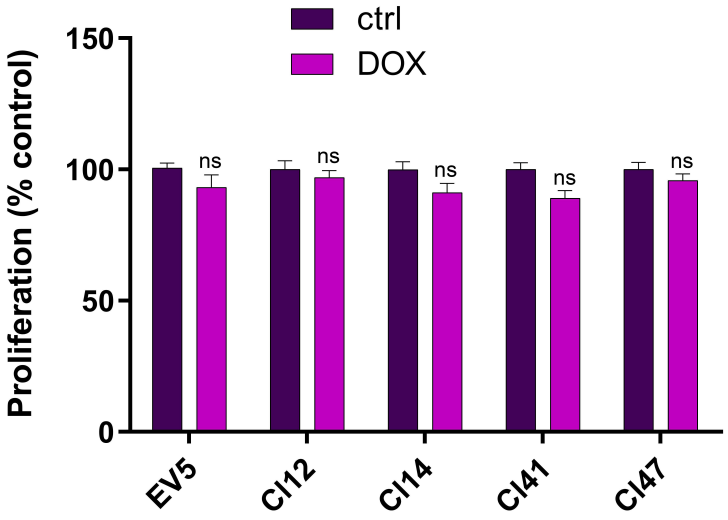

Figure 4.6: **The effect of *QSOX1* induction by DOX on cellular viabilitty by the crystal violet assay.** Cells were seeded in 96-well plates in low confluence ($3 \cdot 10^3$ cells/cm^2), incubated for 120 hours and stained with crystal violet. **DOX** refers to cells cultivated with DOX for the 120 hours of the experiment while **ctrl** refers to cells cultivated without DOX completely. Statistical significance was assessed by two-way ANOVA test by means of GraphPad PRISM software. Ns: $p > 0.05$, *: ≤ 0.05, **: ≤ 0.01, *** ≤ 0.001 and **** < 0.0001. Data are shown as mean $\pm$ SEM (n=2).

4.2.2 QSOX1 knockdown and knockout

To define the effect of loss of *QSOX1*, we have engineered *QSOX1* knockdown *($QSOX1^{+/-}$)* and *QSOX1* knockout *($QSOX1^{-/-}$)* clones based on the MDA-MB-231 cell line.

We have transfected the MDA-MB-231 cells with LentiCRISPR (pXPR_001) vector plasmid with cloned sgRNA targeting exon 6 of *QSOX1* using lipofectamine transfection and sorted the surviving cells via single cell sorting with flow cytometer. We have obtained numerous clones that were afterwards tested for *QSOX1* expression on mRNA level (see Figure 4.7A) and clones with the lowest expression (Cl5, Cl16, Cl17, Cl29 and Cl33) were selected for further testing on protein level (see Figure 4.7C and 4.7D). All of our selected clones showed significantly lower QSOX1 protein level on western blots or diminished secretion, however none of them was a complete knockout (although some of them showed diminished secretion into medium - Cl17, Cl29 and Cl33). With this in mind, we further refer to these clones as knockdown clones.

In order to obtain a complete *QSOX1* knockout cell line, we have repeated the transfection on three of the *QSOX1* knockdown clones (Cl16, Cl17, Cl33). The obtained clones (named after the original knockdown clone and appropriate plate and well number, see Table 3.1) were also tested with qPCR (see Figure 4.8A) and potential knockouts were further tested on protein level (see Figure 4.8).

The second transfection yielded six possible knockout clones - 2D8, 1B4, 1D1, 1E11, 1E4 and 1G11 that all showed diminished QSOX1 protein level on western blots from cell lysates as well as its secreted form from the conditioned medium.

DNA of all subsequently used clones, as well as a control MDA-MB-231 cell line, was isolated, run on agarose gels (see Figures 4.7 and 4.8) and sequenced for *QSOX1* exon 6 by a contractor company GATC Biotech. Importantly, not only the knockdown cell lines (Figure 4.7B) but also some of the knockout (Figure 4.8B) ones were found to have two size-different alleles that were sequenced separately.

Very interestingly, the sequencing results indicate that a similar sequence was inserted into the cleavage site (see Figure 4.9).

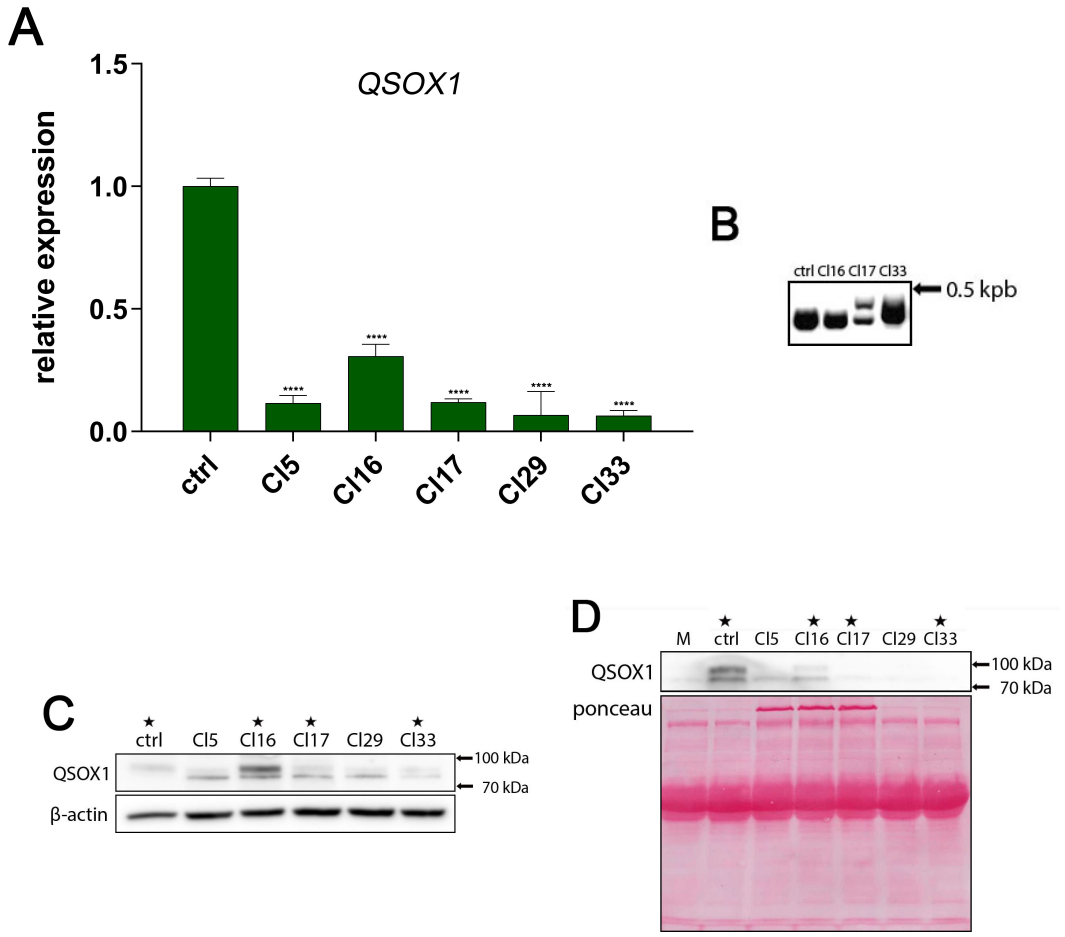

Figure 4.7: **First CRISPR/Cas9-edited cells testing for loss of QSOX1. A** Relative *QSOX1* mRNA expression of CRISPR/Cas9 edited cells. *QSOX1* expression was normalized *via* GenEx software to *IPO8*. Statistical significance was assessed by t-test by means of GraphPad PRISM software. Ns: $p > 0.05$, *: ≤ 0.05, **: ≤ 0.01, *** ≤ 0.001 and **** < 0.0001. Data are shown as geomean ± SEM (n=4). Only selected clones are shown; **B** *QSOX1* exon 6 PCR product from *QSOX1*$^{+/-}$ clones analysis on an agarose gel; **C** QSOX1 protein level in the lysates. 50 µl of total protein from cell lysate was separated by reducing SDS-PAGE followed by Western blotting, β-actin was used as a loading control; **D** QSOX1 protein level in the conditioned medium. 20 µl of centrifuged cell medium was separated by reducing SDS-PAGE followed by Western blotting, ponceau S was used as a loading control. DNA of clones marked with a star was sequenced.

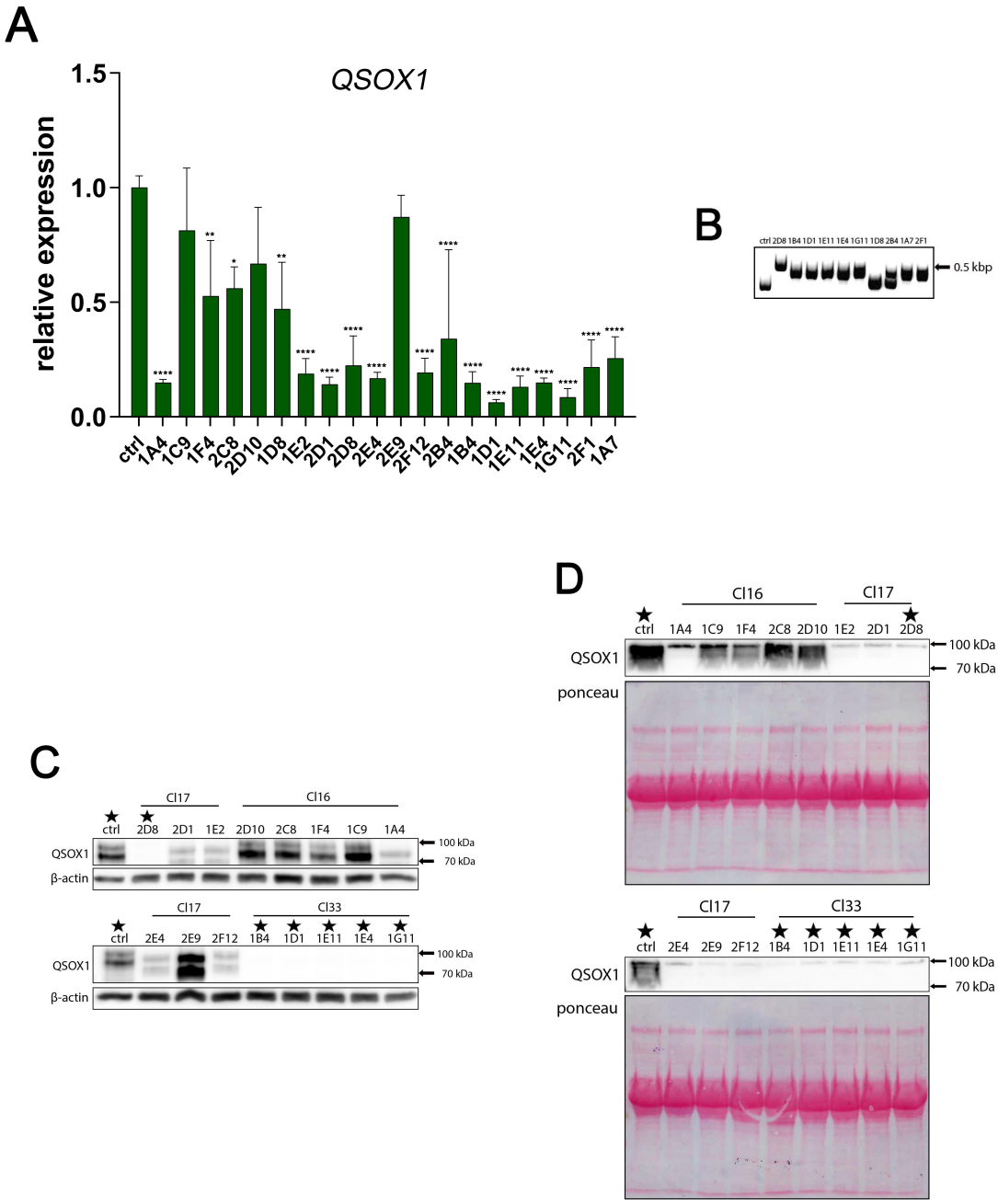

Figure 4.8: **Second CRISPR/Cas9-edited cells testing for loss of QSOX1. A** Relative *QSOX1* mRNA expression of CRISPR/Cas9 edited cells. *QSOX1* expression was normalized *via* GenEx software to *IPO8*. Statistical significance was assessed by t-test by means of GraphPad PRISM software. Ns: $p > 0.05$, *: ≤ 0.05, **: ≤ 0.01, *** ≤ 0.001 and **** < 0.0001. Data are shown as geomean ± SEM (n=3). Only selected clones are shown; **B** *QSOX1* exon 6 PCR product from *QSOX1*$^{-/-}$ clones analysis on an agarose gel; **C** QSOX1 protein level in the lysates. 45 µl of total protein from cell lysate was separated by reducing SDS-PAGE followed by Western blotting, β-actin was used as a loading control; **D** QSOX1 protein level in the conditioned medium. 20 µl of centrifuged cell medium was separated by reducing SDS-PAGE followed by Western blotting, ponceau S was used as a loading control. DNA of clones marked with a star was sequenced.

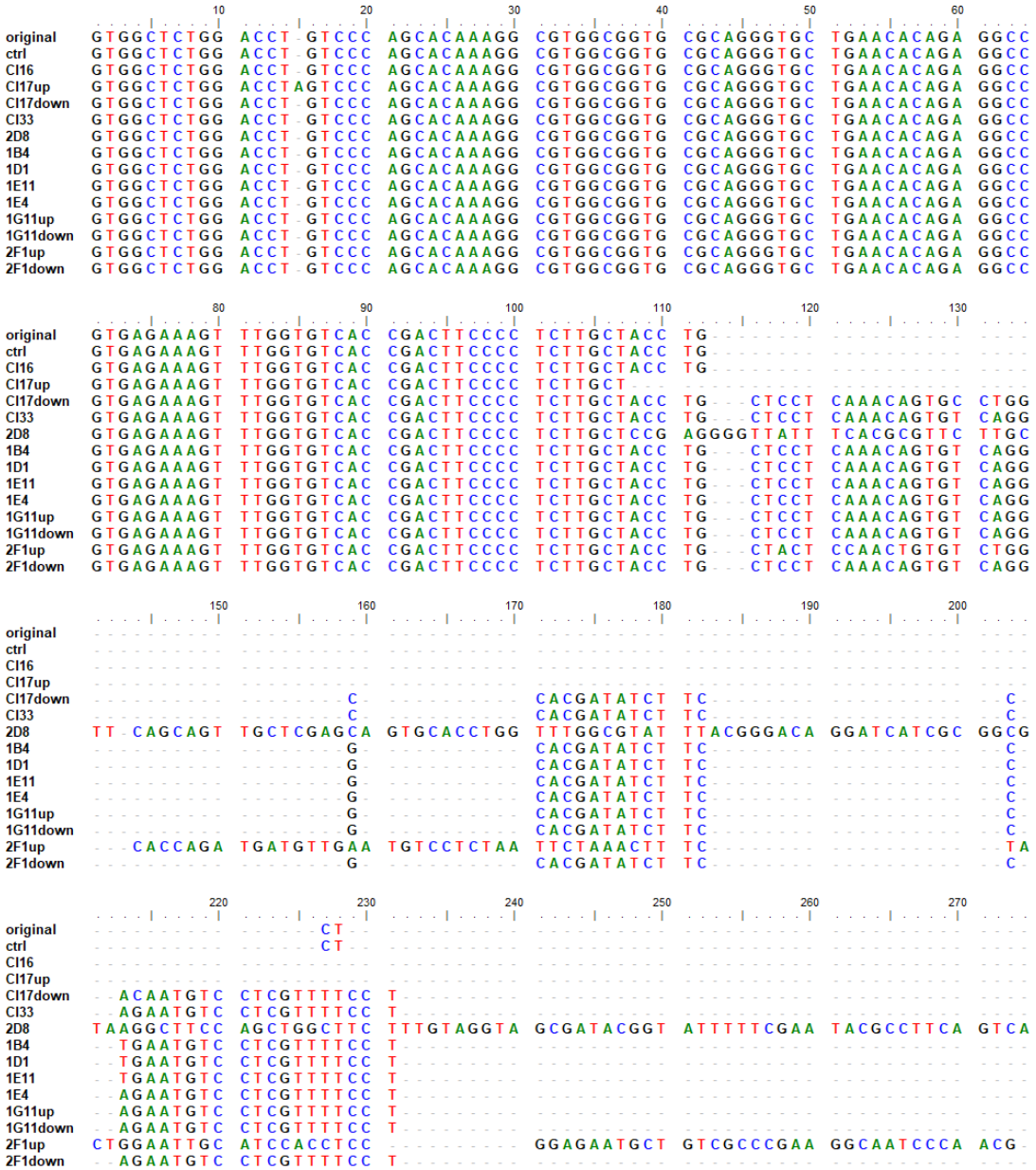

Figure 4.9: ***QSOX1* knockout sequence alignment.** DNA of selected knockdown and knockout cell lines was sequenced for *QSOX1* exon 6 which served as a cleavage site for CRISPR/Cas9 editing. **up** and **down** refer to the position of DNA band isolated from agarose gel before sequencing; **original** refers to an original sequence available at ensembl.org; **ctrl** refers to sequenced MDA-MB-231 sequence from our cells.

4.2.3 Proliferation

As the main focus of this thesis is the effect of QSOX1 sulfhydryl oxidase on cancer cells, we have assessed the effect of QSOX1 on proliferation of cancer cells either overexpressing or knocking out *QSOX1*.

For the *QSOX1*-overexpressing clones, we have used an xCelligence monitoring system of cell proliferation based on measuring the impedance. When electric current passes through the plate well, the impedance between the electrodes is affected by the presence of cells. When the cells grow and multiply, the total impedance of the circuit increases appropriately and is used for the subsequent cell index calculation (see Figure 4.10A and Figures S4-S6; cell index is defined as $(Z_n\text{-}Z_b)/15$, where Z_n and Z_b are the impedance values in the presence and absence of cells, respectively). No significant change in proliferation of the *QSOX1*-overexpressing clones (Cl12, Cl14, Cl41 or Cl47) was recorded and there is no difference in the slope (representing the rate of cellular proliferation, calculated by means of GraphPad PRISM) and doubling time (calculated either by means of xCelligence software or online on http://www.doubling-time.com/compute.php webpage) of cells treated and not treated with DOX (see Figure 4.10A).

The *QSOX1*-overexpressing cells were also analyzed *via* the comparison of the visual images obtained from JuLi live cell movie analyzer (see Figure 4.11A and Figures S7-S9). The built-in software of this appliance is able to recognize the cell periphery from the background and therefore calculate the confluence of the scanned location, measuring the space taken up by the cells. This approach had similar results to the previous one and did not show any significant difference in the proliferation of neither of the overexpressing clones when comparing the slope and doubling time of cells treated and not treated with DOX (see Figure 4.11A).

As a high-throughput procedure measuring cellular proliferation, we have used the IncuCyte instrument capable of scanning 60 wells at the same time and providing us with data illustrating the cellular confluence of two locations of the same well in time, measuring the cell confluence similartly to JuLi. After careful manual analysis of the data, the results seem to be the most trustworthy and reproducible method since all cells are seeded and grown under identical conditions at the same time, limiting the variables commonly encountered during analysis of many experiments performed separately.

While some of the overexpressing clones showed a certain significance in proliferation change when compared to the control MDA-MB-231 cells, similar trend could be seen in the empty vector clones (EV) treated and not treated with DOX (see Figures 4.12-4.13). This result leads to a conclusion that the observed change in proliferation rate is rather due to presence of doxycycline alone than due to overexpression of *QSOX1*. On the other hand, depletion of QSOX1 in the MDA-MB-231 cells leads to a significant decrease in cellular proliferation (see Figure 4.14). The role of QSOX1 in this phenomenon was confirmed by obtaining the same result when treating the MDA-MB-231 with ebselen, a documented inhibitor of QSOX1 activity [Hanavan et al., 2015].

Except for the change in cellular growth and proliferation, we have noticed a quite interesting tendency of the CRISPR clones to change their morphology when compared to control MDA-MB-231 cells. This can be visible mainly in the early phase of cellular growth, approximately at 5-25% of confluence (see Figure 4.15). The cells are usually more round with less visible or completely diminished lamellipodia suggesting a possible involvement of QSOX1 in migration and invasion.

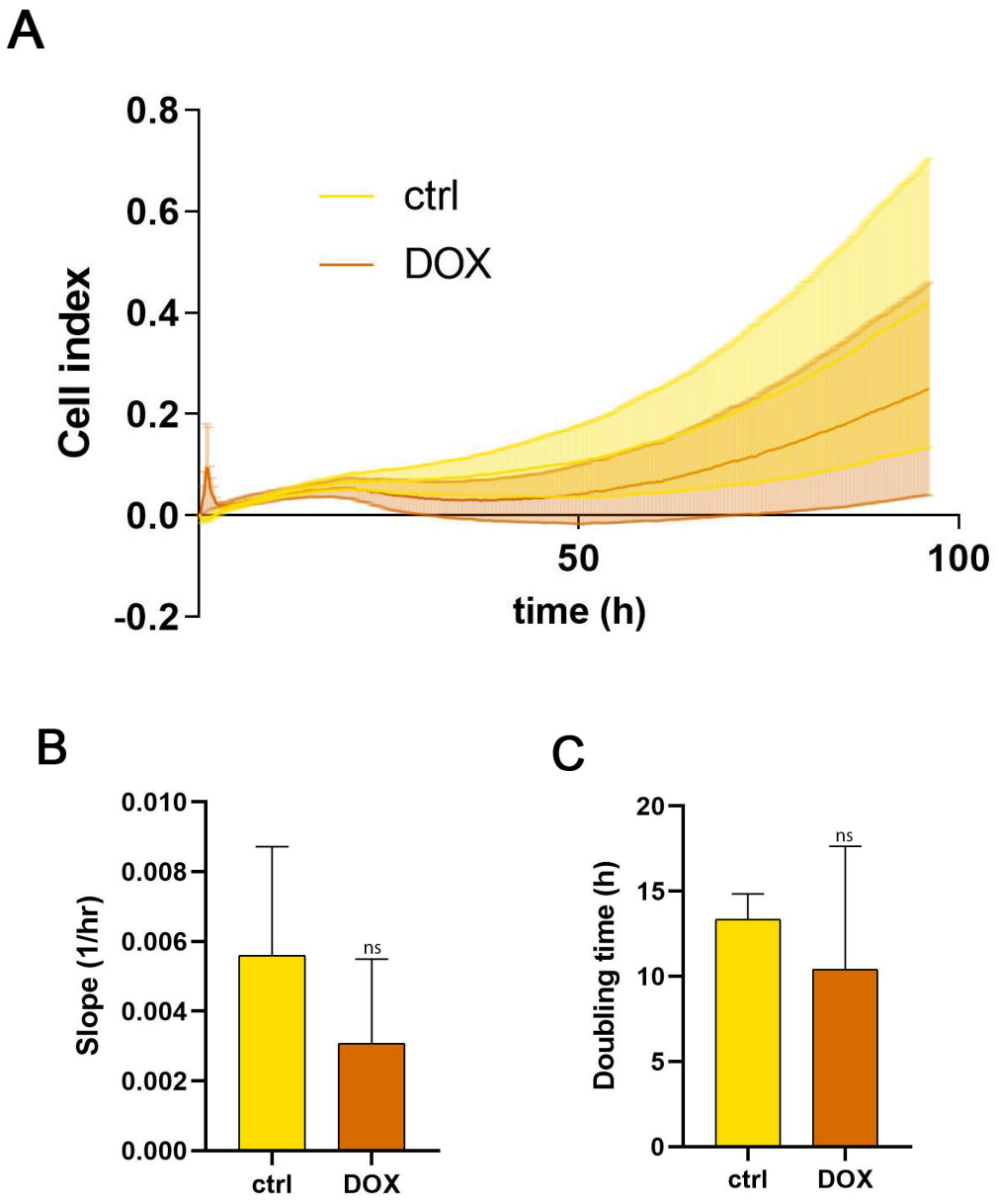

Figure 4.10: **Effect of QSOX1v1 induction on cellular proliferation (Cl12) - xCelligence.** **A** Growth curves comparison of Cl12 obtained from xCelligence; **B** slopes of shown curves representing their steepness, calculated by xCelligence software; **C** graph representing the time needed for the cell population to double, calculated by xCelligence software. Cells were incubated with or without 250 ng/ml of DOX for 120 hours. Statistical significance were assessed by t-test by means of GraphPad PRISM software. Ns: $p > 0.05$, *: ≤ 0.05, **: ≤ 0.01, *** ≤ 0.001 and **** < 0.0001. Data are shown as mean $\pm$ SEM (n=4).

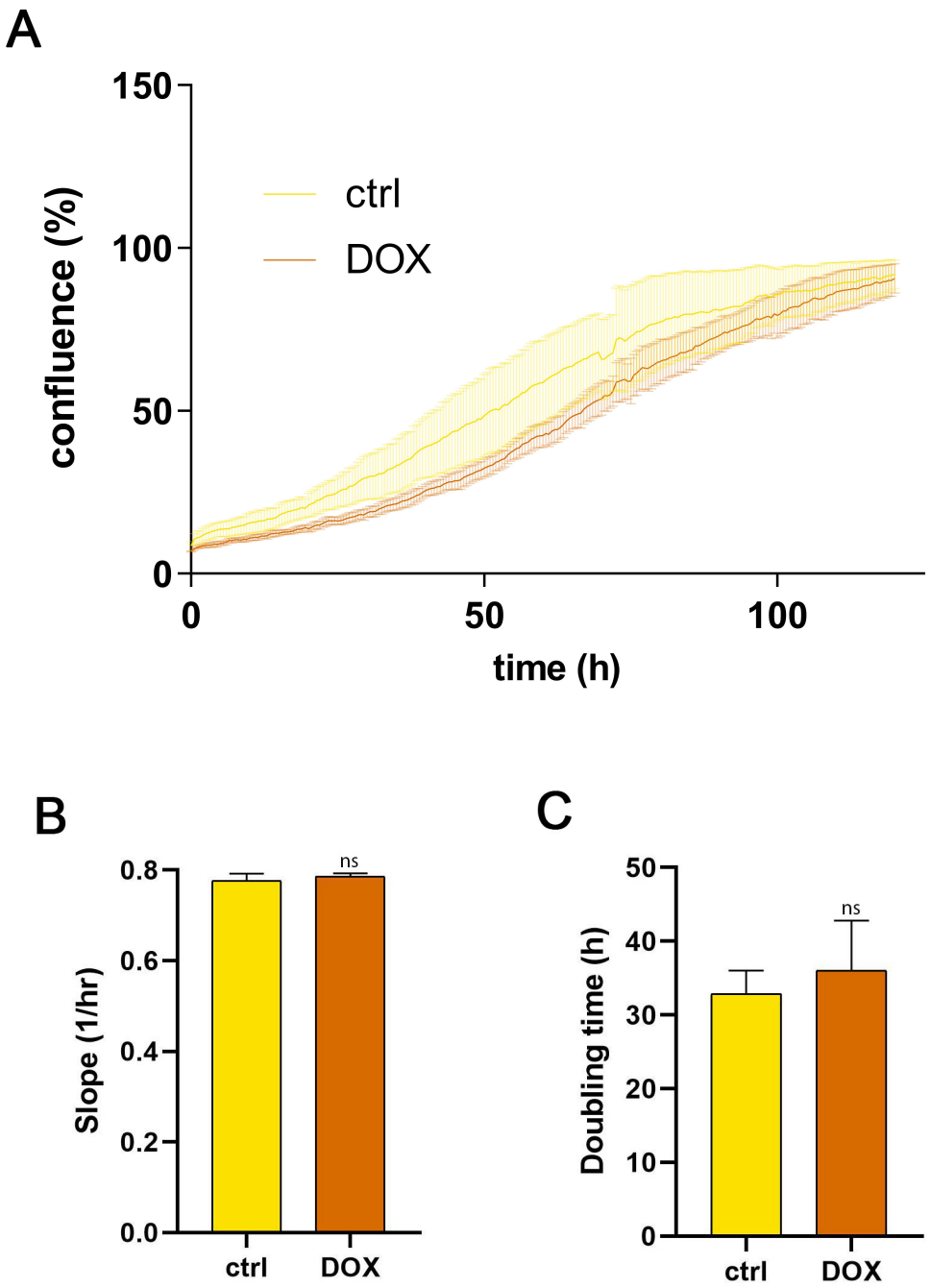

Figure 4.11: **Effect of QSOX1v1 induction on cellular proliferation (Cl12) - JuLi.** **(a)** Growth curves comparison of Cl14 obtained from JuLi; **(b)** slopes of shown curves representing their steepness, calculated in GraphPad PRISM; **(c)** graph representing the time needed for the cell population to double, calculated online (http://www.doubling-time.com/compute.php). Cells were incubated with or without 250 ng/ml of DOX for 120 hours. Statistical significance was assessed by t-test by means of GraphPad PRISM software. Ns: $p > 0.05$, *: ≤ 0.05, **: ≤ 0.01, *** ≤ 0.001 and **** < 0.0001. Data are shown as mean $\pm$ SEM (n=4).

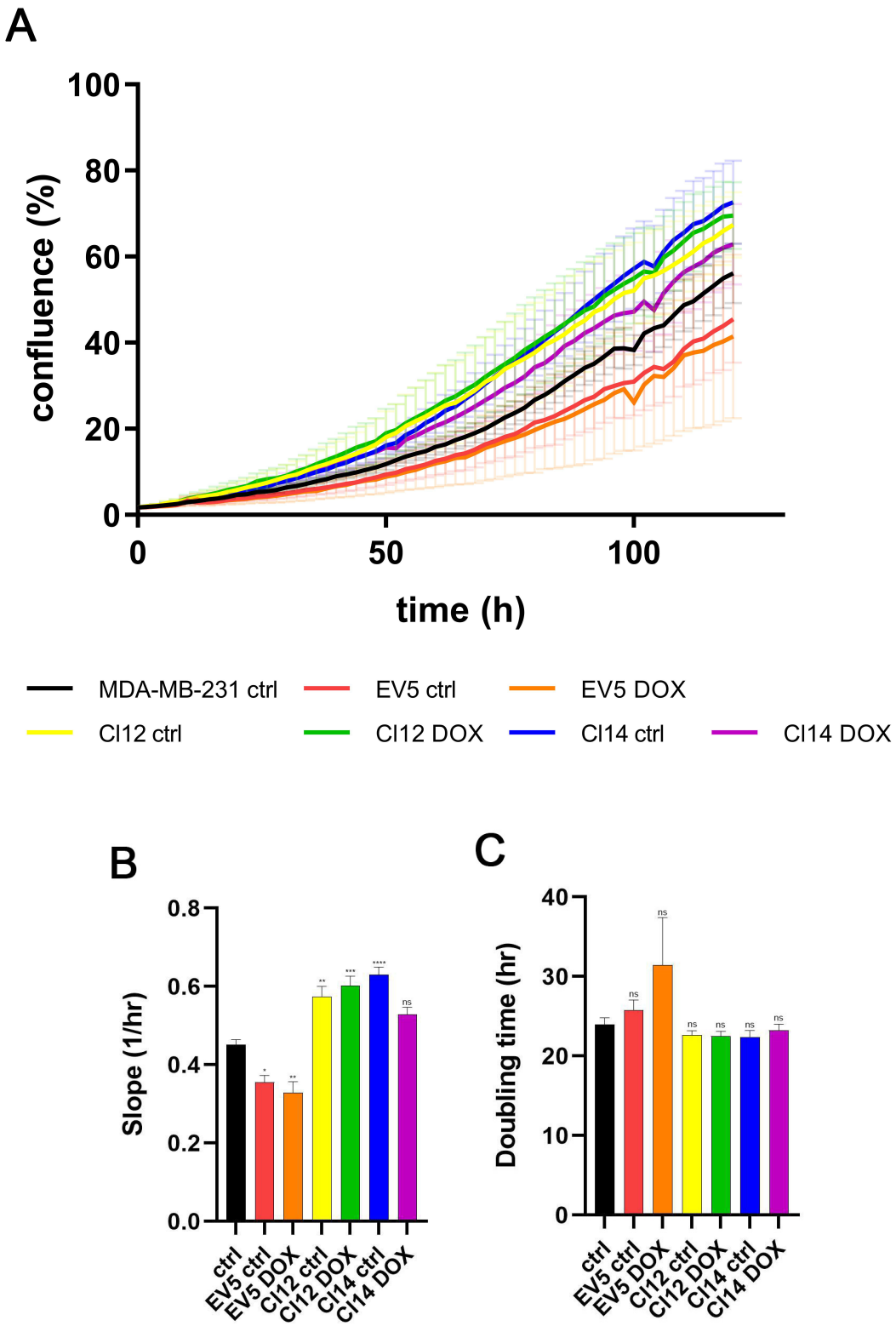

Figure 4.12: **Effect of QSOX1v1 induction on cellular proliferation - IncuCyte.** **A** Growth curve comparison of control cells (not treated MDA-MB-231) with *QSOX1v1*-overexpressing cells; **B** slopes of shown curves representing their steepness, claculated in GraphPad PRISM; **C** graph representing the time needed for the cell population to double, calculated online (http://www.doubling-time.com/compute.php). Statistical significance was assessed by one-way ANOVA test by means of GraphPad PRISM software. Ns: $p > 0.05$, *: ≤ 0.05, **: ≤ 0.01, *** ≤ 0.001 and **** < 0.0001. Data are shown as mean $\pm$ SEM (n=4).

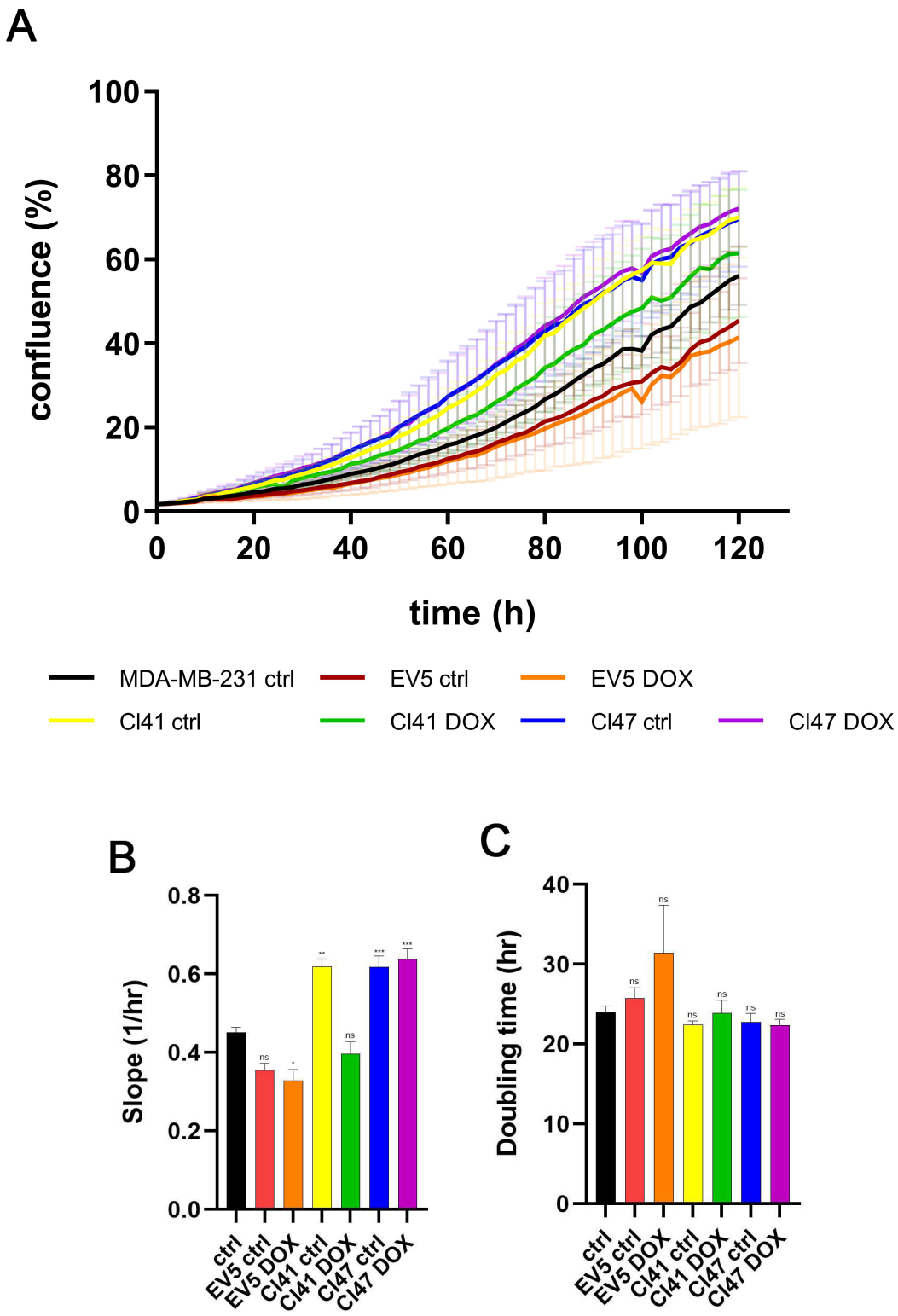

Figure 4.13: **Effect of QSOX1v2 induction on cellular proliferation - IncuCyte** **A** Growth curve comparison of control cells (not treated MDA-MB-231) with QSOX1v2-overexpressing cells); **B** slopes of shown curves representing their steepness, claculated in GraphPad PRISM; **C** graph representing the time needed for the cell population to double, calculated online (http://www.doubling-time.com/compute.php). Statistical significance was assessed by one-way ANOVA test by means of GraphPad PRISM software. Ns: $p > 0.05$, *: ≤ 0.05, **: ≤ 0.01, *** ≤ 0.001 and **** < 0.0001. Data are shown as mean $\pm$ SEM (n=4).

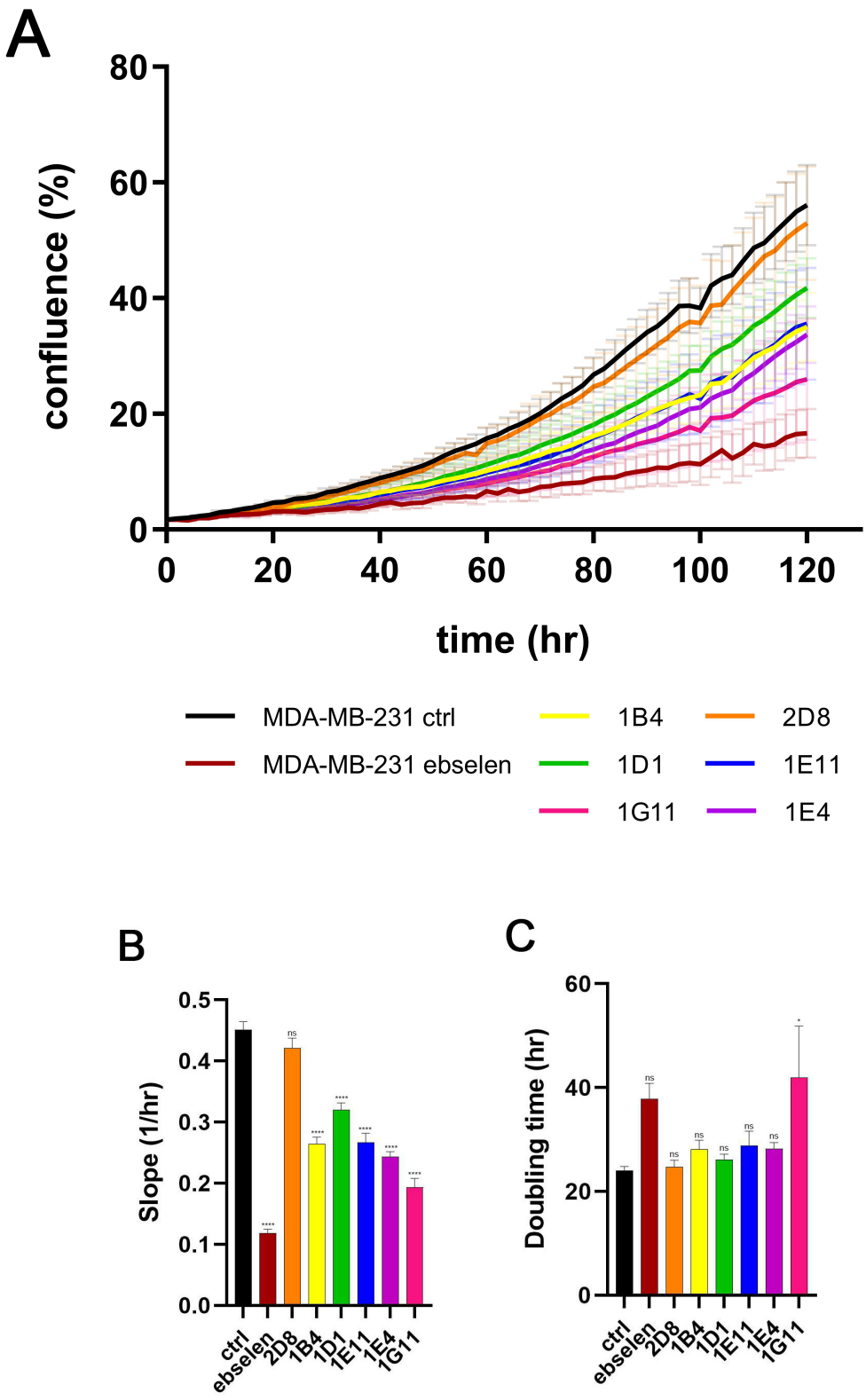

Figure 4.14: **Effect of putative *QSOX1*$^{-/-}$ clones on cellular proliferation - IncuCyte. A** Growth curve comparison of control cells (not treated MDA-MB-231) with *QSOX1* knockout cells *(QSOX1*$^{-/-}$*)*; **B** slopes of shown curves representing their steepness, claculated in GraphPad PRISM; **C** graph representing the time needed for the cell population to double, calculated online (http://www.doubling-time.com/compute.php). Statistical significance was assessed by one-way ANOVA test by means of GraphPad PRISM software. Ns: $p > 0.05$, *: ≤ 0.05, **: ≤ 0.01, *** ≤ 0.001 and **** < 0.0001. Data are shown as mean $\pm$ SEM (n=4).

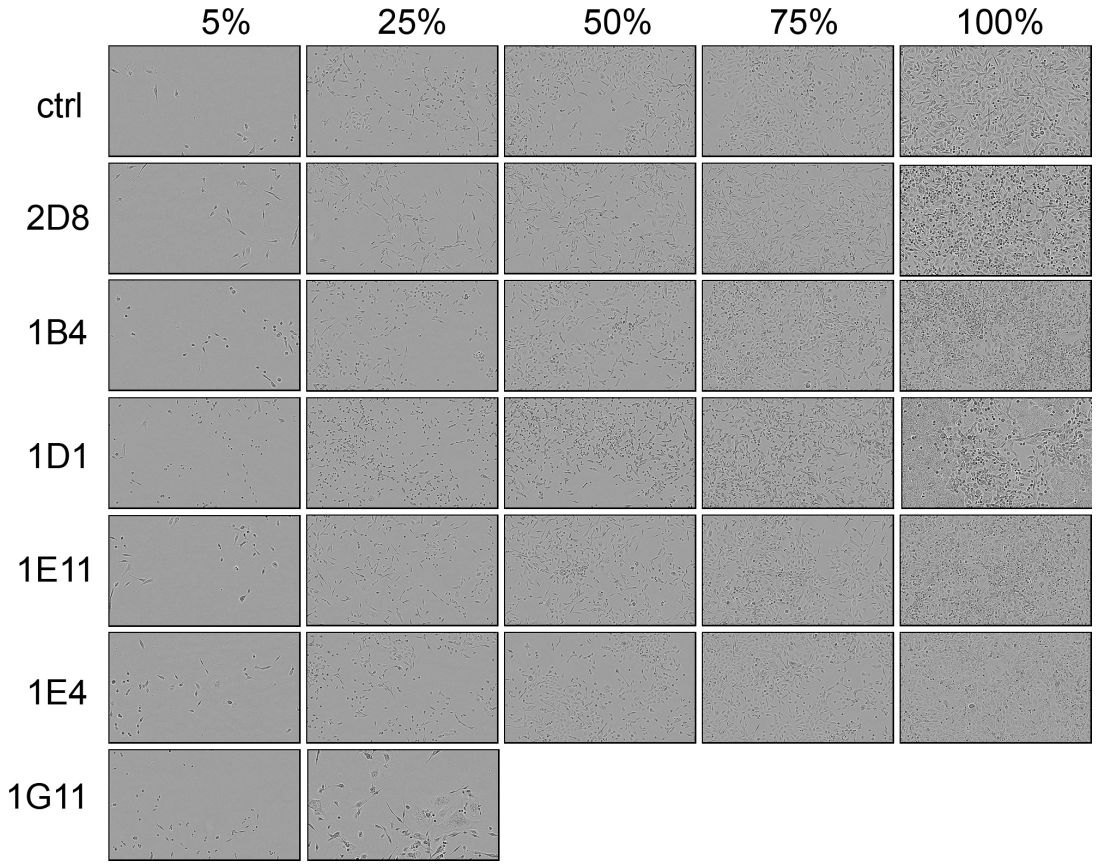

Figure 4.15: **Phenotype of *QSOX1*$^{-/-}$ clones in different confluence.** Images were taken during the incucyte experiment during 120 hour incubation. We were unable to obtain images of clone 1G11 in 50% and higher confluence.

4.3 Hypoxia

As already mentioned in the introduction, some literature states that QSOX1 is regulated by partial oxygen pressure due to the hypoxia-response elements in its DNA sequence [Shi et al., 2013].

In the following section, we test whether protein level and also secretion of QSOX1 to extracellular space is regulated by hypoxia using several hypoxia-mimicking strategies such as deferoxamine (DFO, an iron chelator), $CoCl_2$ (capable of exchanging the iron in iron-dependent enzymes for cobalt thus mimicking iron deprivation) [Guo et al., 2006] and a hypoxic chamber.

4.3.1 Hypoxia and hypoxia-mimicking conditions

To assess the effect of hypoxia or hypoxia-mimicking conditions on the specific cell lines we used a panel of cell lines consisting of breast (MCF10A, MCF7, MDA-MB-231) and pancreatic origin (Panc-1). Every cell line was incubated for 48 hours with either 100µM DFO, 100µM $CoCl_2$ or in the hypoxic chamber with 0.1 % of O_2. Since it was also reported that QSOX1 can be induced upon trypsinization or scraping of the cells manually [Coppock et al., 1993], the cells were harvested after instant deep freezing with dry ice.

To be certain that our treatments induced hypoxia or hypoxia mimicking conditions, we assessed the mRNA expression of the known hypoxic markers – carbonic anhydrase 9 (*CA9*) and heme oxygenase 1 (*HMOX1*) by qPCR (see Figure 4.16). While with the *CA9* we can see a considerable increase in expression under decreased oxygen concentration and also with DFO and $CoCl_2$ (see Figure 4.16A), the change in the relative expression of *HMOX1* upon hypoxia is significant only with the MCF10A cell line and not significant in the remaining cell lines, although a similar increasing trend could be seen for DFO and 0.1% O_2 (see Figure 4.16B).

At the same time, we also determined the relative mRNA expression of *QSOX1* under the already described conditions (see Figure 4.16C), leading to a conclusion that all cell lines respond to DFO and 0.1% O_2 in a noticeable way with increased relative *QSOX1* mRNA expression that correlates to the one of *CA9*. However, in the case of MDA-MB-231, the response was not statistically significant.

To determine the situation at the protein level we isolated protein samples from cells incubated under the same conditions and carried out SDS-PAGE followed by Western blotting. To determine whether our treatment induced hypoxia in the cells, we have assessed the protein level of CA9, HMOX1, HIF1α as well as HIF2α all of which are induced by hypoxic conditions (see Figure 4.17 - 4.19). We have performed a densitometry measurement of the bands, normalized to appropriate β-actin bands to get a normalized response (see Figure 4.18-4.20).

As expected, the carbonic anhydrase on a protein level responds on a very similar manner as it does at the mRNA level (see Figure 4.18C)– a considerable, at least 5-fold, 10-fold and 30-fold increase in MCF10As treated by $CoCl_2$, DFO and decreased oxygen, respectively. The same trend is visible with the remaining cell lines. Panc-1 cells show a response only in hypoxia but not with DFO and $CoCl_2$.

Very interestingly, HMOX1 is almost non-detectable on the Western blots for MCF10A, MCF7 as well as MDA-MB-231 whilst there is a significant difference in the Panc-1 cell line (see Figure 4.17). It seems that the basal expression of HMOX1 in Panc-1 is significantly increased when compared to other cell lines in our study which is in agreement with the literature [Han et al., 2018, Berberat et al., 2005].

When detecting HIF1α we had some difficulties since the protein is degraded rapidly in normoxia. However, after several attempts, we succeeded in its isolation and visualization even though we obtained two visible bands instead of one (see Figure 4.17). Nonetheless, only the

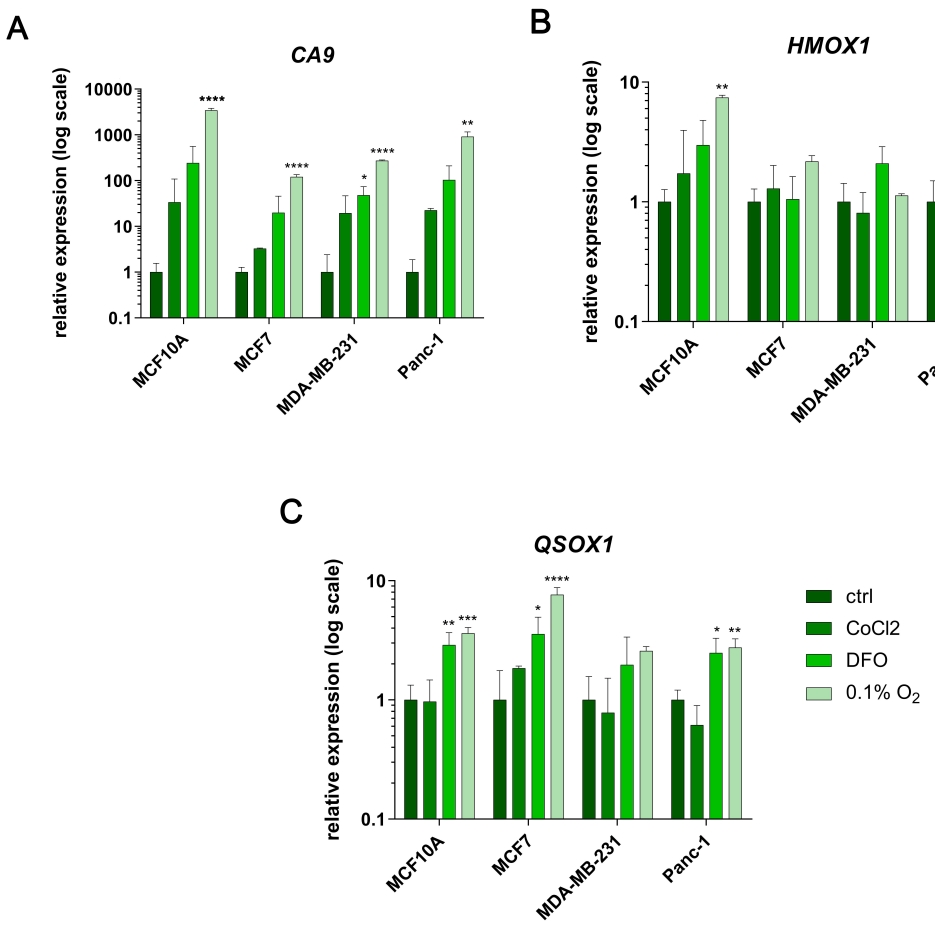

Figure 4.16: **Relative mRNA expression of *CA9*, *HMOX1* and *QSOX1* in MCF10A, MCF7, MDA-MB-231 and Panc-1 cells. A**; *CA9*; **B** *HMOX1*; **C** *QSOX1*; normalized *via* GenEx software to *18S*. Statistical significance was assessed by one-way ANOVA test (each cell line separately) by means of GraphPad PRISM software. No sign: $p > 0.05$, *: ≤ 0.05, **: ≤ 0.01, *** ≤ 0.001 and **** < 0.0001. Data are shown as mean $\pm$ SEM (n=3, except for the MCF10A DFO sample where n=2). Cells were incubated with the reagents or under different O_2 concentrations for 48 hours, then harvested.

upper band is upregulated by hypoxia and corresponds to the predicted size of 120 kDa. The identity of the lower band remains to be determined.

Nonetheless, HIF1α seems to be mostly upregulated in samples treated with DFO (see Figure 4.18A). The same result applies with HIF2α and MCF7 cells while in the case of MCF10A, MDA-MB-231 and Panc-1, the strongest inducer of HIF2α seems to be the hypoxic chamber (see Figure 4.18B).

The quantification of relative expression of QSOX1 itself did not show any visible trend in QSOX1 protein-induction upon either chemically- or physically-induced hypoxia. The only cell line that showed any induction was MCF7, where the protein level increased upon DFO treatment almost 4-fold (see Figure 4.18E).

Since QSOX1 is also secreted to the medium, we carried out an experiment determining whether the hypoxia or hypoxia-mimicking conditions affect the secretion of QSOX1. Before harvesting cells for protein isolation, small amount of medium was removed from the cells, centrifuged and assessed by reducing SDS-PAGE followed by Western blotting.

A slight change in the QSOX1 secretion occurs when the malignant cell lines such as MCF7,

MDA-MB-231 and Panc-1 are subjected to the hypoxic environment, while no change is visible with the non-malignant MCF10A cells (see Figure 4.19, 4.20). To address the excessively high error bars in this experiment, we reffer to the appendix (see Figure S10 where we show both western blots used for this densitometry.

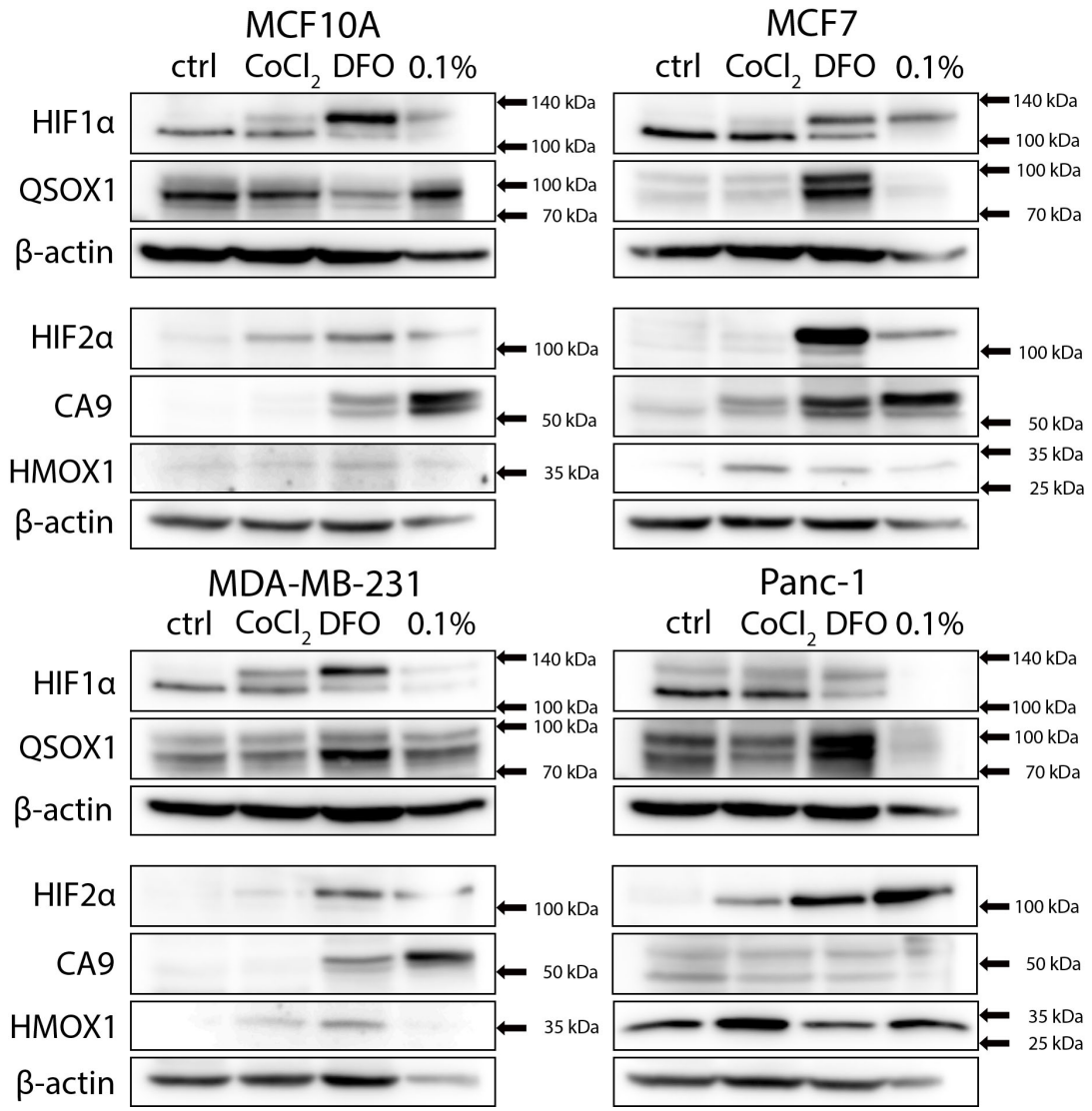

Figure 4.17: **Protein levels of HIF1α, QSOX1, HIF2α, CA9 and HMOX1 in hypoxic or hypoxia-mimicking conditions in MCF10A, MCF7, MDA-MB-231 and Panc-1 cells.** 80 µg of total protein from cell lysate was separated by reducing SDS-PAGE followed by Western blotting, β-actin was used as a loading control. Cells were incubated with the reagents or under different O_2 concentrations for 48 hours, then harvested.

While the *QSOX1*-knockout cells showed a different phenotype from the control MDA-MB-231 cell line, the four tested cell lines (MCF10A, MCF7, MDA-MB-231 and Panc-1) either under the hypoxia-mimicking conditions or in the hypoxic atmosphere (0.1% O_2) did not undergo any phenotypical change (see Figure 4.21).

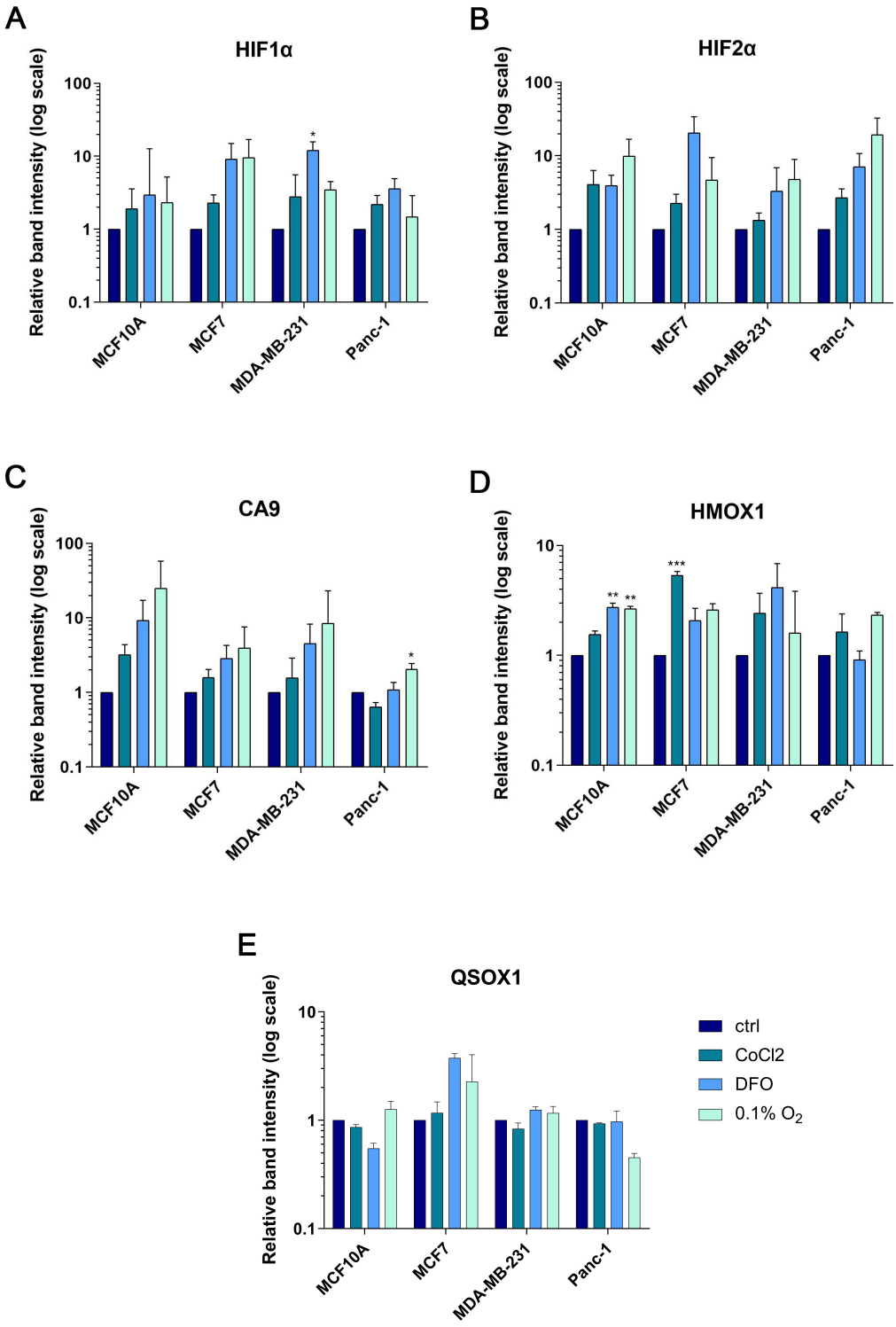

Figure 4.18: **Densitometry of HIF1α, HIF2αm CA9, HMOX1 and QSOX1 in hypoxic and hypoxia-mimicking conditions in MCF10A, MCF7, MDA-MB-231 and Panc-1 cells (see Figure 4.17). A** HIF1α; **B** HIF2α; **C** CA9; **D** HMOX1; **E** QSOX1. Statistical significance was assessed by one-way ANOVA test (each cell line separately) by means of GraphPad PRISM software. No sign: $p > 0.05$, *: ≤ 0.05, **: ≤ 0.01, *** ≤ 0.001 and **** < 0.0001. Data are shown as mean $\pm$ SEM (n=3).

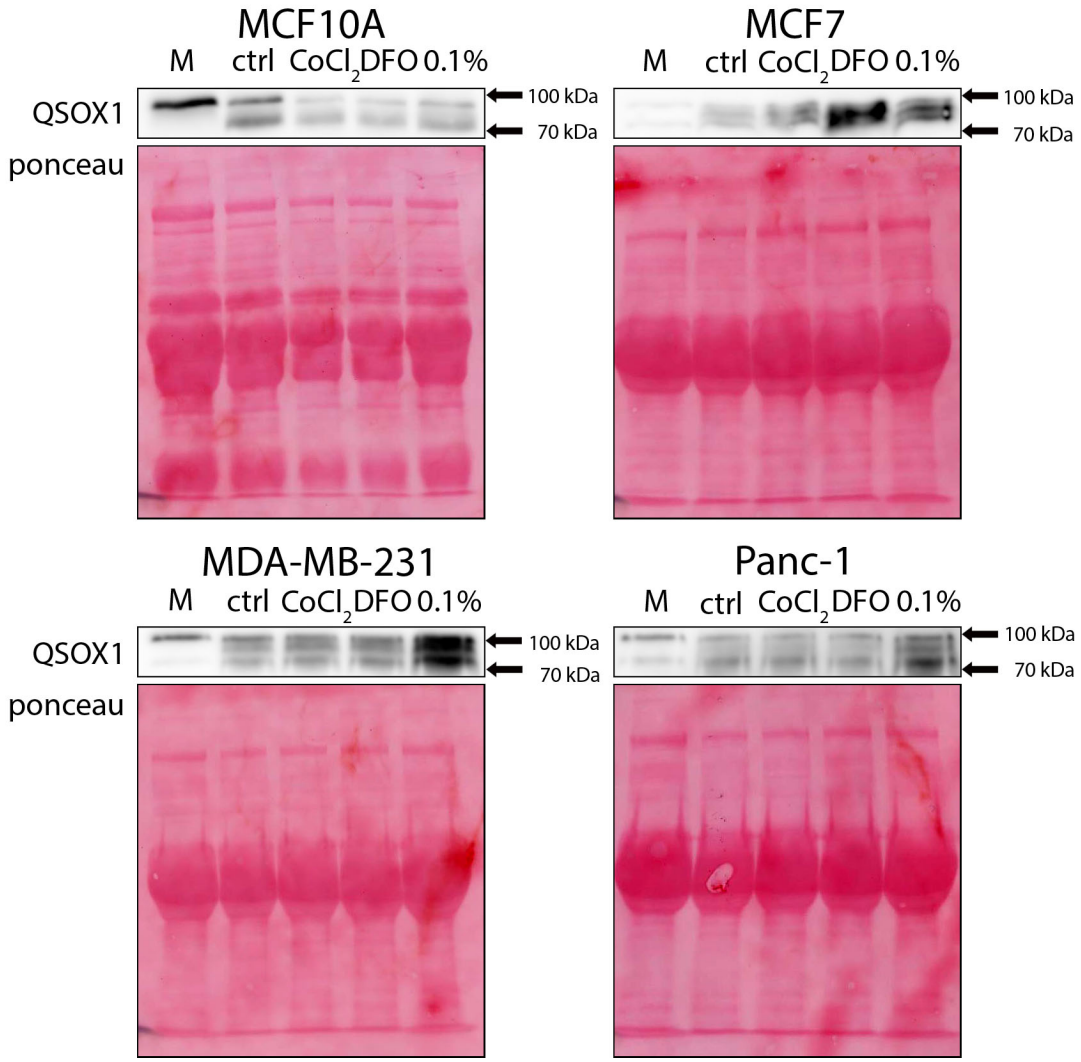

Figure 4.19: **Secreted QSOX1 protein level in hypoxic and hypoxia-mimicking conditions in MCF10A, MCF7, MDA-MB-231 and Panc-1 cells.** 20 µl of centrifuged cell medium was separated by reducing SDS-PAGE followed by Western blotting, ponceau S was used as a loading control. Cells were incubated with the reagents or under different O_2 concentrations for 48 hours, then the medium was harvested.

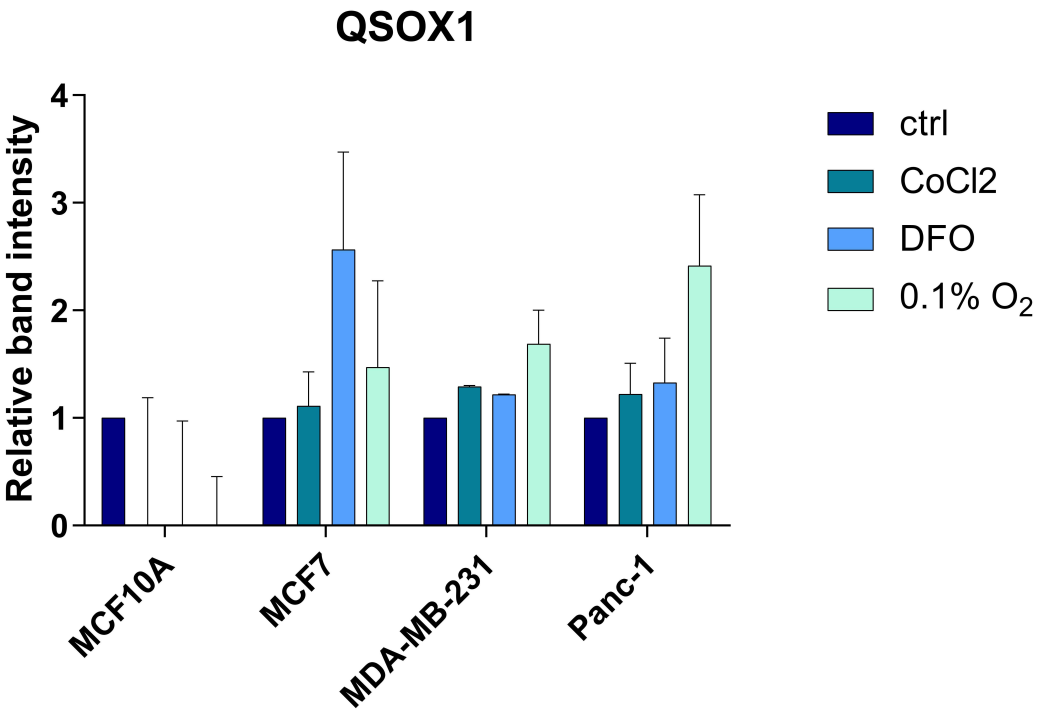

Figure 4.20: **Densitometry of secreted QSOX1 protein level in MCF10A, MCF7, MDA-MB-231 and Panc-1 cells under hypoxia or hypoxia-mimicking conditions(see Figures 4.19).** Statistical significance was assessed by one-way ANOVA test (each cell line separately) by means of GraphPad PRISM software. No sign: $p > 0.05$, *: ≤ 0.05, **: ≤ 0.01, *** ≤ 0.001 and **** < 0.0001. Data are shown as mean $\pm$ SEM (n=2).

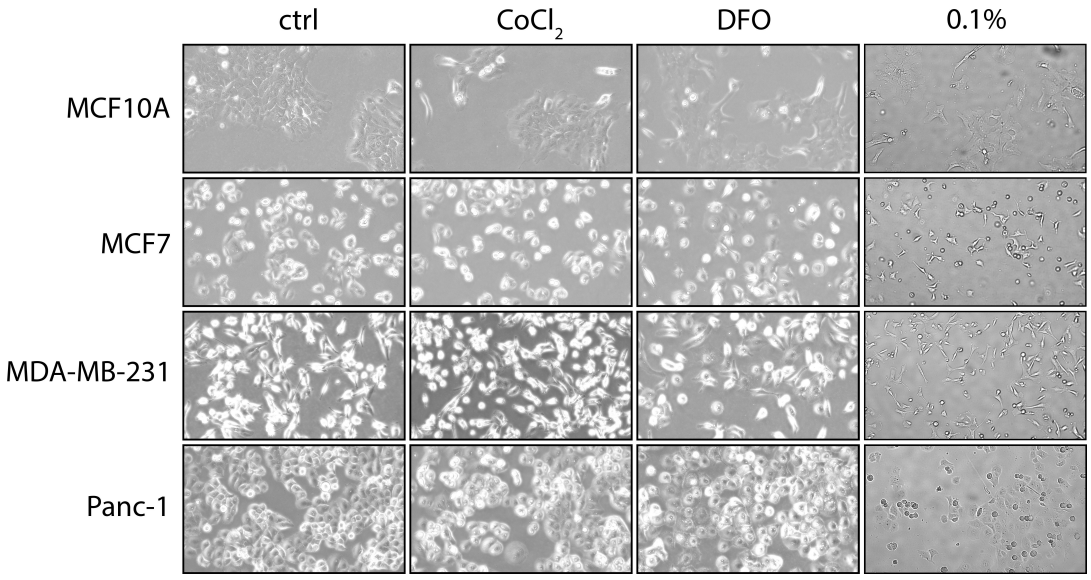

Figure 4.21: **Phenotype of MCF10A, MCF7, MDA-MB-231 and Panc-1 cells in various hypoxia-inducing and hypoxia-mimicking treatments.** Cells were incubated with the reagents or under 0.1% O_2 concentration for 48 hours, pictures were taken before the harvest.

4.3.2 Hypoxia titration

For further understanding of how normal and malignant cells respond to hypoxia, we have carried out an oxygen titration assay. The cells were incubated for 48 hours in environments with different oxygen concentrations and harvested using the same procedure as mentioned in chapter Hypoxia control.

The relative mRNA expression of *CA9* shows a very apparent trend when the expression significantly increases up to 1000-fold in MCF10A in 0% O_2 and decreasing gradually, with 5% of O_2 showing the effect similar to normoxic environment for the malignant cell lines (see Figure 4.22A).

Again, we cannot confirm this correlation with *HMOX1* (see Figure 4.22B). The expression increases slightly in 0% in all cell lines but fluctuates under the remaining oxygen concentrations.

Very similar results were obtained for the *QSOX1* mRNA (see Figure 4.22C) where it seems to respond to hypoxic conditions in MCF10A and MDA-MB-231 cells by increasing up to 4-fold in case of concentrations lower than 1% of oxygen, but the changes in other cell lines are only slightly increased.

As expected, on the protein level we can see a very similar trend with CA9 expression (see Figures 4.23 and4.24C) – steep increase in 0% O_2 decreasing gradually with higher oxygen concentrations with the only difference Panc-1 being the cell line where the *CA9* expression increases 10-fold with 0% O_2 and stays increased until 5% O_2.

The HIF1α and HIF2α react to the changes of O_2 concentration very differently (see Figures 4.23, 4.24A and 4.24B). Both proteins increase in expression when O_2 decreases to 0% but while HIF1α starts to decrease gradually with higher O_2 concentrations, HIF2α remains upregulated even in 5%, suggesting that HIF1α is more of an acute hypoxia response factor, whilst HIF2α probably reacts already to less radical changes.

Very importantly, when we assessed the influence of change of oxygen concentrations on QSOX1 protein level within the cell in this experiment, our results suggest that MCF7 and MDA-MB-231 cell lines seem to be influenced by oxygen tension and upregulate QSOX1, while MCF10A do not respond much and Panc-1 cells even seem to have lower amounts of QSOX1 concentrations below 1% O_2 compared to control and this conclusion is extremely significant according to one way ANOVA test by GraphPad PRISM (see Figure 4.24D).

On the other hand, all cells show a tendency to secrete QSOX1 into the medium when exposed to low oxygen tension below 1% (see Figures 4.25 and 4.26). The massive excretion could be seen in Panc-1 cells, suggesting that the above mentioned lower levels of cellular QSOX1 might be because of the excessive secretion into the medium. This is potentially a very important information as a link between secretion of QSOX1 and hypoxia has not been studied and described so far.

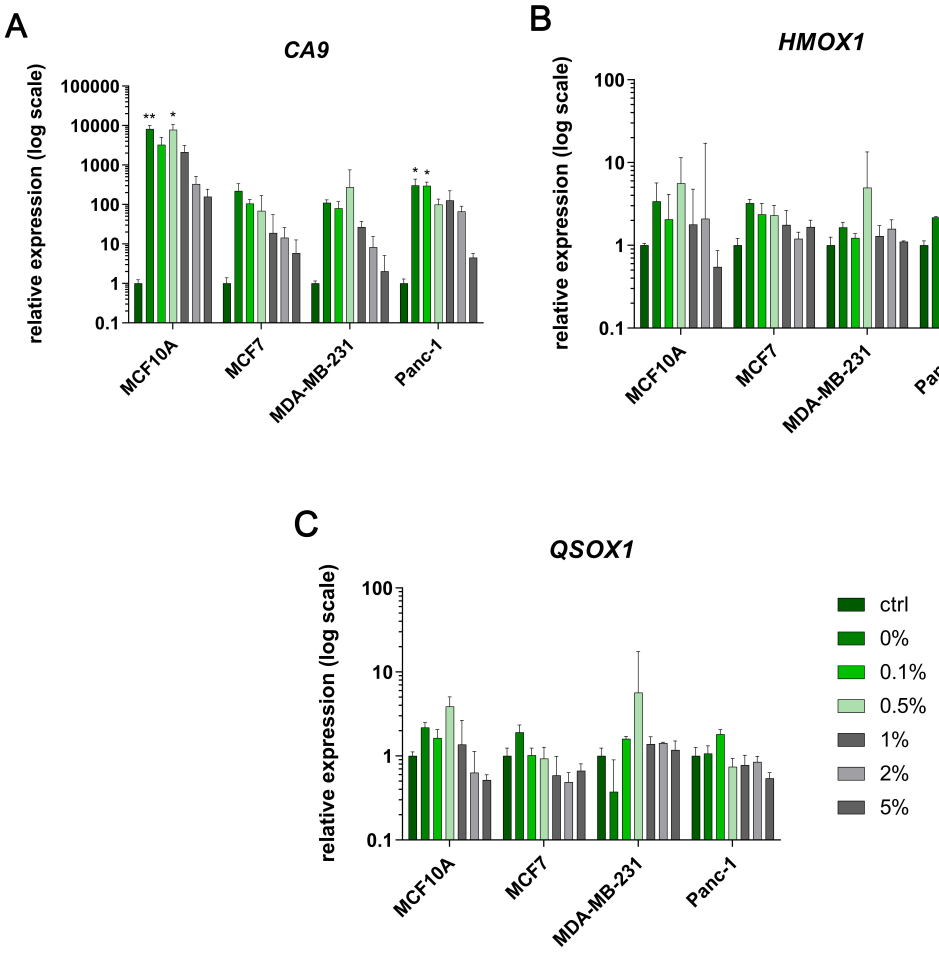

Figure 4.22: **Relative mRNA expression of *CA9*, *HMOX1* and *QSOX1* in MCF10A, MCF7, MDA-MB-231 and Panc-1 cells. A** *CA9*; **B** *HMOX1*; **C** *QSOX1*; normalized *via* GenEx software to *IPO8*. Statistical significance was assessed by one-way ANOVA test (each cell line separately) by means of GraphPad PRISM software. No sign: $p > 0.05$, *: ≤ 0.05, **: ≤ 0.01, *** ≤ 0.001 and **** < 0.0001. Data are shown as mean $\pm$ SEM (n=3). Cells were incubated in hypoxic chamber for 48 hours under different O_2 concentrations, then harvested.

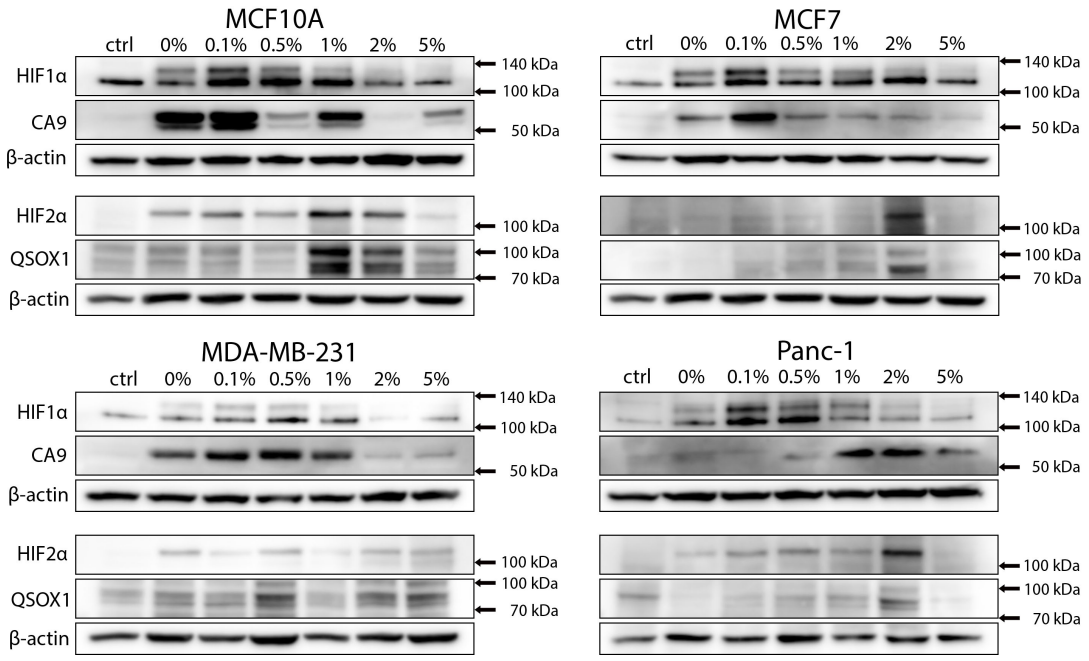

Figure 4.23: **Protein levels of HIF1α, HIF2α, CA9, HMOX1 and QSOX1 in response to 0-5% O_2 in MCF10A, MCF7, MDA-MB-231 and Panc-1 cells.** 60 µg of total protein from cell lysate was separated by reducing SDS-PAGE followed by Western blotting, β-actin was used as a loading control. Cells were incubated in hypoxic chamber for 48 hours under different O_2 concentrations, then harvested.

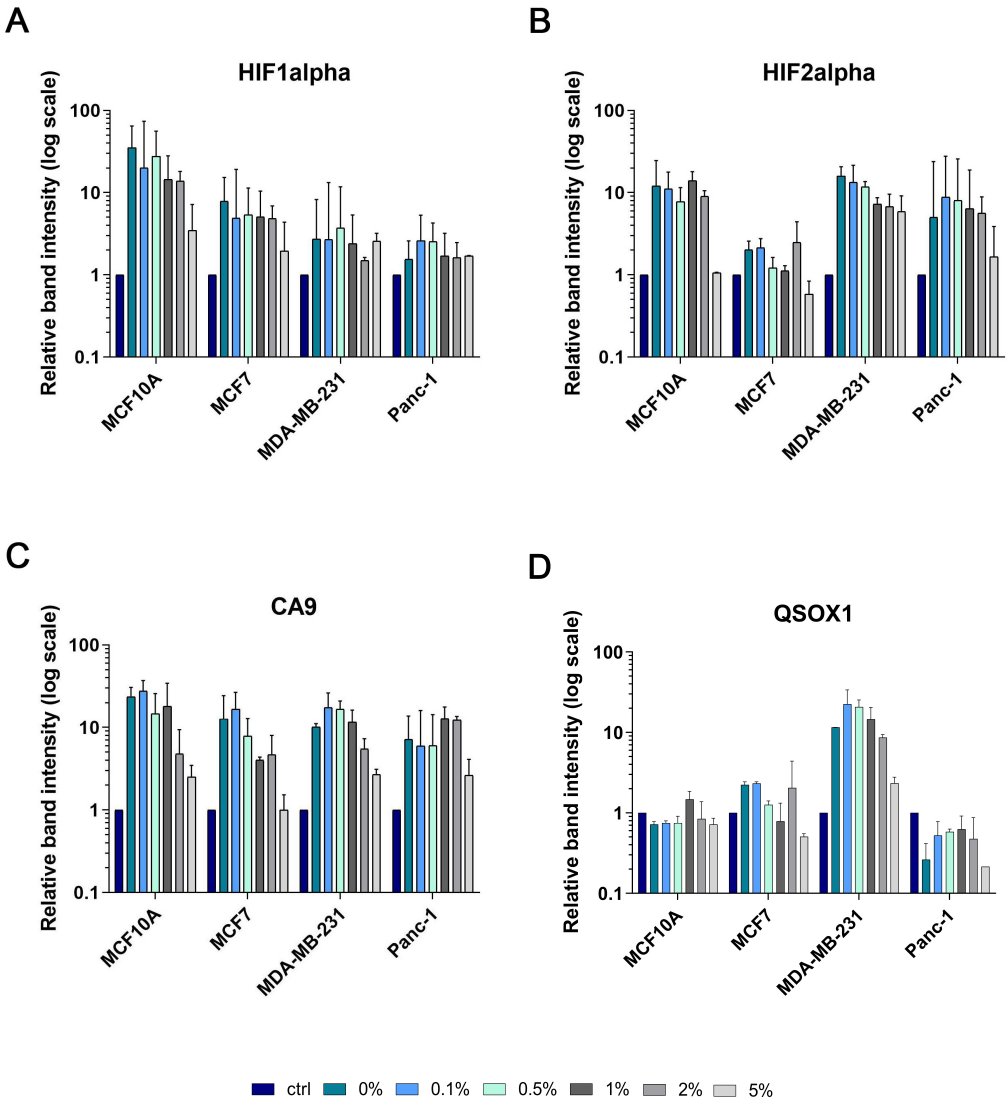

Figure 4.24: **Densitometry of HIF1α, HIF2α, CA9 and QSOX1 protein levels under 0-5% O_2 in MCF10A, MCF7, MDA-MB-231 and Panc-1 cells' lysate (see Figure 4.23). A** HIF1α; **B** HIF2α; **C** CA9; **D** QSOX1. Statistical significance was assessed by one-way ANOVA test (each cell line separately) by means of GraphPad PRISM software. No sign: $p > 0.05$, *: ≤ 0.05, **: ≤ 0.01, *** ≤ 0.001 and **** < 0.0001. Data are shown as mean $\pm$ SEM (n=3). Cells were incubated in hypoxic chamber for 48 hours under different O_2 concentrations, then harvested.

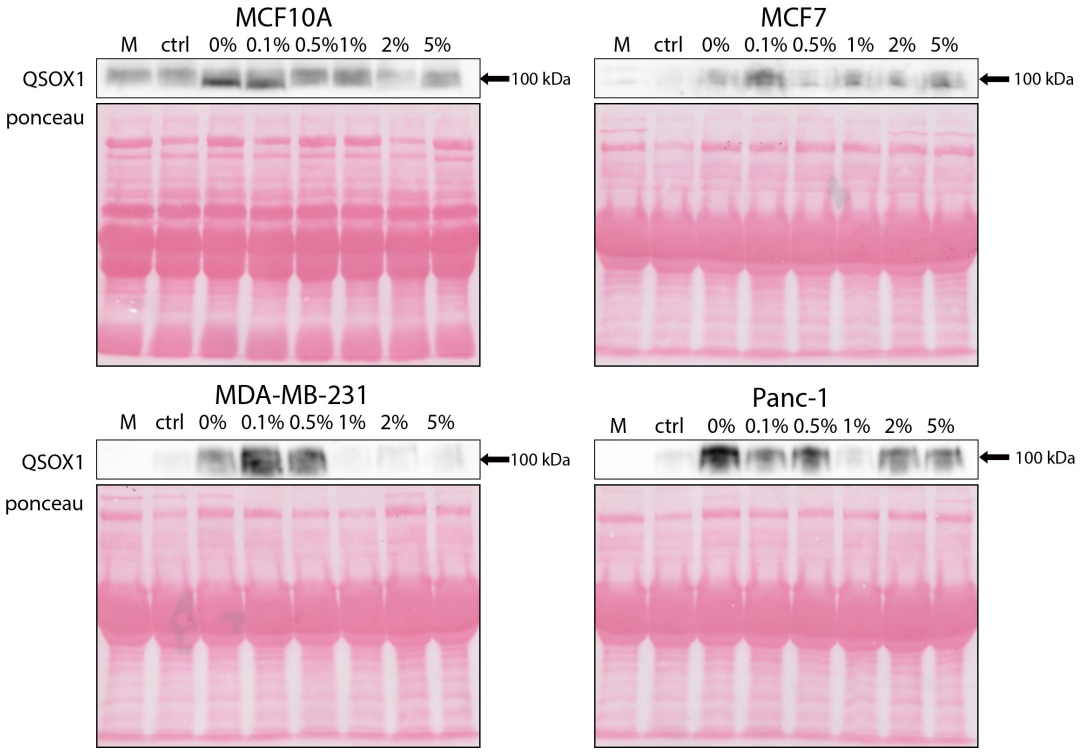

Figure 4.25: **Secreted QSOX1 protein level in conditioned medium in MCF10A, MCF7, MDA-MB-231 and Panc-1 cells under 0-5% O_2.** 20 µl of centrifuged cell medium was separated by reducing SDS-PAGE followed by Western blotting, ponceau S was used as a loading control. Cells were incubated in hypoxic chamber for 48 hours under different O_2 concentrations, then the medium was harvested and analysed.

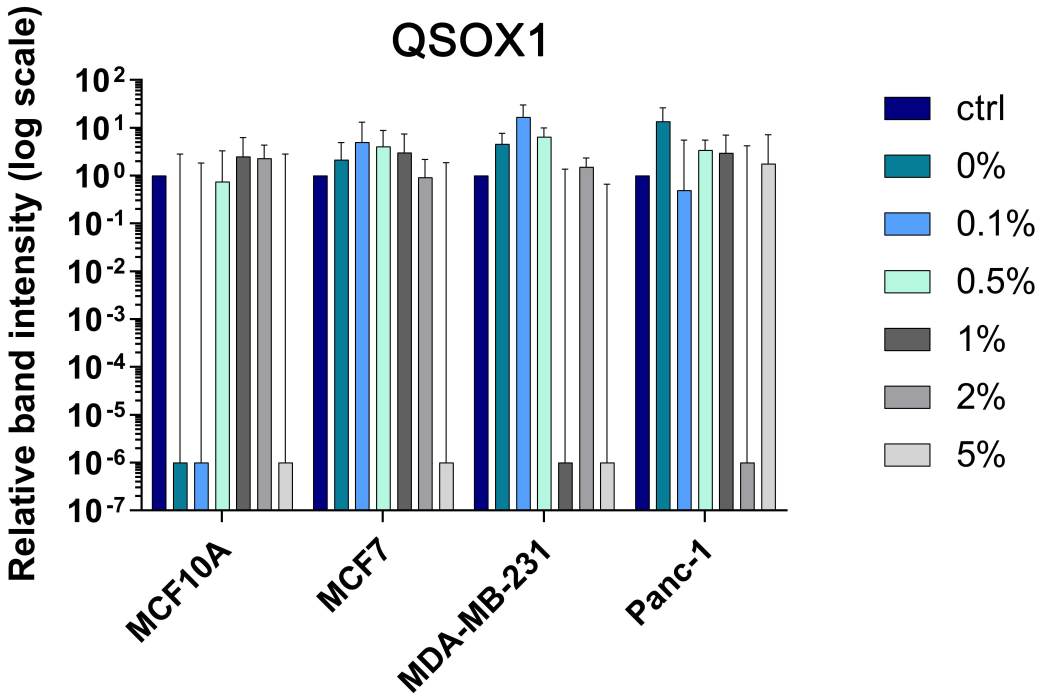

Figure 4.26: **Densitometry of secreted QSOX1 protein level in conditioned medium under 0-5% O_2 in MCF10A, MCF7, MDA-MB-231 and Panc-1 cells (see Figure 4.25).** Statistical significance was assessed by one-way ANOVA test (each cell line separately) by means of GraphPad PRISM software. Ns: $p > 0.05$, *: ≤ 0.05, **: ≤ 0.01, *** ≤ 0.001 and **** < 0.0001. Data are shown as mean $\pm$ SEM (n=3). Cells were incubated in hypoxic chamber for 48 hours under different O_2 concentrations, then harvested.

5. Discussion

QSOX1 is a sulfhydryl oxidase playing an important role in intracellular, as well as extracellular processes, such as oxidative protein folding or extracellular matrix (ECM) remodeling and formation [Hoober et al., 1999b, Ilani et al., 2013]. Its two forms can be found on the membrane of rough endoplasmatic reticulum (ER) [Thorpe et al., 2002], in the Golgi apparatus (GA) and in the ECM [Rudolf et al., 2013] where it is actively secreted by almost every cell type.

Due to the possible involvement in extracellular matrix transformation and concurrent upregulation in several types of cancer including cancer stem-like cells [Antwi et al., 2009, Baek et al., 2018, Katchman et al., 2013, Soloviev et al., 2013, Rychtarcikova et al., 2017], QSOX1 represents an attractive target for antineoplastic treatment and therapy. However, our understanding of QSOX1 characteristics, mechanism of action, interaction partners as well as substrates or a way of regulation, is far from complete, requiring further research.

Generally, it was proposed that patients suffering from different types of cancer with increased levels of QSOX1 in the malignant tissues face poor prognosis. This suggestion was based on several studies indicating the role of QSOX1 in cancer cells proliferation, migration and invasion leading to enhanced ability of the cells to form metastases [Katchman et al., 2013, Baek et al., 2018] and therefore to underwhelming outcomes for the patients. The molecular mechanisms of QSOX1 affecting cancer cells are poorly understood so far and warrants further elucidation.

While QSOX1 catalyzes formation of disulfide bonds in order to aid the substrate proteins to reach the native conformation, it also produces hydrogen peroxide. Although H_2O_2, together with other ROS, is useful in defense against pathogens, it is also known to be toxic to cells due to its reactivity with nucleic acids, proteins and lipids and following disruption of normal gene expression. This can lead to vast number of possible outcomes including senescence or apoptosis. At the same time, some of the ROS molecules can operate as signal transducers and, according to literature and our results on cancer stem-like cells, promote cell invasion and metastatic spread in a more complex manner [Pani et al., 2010, Rychtarcikova et al., 2017].

To address the effect of *QSOX1* overexpression or knockout on cancer cells, we constructed three functional experimental models using the triple negative MDA-MB-231 breast cancer cell line - (1) *QSOX1v1*- and *QSOX1v2*-overexpressing cell lines based on TetON3G-inducible system, enabling a full control over the protein induction *via* direct activation of the pTRE3G promoter by addition of tetracycline-derivative doxycycline. The pTRE3G-BI-mCherry vector used for this purpose contains a bidirectional pTRE3G promoter, one inducing the gene of interest while the other controls fluorescent mCherry protein induction; (2) stable *QSOX1* knockdown cell lines constructed using CRISPR/Cas9 system and (3) stable *QSOX1* knockout cell lines created by repeated transfection of the already generated cells that show diminished expression of *QSOX1*.

All of our overexpressing clones showed significant induction of fluorescent protein mCherry after DOX addition (see Figure 4.4). Similarly, QSOX1 protein was highly induced so that the basal expression in controls (ctrl), as well as in empty vector (EV) and non-induced cells was in fact non-detectable. Interestingly, the western blot of total protein from cell lysate showed multiple bands in the area of predicted and reported size (see Figure 4.3A) for both longer and shorter variant of QSOX1. Since the bands were visible exclusively in the lines of cells with DOX, it is not likely the result of non-specific binding of the QSOX1 antibody and probably reflects posttranstlational modification, such as glycosylation at ASN130 and ADN243 that have been reported [Horowitz et al., 2018].

Besides the QSOX1 protein level within the cell, we also assayed its secretion outside the cell. The medium was collected shortly before the cell harvest, centrifuged and transported to new tubes to avoid contamination with floating cells. According to our results (see Figure 4.3B), the secretion of QSOX1 into medium correlates with its mRNA expression and protein levels inside the cells. Moreover, in accordance with published literature, both variants of QSOX1 seem to be secreted to the medium, even though in our case this can be due to the fact that we have reached unnaturally high QSOX1 levels.

Neither of the clones showed any cell morphology changes after DOX addition (data not shown), most of the cells in the colonies had an elongated phenotype with well visible lamellipodia suggesting their continual movement.

In order to define the role of *QSOX1*-overexpression on the viability and proliferation of cancer cells, we first determined an induction curve for DOX-dependent *QSOX1*-overexpression. This allowed us to detect when the protein is actually induced and how stable it is in our model. According to our findings, significantly higher levels of QSOX1 protein were induced after 24 hours of incubation with DOX in all clones irrespective of the isoform expressed (see Figure 4.5 and Figures S1-S3). It is important to realize that the graph plots relative band intensity of *QSOX1*-overexpressing clones, meaning that the signal obtained from the western blots was too strong to enable proper basal expression quantification and thus 0 band intensity does not necessarily mean null overall QSOX1 level.

Thus we have prepared a useful model of cell lines that exhibits very high protein level of QSOX1v1 or QSOX1v2 upon doxycycline addition.

As the objective of this project was to help clarify the role of QSOX1 in cancerogenesis, we have focused our work towards the proliferation of cancerous cells and an influence of QSOX1 on this cellular process. In several earlier academic works, the results indicate that depletion of QSOX1 *via* shRNA/RNAi has a significant effect on cell cycle of multiple cancer cell lines including pancreatic Panc-1 or mammary MCF7, BT549 or BT474 cells [Lake et al., 2016, Knutsvik et al., 2016] resulting in decreased cellular growth *in vitro* and *in vivo*. In our model none of the overexpressing clones showed a significant effect on the proliferation rate, although there was a tendency towards slower growth, yet this could be attributed to the effect of addition of doxycycline as a similar trend could be seen in the empty vector clones (see Figure 4.14.

Our second and third experimental models were prepared using CRISPR/Cas9 technology. We have designed a vector introducing a double-strand nick into the exon 6 of *QSOX1* coding sequence. The double-strand is randomly ligated back together by either homology directed repair (HDR) or non-homologous end joining (NHEJ), ideally resulting in a cell line with mutated *QSOX1* gene that has lost QSOX1 protein expression.

After our first attempt at transfecting the cells with our vector, we have obtained only cells with partially inactivated *QSOX1* with downregulated mRNA expression and decreased protein level (see Figures 4.7A and 4.7C). We have explained this results as a possibility that only one allele was affected and the generated clones represented heterozygotes. On the other hand, it is also possible that the introduced change in *QSOX1* gene leads to translation of QSOX1 in a defective form, probably unable to fold into its native conformation but still persisting in the cell. This explanation is supported by the fact that even though, there are bands visible on western blot of total cell lysate (see Figure 4.7C), there are either none or much weaker bands of QSOX1 present on the western blots from cell medium (see Figure 4.7D), suggesting that the formed protein is unable to be secreted from the cell (or secreted at much lower level), likely

due to genomic modification introduced by the CRISPR nuclease.

Since our goal was to obtain a knock-out cell lines, we have repeated the transfection of the prepared CRISPR/Cas9 constructs. We have used the already knocked-down cells for these purposes in order to knock out the remaining functional allele. The result showed we have obtained the desired knockout cells all of which originated from the parental Cl17 and Cl33 (see Figure 4.8C). On the other hand, clones originated from parental Cl16 still contained QSOX1 protein. After carefull analysis of the sequencing results (see Figure 4.9), we came to a conclusion that clone 16 has a deletion of a TTC triplet coding for the F242 but otherwise it is identical to the wild type allele and produces QSOX1 protein, therefore this clone was edited by CRISPR but the resulting allele is not a knockout and produces a modified protein which probably has different turnover and is less secreted into the medium.

To verify that the resulting *QSOX1*$^{-/-}$ clones are indeed knockouts, genomic DNA of the selected clones, as well as the control cells was isolated and sequenced for the *QSOX1* gene exon 6. The enthralling result of this work is depicted in Figure 4.9 as a sequence alignment scheme which reveals a confounding finding. An identical short sequence was inserted in place of the introduced double-stranded nick in several of our clones. This indicates a possibility of a certain similarity between our target site and an unknown genomic sequence. However, we were unable to acquire any significant hit when running the sequence using the commonly used open-access internet tool Blastn, therefore this question awaits future studies, but we could use the knockout *QSOX1*$^{-/-}$ clones for further experiments, as these have edited DNA and produce no QSOX1.

In order to see whether QSOX1 has any effect on cellular viability and proliferation rate, we utilized our *QSOX1*-overexpressing MDA-MB-231 cells. Unfortunately, induction of high protein levels of QSOX1v1 and QSOX1v2 did not show a statistically significant effect on the number of proliferating cells as could be seen on Figure 4.6 and thus we see that high levels of QSOX1 in cancer cells do not lead to a cell cycle arrest and quiescence as in normal fibroblasts and, similarly, high expression of QSOX1 does not seem to have a significant effect on the proliferation rate of our model cell line MDA-MB-231 (see Figures 4.12 and 4.13). Yet, it is possible that since MDA-MB-231 cells, in comparison to other cell lines, express relatively high level of QSOX1, pushing the amount even higher did not result in any stronger effect. The other possible explanation is that the overexpression induces such high levels that they are not physiologic and the protein may not be functioning similarly to the normal situation.

Since no effect was seen in the cells with high levels of QSOX1, we moved forward and tested the effect of loss of *QSOX1* using CRISPR/Cas9 knockout cells that according to our data lack production of normal functional QSOX1 in any isoform and do not secrete it in the medium either (see Figure 4.8).

Importantly, in our experiments, *QSOX1*-knockout cells showed a significant decrease in proliferation while when compared to a designated control (see Figures 4.14-4.13). This finding was confirmed by inhibiting QSOX1 activity in original MDA-MB-231 cells by an inhibitory compound ebselen, leading to the very same results, pointing towards an assumption that this phenotype is indeed induced by loss of *QSOX1* and not a consequence of potential intrinsic changes accompanying the CRISPR/Cas9 editing process.

The fact that we see a reduction in cell growth after *QSOX1* knockout is not consistent with data published by Hellebrekers *et al.*. The difference may be a repercussion of using a different cell type for purposes of our assays, since Hellebrekers *et al.* were using human umbilical vein endothelial cells while in our experiments, MDA-MB-231 epithelial mammary cancer cell line was used. On the other hand, Pernodet *et al.*, who associate *QSOX1*-overexpression with

decreased tumor growth, performed their experiments (among other cell lines) on MDA-MB-231 as well, interpreting the outcomes contradictory to ours as well as to data of Katchman *et al.* [Pernodet et al., 2012, Katchman et al., 2011]. This difference in experimental work was already addressed by Lake and Faigle in 2014, referring to Pernodet's work as "very hard to interpret" and favoring the study of Katchman's group [Katchman et al., 2011, Lake and Faigel, 2014].

While part of the academic community disputes over the role of QSOX1 in tumor proliferation and invasiveness, Morel *et al.* introduces another possible point of view on QSOX1 involvement in tumor biology. Despite the fact, that QSOX1 actively participates on intracellular ROS formation in form of hydrogen peroxide, the insights of Morel's group suggest that overexpression of *QSOX1* significantly contributes to protection of a cell against oxidative-stress induced apoptosis [Morel et al., 2007]. In Morel's work, QSOX1 is upregulated upon treatment with H_2O_2 which seems as striking since the only explanation for this peculiar behavior would be a positive feedback loop in which H_2O_2 induces QSOX1 expression, producing even more H_2O_2 as a consequence.

Another cellular process, described for the first time on the massively proliferating tumor cells, dealing with a reduction of a risk of ROS-induced apoptosis is a well-studied Warburg effect, that pushes cancerous cells towards an aerobic glycolysis. According to the literature, Warburg effect is, among others, caused by activation of HIFs, stabilization of which is initiated during significant pO_2 decrease in tumor and other tissues [Denko, 2008]. Furthermore, hydrogen peroxide can indirectly promote HIF stabilization by removing catalytic iron from prolyl-hydroxylases (PHDs) that under normal circumstances drives HIF towards proteasomal degradation, thus inhibiting their activity [Gerald et al., 2004]. A different downstream target of HIF transcriptional activity is supposedly our gene of interest, *QSOX1*. Therefore, the alleged conclusion made by Morel *et al.* that QSOX1 is induced by higher H_2O_2 concentration may be correct but in a more indirect way than previously proposed. Instead of direct influence on *QSOX1* expression (the aforementioned positive feedback loop), H_2O_2 triggers HIF stabilization, followed by induction of its downstream targets (together with *QSOX1*) and enhances the Warburg effect, that is afterwards inherently leading to increased protection against ROS-induced apoptosis.

The findings that QSOX1 is a hypoxia-inducible transcription factor target can be attributed to Shi *et al.* who in 2013 stated that HIF1 contributes to hypoxia-induced pancreatic cancer cells invasion *via* promoting *QSOX1* expression [Shi et al., 2013]. This idea is not altogether that revolutionary - the closely related Ero1α oxidase is known to be a hypoxia inducible protein, which can lead us to an assumption that QSOX1 may be regulated in a similar manner. According to Shi *et al.*, the *QSOX1* gene contains two HRE segments on which stabilized HIF1 binds upon hypoxic conditions and promotes *QSOX1* transcription. In order to see whether this regulation takes place also in normal cells and is valid not only in the used Panc-1 cells, we performed a set of experiments that induce hypoxia-mimicking conditions *via* chemical treatment with $CoCl_2$ and DFO or, by using a hypoxia chamber, expose the cells to real gradual loss of oxygen. In our experiments, we did see an induction of *QSOX1* transcription but were unable to detect an increased level of protein within the cell as reported by Shi *et al.*, using an identical cell line Panc-1 (see Figures 4.17-4.18 and 4.23-4.24). We have shown that all tested cells do respond to decreased oxygen concentrations by moderately increasing *QSOX1* transcription (see Figure 4.22C), there was a slight increase in protein levels within the cells as well (see Figure 4.24D) but the biggest change was in the amount of secreted QSOX1 in the medium, which increased in all tested cell lines when oxygen tension was very low (see Figures 4.19-4.20

and 4.25-4.26). Our findings suggest that the trancription of *QSOX1* is induced by hypoxia and also by addition of DFO. The produced protein is then secreted into the extracellular space while at the same time the actual protein content within the cell does not change significantly. This is a new and very important finding that has not been observed and described so far. Although we can only speculate at this point, it is possible that some HIF1-responsive protease such as furin protease could be activated and shed the QSOX1 from cell surface [McMahon et al., 2005]. This is yet to be confirmed by further experiments.

Importantly, while QSOX1 seems to be regulated by hypoxia in some types of cancer, hypoxia itself is often associated with invasive and metastatic phenotype [Cannito et al., 2008]. Not only that it actively affects surrounding epithelial cells to proliferate and form new bloodstream vessels that are usually leaky (which is ideal for cancer cell intravasation followed by transfer of the cells to the secondary tumor sites). It also leads to lowering extracellular pH due to the activation of carbonic anhydrases (see Figures 4.22A and 4.23), favoring matrix degradation by MMPs and cathepsins [Rofstad et al., 2006].

Altogether, the information available to date lead us to the conclusion that *QSOX1* is highly expressed in various cancer tissues and plays a role in enhancement of cellular growth and migratory abilities. Possibly, when the tumor mass reaches size that does not allow for sufficient amounts of oxygen to reach the tissue equally, the hypoxic environment results in even higher levels of QSOX1 in cancerous cells and secretion into extracellular space while the tumor-supporting fibroblasts are depleted of QSOX1 as Ilani *et al.* suggest in their research [Ilani et al., 2013]. This enables the tumor cells to detach from their surroundings and escape from hypoxia-induced oxidative stress. This could be facilitated by secreted QSOX1, which indirectly activates the MMPs leading to ECM degradation and rapid cancer cell migration and dissemination.

As the growing body of evidence suggest the most important role of QSOX1 in cancer lays in its notable ability to induce cellular migration and invasiveness. Sadly, due to technical problems we have encountered, as well as for time reasons, we were unable to perform experiments concerning this matter and we are planning on proceeding with that in the near future.

Since metastases represent the leading cause of death by cancer due to failure of the colonized organs [Steeg, 2006], it is considered an eminent part of contemporary cancer biology. For cells to be able to detach and leave the place of primary tumor mass, they have to undergo a very specific and demanding conversion that is characterized as an epithelial-mesenchymal transition (EMT). Apart for loss of polarity and detachment from surrounding cells, the cells are forced to increase their interactions with the extracellular matrix but also migrate through the ECM towards blood and lymphatic vessels to use this already existing stream to establish secondary tumors in distant sites of the body [Steeg, 2006].

Very interestingly, QSOX1 was found to have a certain role in all aforementioned processes [Lake and Faigel, 2014, Katchman et al., 2011] needed for successful transition, however, it is rather disputable whether its role is vital or if it is redundant so that other proteins can take its place during this particularly important part of initiation of tumor dissemination.

Nonetheless, it is becoming clear that after QSOX1 is secreted to the ECM, it continues in its dedicated work of a sulfhydryl oxidase by formation of disulfide bonds within its substrate range. This activity was described in 2013 by Ilani *et al.* as means of incorporation of laminin into ECM [Ilani et al., 2013] and in 2011 by Katchman *et al.* as an indirect activation of matrix metalloproteinases 2 and 9 [Katchman et al., 2011] - proteins commonly present in the ECM in an inactive state. While RNAi-induced depletion of QSOX1 in stromal fibroblasts results in inability of ECM to provide a sufficient cell-matrix adhesion leading to detached but still viable cells [Ilani et al., 2013], activation of MMPs is associated with ECM degradation and therefore

easier progression of migrating cancer cells.

Other reports mention a correlation between angiogenesis and silencing of QSOX1 where knockout of tumor epithelial cells leads to an increase in growth [Hellebrekers et al., 2007]. As a reaction to this claim, Lake and Faigel [Lake and Faigel, 2014] in their latest review on emerging role of QSOX1 in cancer propose that "QSOX1 may help the tumor cells to invade through the basement membrane and gain access to the bloodstream, but once circulating tumor cells intravasate back into a tissue and begin to grow at a metastatic site, QSOX1 is no longer required and so its expression is turned off, enabling an angiogenic phenotype to emerge".

6. Conclusions

Conclusions reached within this study can be summarized in following points:

- We assessed QSOX1 protein level in non-malignant MCF10A and malignant MCF7, MDA-MB-231, BT474, T47D breast cancer cell lines as well as pancreatic cancer cell lines Panc-1 and PaTu-8902 and non-malignant fibroblasts cells BJ, finding the highest level in MDA-MB-231 and Panc-1 cells. Moreover, MDA-MB-231 cells showed also the highest secretion of QSOX1 into the medium.
- We have set up an experimental model of MDA-MB-231 cells inducibly overexpressing both variants of *QSOX1* and observed no significant effect of *QSOX1* overexpresion on proliferation of MDA-MB-231 breast cancer cells.
- We have successfully generated $QSOX1^{-/-}$ knockout MDA-MB-231 breast cancer cell line using CRISPR/Cas9 technology. Importantly, $QSOX1^{-/-}$ cells exhibit significant attenuation of cellular growth and proliferation, supporting the important role of QSOX1 in cancerogenesis.
- We have observed a modest increase in *QSOX1* expression in MCF10A, MCF7, MDA-MB-231 and Panc-1 cell lines under decreased oxygen levels and we consistently observe enhanced secretion of QSOX1 into the extracellular space rather than its accumulation within the cells, suggesting that hypoxia regulates not only its transcription but also its secretion.

In the near future, our work on QSOX1 characterization will focus on its role in migration and invasiveness in cancer cells, its interaction partners like MMPs, the possibility of regulation by estrogen and the effect of QSOX1 on spheres.

Bibliography

[Ahmed et al., 1975] Ahmed, A. K., Schaffer, S., and Wetlaufer, D. (1975). Nonenzymic reactivation of reduced bovine pancreatic ribonuclease by air oxidation and by glutathione oxidoreduction buffers. *Journal of Biological Chemistry*, 250(21):8477–8482.

[Anelli et al., 2003] Anelli, T., Alessio, M., Bachi, A., Bergamelli, L., Bertoli, G., Camerini, S., Mezghrani, A., Ruffato, E., Simmen, T., and Sitia, R. (2003). Thiol-mediated protein retention in the endoplasmic reticulum: the role of erp44. *The EMBO journal*, 22(19):5015–5022.

[Anfinsen, 1973] Anfinsen, C. B. (1973). Principles that govern the folding of protein chains. *Science*, 181(4096):223–230.

[Antwi et al., 2009] Antwi, K., Hostetter, G., Demeure, M. J., Katchman, B. A., Decker, G. A., Ruiz, Y., Sielaff, T. D., Koep, L. J., and Lake, D. F. (2009). Analysis of the plasma peptidome from pancreas cancer patients connects a peptide in plasma to overexpression of the parent protein in tumors. *Journal of proteome research*, 8(10):4722–4731.

[Arner and Holmgren, 2006] Arner, E. S. and Holmgren, A. (2006). The thioredoxin system in cancer. 16(6):420–426.

[Baek et al., 2018] Baek, J. A., Song, P. H., Ko, Y., and Gu, M. J. (2018). High expression of qsox1 is associated with tumor invasiveness and high grades groups in prostate cancer. *Pathology-Research and Practice*, 214(7):964–967.

[Baluk et al., 2005] Baluk, P., Hashizume, H., and McDonald, D. M. (2005). Cellular abnormalities of blood vessels as targets in cancer. *Current opinion in genetics & development*, 15(1):102–111.

[Benayoun et al., 2001] Benayoun, B., Esnard-Fève, A., Castella, S., Courty, Y., and Esnard, F. (2001). Rat seminal vesicle fad-dependent sulfhydryl oxidase biochemical characterization and molecular cloning of a member of the new sulfhydryl oxidase/quiescin q6 gene family. *Journal of Biological Chemistry*, 276(17):13830–13837.

[Berberat et al., 2005] Berberat, P. O., Dambrauskas, Z., Gulbinas, A., Giese, T., Giese, N., Künzli, B., Autschbach, F., Meuer, S., Büchler, M. W., and Friess, H. (2005). Inhibition of heme oxygenase-1 increases responsiveness of pancreatic cancer cells to anticancer treatment. *Clinical cancer research*, 11(10):3790–3798.

[Bertini et al., 1999] Bertini, R., Howard, O. Z., Dong, H.-F., Oppenheim, J. J., Bizzarri, C., Sergi, R., Caselli, G., Pagliei, S., Romines, B., Wilshire, J. A., et al. (1999). Thioredoxin, a redox enzyme released in infection and inflammation, is a unique chemoattractant for neutrophils, monocytes, and t cells. *Journal of Experimental Medicine*, 189(11):1783–1789.

[Blasco, 2005] Blasco, M. A. (2005). Telomeres and human disease: ageing, cancer and beyond. *Nature Reviews Genetics*, 6(8):611.

[Brenton et al., 2005] Brenton, J. D., Carey, L. A., Ahmed, A. A., and Caldas, C. (2005). Molecular classification and molecular forecasting of breast cancer: ready for clinical application? *Journal of clinical oncology*, 23(29):7350–7360.

[Bulleid and Ellgaard, 2011] Bulleid, N. J. and Ellgaard, L. (2011). Multiple ways to make disulfides. *Trends in biochemical sciences*, 36(9):485–492.

[Cabibbo et al., 2000] Cabibbo, A., Pagani, M., Fabbri, M., Rocchi, M., Farmery, M. R., Bulleid, N. J., and Sitia, R. (2000). Ero1-l, a human protein that favors disulfide bond formation in the endoplasmic reticulum. *Journal of Biological Chemistry*, 275(7):4827–4833.

[Cailleau et al., 1974] Cailleau, R., Young, R., Olive, M., and Reeves Jr, W. (1974). Breast tumor cell lines from pleural effusions. *Journal of the National Cancer Institute*, 53(3):661–674.

[Cannito et al., 2008] Cannito, S., Novo, E., Compagnone, A., Valfrè di Bonzo, L., Busletta, C., Zamara, E., Paternostro, C., Povero, D., Bandino, A., Bozzo, F., et al. (2008). Redox mechanisms switch on hypoxia-dependent epithelial–mesenchymal transition in cancer cells. *Carcinogenesis*, 29(12):2267–2278.

[Cao et al., 2009] Cao, Y., Fu, Y.-L., Yu, M., Yue, P.-b., Ge, C.-H., Xu, W.-X., Zhan, Y.-Q., Li, C.-Y., Li, W., Wang, X.-H., et al. (2009). Human augmenter of liver regeneration is important for hepatoma cell viability and resistance to radiation-induced oxidative stress. *Free Radical Biology and Medicine*, 47(7):1057–1066.

[Cha et al., 2009] Cha, M.-K., Suh, K.-H., and Kim, I.-H. (2009). Overexpression of peroxiredoxin i and thioredoxin1 in human breast carcinoma. *Journal of Experimental & Clinical Cancer Research*, 28(1):93.

[Chae et al., 1994] Chae, H. Z., Chung, S. J., and Rhee, S. G. (1994). Thioredoxin-dependent peroxide reductase from yeast. *Journal of Biological Chemistry*, 269(44):27670–27678.

[Choi, 2012] Choi, S. (2012). *Encyclopedia of Signaling Molecules*. Springer.

[Clare et al., 1984] Clare, D. A., Horton, H. R., Stabel, T. J., Swaisgood, H. E., and Lecce, J. G. (1984). Tissue distribution of mammalian sulfhydryl oxidase. *Archives of biochemistry and biophysics*, 230(1):138–145.

[Clare et al., 1988] Clare, D. A., Pinnix, I. B., Lecce, J. G., and Horton, H. R. (1988). Purification and properties of sulfhydryl oxidase from bovine pancreas. *Archives of biochemistry and biophysics*, 265(2):351–361.

[Coppock et al., 1998] Coppock, D. L., Cina-Poppe, D., and Gilleran, S. (1998). The quiescin q6 gene (qscn6) is a fusion of two ancient gene families: thioredoxin and erv1. *Genomics*, 54(3):460–468.

[Coppock et al., 1993] Coppock, D. L., Kopman, C., Scandalis, S., and Gilleran, S. (1993). Preferential gene expression in quiescent human lung fibroblasts. *Cell growth and differentiation*, 4:483–483.

[Coppock and Thorpe, 2006] Coppock, D. L. and Thorpe, C. (2006). Multidomain flavin-dependent sulfhydryl oxidases. *Antioxidants & redox signaling*, 8(3-4):300–311.

[Dai et al., 2015] Dai, X., Li, T., Bai, Z., Yang, Y., Liu, X., Zhan, J., and Shi, B. (2015). Breast cancer intrinsic subtype classification, clinical use and future trends. *American journal of cancer research*, 5(10):2929.

[Daithankar et al., 2009] Daithankar, V. N., Farrell, S. R., and Thorpe, C. (2009). Augmenter of liver regeneration: substrate specificity of a flavin-dependent oxidoreductase from the mitochondrial intermembrane space. *Biochemistry*, 48(22):4828–4837.

[Das et al., 2013] Das, P., Siegers, G. M., and Postovit, L.-M. (2013). Illuminating luminal b: Qsox1 as a subtype-specific biomarker. *Breast Cancer Research*, 15(3):104.

[De La Motte and Wagner, 1987] De La Motte, R. S. and Wagner, F. W. (1987). Aspergillus niger sulfhydryl oxidase. *Biochemistry*, 26(23):7363–7371.

[Denko, 2008] Denko, N. C. (2008). Hypoxia, hif1 and glucose metabolism in the solid tumour. *Nature Reviews Cancer*, 8(9):705.

[Dessein et al., 1984] Dessein, A., Lenzi, H., Bina, J. C., Carvalho, E., Weiser, W., Andrade, Z. d. A., and David, J. R. (1984). Modulation of eosinophil cytotoxicity by blood mononuclear cells from healthy subjects and patients with chronic schistosomiasis mansoni. *Cellular immunology*, 85(1):100–113.

[Dias-Gunasekara et al., 2005] Dias-Gunasekara, S., Gubbens, J., van Lith, M., Dunne, C., Williams, J. G., Kataky, R., Scoones, D., Lapthorn, A., Bulleid, N. J., and Benham, A. M. (2005). Tissue-specific expression and dimerization of the endoplasmic reticulum oxidoreductase ero1β. *Journal of Biological Chemistry*, 280(38):33066–33075.

[Dijkman et al., 2013] Dijkman, W. P., de Gonzalo, G., Mattevi, A., and Fraaije, M. W. (2013). Flavoprotein oxidases: classification and applications. *Applied microbiology and biotechnology*, 97(12):5177–5188.

[Dixon et al., 2008] Dixon, B. M., Heath, S.-H. D., Kim, R., Suh, J. H., and Hagen, T. M. (2008). Assessment of endoplasmic reticulum glutathione redox status is confounded by extensive ex vivo oxidation. *Antioxidants & redox signaling*, 10(5):963–972.

[Ema et al., 1999] Ema, M., Hirota, K., Mimura, J., Abe, H., Yodoi, J., Sogawa, K., Poellinger, L., and Fujii-Kuriyama, Y. (1999). Molecular mechanisms of transcription activation by hlf and hif1α in response to hypoxia: their stabilization and redox signal-induced interaction with cbp/p300. *The EMBO journal*, 18(7):1905–1914.

[Endoh et al., 2004] Endoh, H., Tomida, S., Yatabe, Y., Konishi, H., Osada, H., Tajima, K., Kuwano, H., Takahashi, T., and Mitsudomi, T. (2004). Prognostic model of pulmonary adenocarcinoma by expression profiling of eight genes as determined by quantitative real-time reverse transcriptase polymerase chain reaction. *Journal of clinical oncology*, 22(5):811–819.

[Evan and Littlewood, 1998] Evan, G. and Littlewood, T. (1998). A matter of life and cell death. *Science*, 281(5381):1317–1322.

[Ferecatu et al., 2014] Ferecatu, I., Gonçalves, S., Golinelli-Cohen, M.-P., Clémancey, M., Martelli, A., Riquier, S., Guittet, E., Latour, J.-M., Puccio, H., Drapier, J.-C., et al. (2014). The diabetes drug target mitoneet governs a novel trafficking pathway to rebuild an fe-s cluster into cytosolic aconitase/iron regulatory protein 1. *Journal of Biological Chemistry*, 289(41):28070–28086.

[Fetzner and Steiner, 2010] Fetzner, S. and Steiner, R. A. (2010). Cofactor-independent oxidases and oxygenases. *Applied microbiology and biotechnology*, 86(3):791–804.

[Fidler, 2003] Fidler, I. J. (2003). The pathogenesis of cancer metastasis: the'seed and soil'hypothesis revisited. *Nature reviews cancer*, 3(6):453.

[Frand and Kaiser, 1999] Frand, A. R. and Kaiser, C. A. (1999). Ero1p oxidizes protein disulfide isomerase in a pathway for disulfide bond formation in the endoplasmic reticulum. *Molecular cell*, 4(4):469–477.

[Fukumoto et al., 2006] Fukumoto, A., Tomoda, K., Yoneda-Kato, N., Nakajima, Y., and Kato, J.-y. (2006). Depletion of jab1 inhibits proliferation of pancreatic cancer cell lines. *FEBS letters*, 580(25):5836–5844.

[Gerald et al., 2004] Gerald, D., Berra, E., Frapart, Y. M., Chan, D. A., Giaccia, A. J., Mansuy, D., Pouysségur, J., Yaniv, M., and Mechta-Grigoriou, F. (2004). Jund reduces tumor angiogenesis by protecting cells from oxidative stress. *Cell*, 118(6):781–794.

[Gess et al., 2003] Gess, B., Hofbauer, K.-H., Wenger, R. H., Lohaus, C., Meyer, H. E., and Kurtz, A. (2003). The cellular oxygen tension regulates expression of the endoplasmic oxidoreductase ero1-lα. *European journal of biochemistry*, 270(10):2228–2235.

[Gil-Bea et al., 2012] Gil-Bea, F., Akterin, S., Persson, T., Mateos, L., Sandebring, A., Avila-Cariño, J., Gutierrez-Rodriguez, A., Sundström, E., Holmgren, A., Winblad, B., et al. (2012). Thioredoxin-80 is a product of alpha-secretase cleavage that inhibits amyloid-beta aggregation and is decreased in alzheimer's disease brain. *EMBO molecular medicine*, 4(10):1097–1111.

[Gillen et al., 2010] Gillen, S., Schuster, T., Zum Büschenfelde, C. M., Friess, H., and Kleeff, J. (2010). Preoperative/neoadjuvant therapy in pancreatic cancer: a systematic review and meta-analysis of response and resection percentages. *PLoS medicine*, 7(4):e1000267.

[Giorda et al., 1996] Giorda, R., Hagiya, M., Seki, T., Shimonishi, M., Sakai, H., Michaelson, J., Francavilla, A., Starzl, T. E., and Trucco, M. (1996). Analysis of the structure and expression of the augmenter of liver regeneration (alr) gene. *Molecular Medicine*, 2(1):97.

[Global Cancer Observatory, 2018] Global Cancer Observatory (2018). Cancer Today. http://gco.iarc.fr/today/fact-sheets-cancers. [Online; accessed 25-April-2019].

[Go and Jones, 2010] Go, Y.-M. and Jones, D. P. (2010). Redox control systems in the nucleus: mechanisms and functions. *Antioxidants & redox signaling*, 13(4):489–509.

[Goldsmith, 1987] Goldsmith, L. A. (1987). Sulfhydryl oxidase from rat skin. In *Methods in enzymology*, volume 143, pages 510–515. Elsevier.

[Griffiths and Olin, 2012] Griffiths, C. L. and Olin, J. L. (2012). Triple negative breast cancer: a brief review of its characteristics and treatment options. *Journal of pharmacy practice*, 25(3):319–323.

[Gross et al., 2006] Gross, E., Sevier, C. S., Heldman, N., Vitu, E., Bentzur, M., Kaiser, C. A., Thorpe, C., and Fass, D. (2006). Generating disulfides enzymatically: reaction products and electron acceptors of the endoplasmic reticulum thiol oxidase ero1p. *Proceedings of the National Academy of Sciences*, 103(2):299–304.

[Grumbt et al., 2007] Grumbt, B., Stroobant, V., Terziyska, N., Israel, L., and Hell, K. (2007). Functional characterization of mia40p, the central component of the disulfide relay system of the mitochondrial intermembrane space. *Journal of Biological Chemistry*, 282(52):37461–37470.

[Guo et al., 2006] Guo, M., Song, L.-P., Jiang, Y., Liu, W., Yu, Y., and Chen, G.-Q. (2006). Hypoxia-mimetic agents desferrioxamine and cobalt chloride induce leukemic cell apoptosis through different hypoxia-inducible factor-1α independent mechanisms. *Apoptosis*, 11(1):67–77.

[Gupta and Venugopal, 2018] Gupta, P. and Venugopal, S. K. (2018). Augmenter of liver regeneration: A key protein in liver regeneration and pathophysiology. *Hepatology Research*, 48(8):587–596.

[Han et al., 2018] Han, L., Jiang, J., Ma, Q., Wu, Z., and Wang, Z. (2018). The inhibition of heme oxygenase-1 enhances the chemosensitivity and suppresses the proliferation of pancreatic cancer cells through the shh signaling pathway. *International journal of oncology*, 52(6):2101–2109.

[Hanahan and Folkman, 1996] Hanahan, D. and Folkman, J. (1996). Patterns and emerging mechanisms of the angiogenic switch during tumorigenesis. *cell*, 86(3):353–364.

[Hanahan and Weinberg, 2000] Hanahan, D. and Weinberg, R. A. (2000). The hallmarks of cancer. *cell*, 100(1):57–70.

[Hanahan and Weinberg, 2011] Hanahan, D. and Weinberg, R. A. (2011). Hallmarks of cancer: the next generation. *cell*, 144(5):646–674.

[Hanavan et al., 2015] Hanavan, P. D., Borges, C. R., Katchman, B. A., Faigel, D. O., Ho, T. H., Ma, C.-T., Sergienko, E. A., Meurice, N., Petit, J. L., and Lake, D. F. (2015). Ebselen inhibits qsox1 enzymatic activity and suppresses invasion of pancreatic and renal cancer cell lines. *Oncotarget*, 6(21):18418.

[Hanschmann et al., 2013] Hanschmann, E.-M., Godoy, J. R., Berndt, C., Hudemann, C., and Lillig, C. H. (2013). Thioredoxins, glutaredoxins, and peroxiredoxins—molecular mechanisms and health significance: from cofactors to antioxidants to redox signaling. *Antioxidants & redox signaling*, 19(13):1539–1605.

[Hayashi et al., 1997] Hayashi, S.-i., Hajiro-Nakanishi, K., Makino, Y., Eguchi, H., Yodoi, J., and Tanaka, H. (1997). Functional modulation of estrogen receptor by redox state with reference to thioredoxin as a mediator. *Nucleic acids research*, 25(20):4035–4040.

[Heckler et al., 2008] Heckler, E. J., Rancy, P. C., Kodali, V. K., and Thorpe, C. (2008). Generating disulfides with the quiescin-sulfhydryl oxidases. *Biochimica et Biophysica Acta (BBA)-Molecular Cell Research*, 1783(4):567–577.

[Hellebrekers et al., 2007] Hellebrekers, D. M., Melotte, V., Viré, E., Langenkamp, E., Molema, G., Fuks, F., Herman, J. G., Van Criekinge, W., Griffioen, A. W., and Van Engeland, M. (2007). Identification of epigenetically silenced genes in tumor endothelial cells. *Cancer research*, 67(9):4138–4148.

[Hirota et al., 1999] Hirota, K., Murata, M., Sachi, Y., Nakamura, H., Takeuchi, J., Mori, K., and Yodoi, J. (1999). Distinct roles of thioredoxin in the cytoplasm and in the nucleus a two-step mechanism of redox regulation of transcription factor nf-κb. *Journal of Biological Chemistry*, 274(39):27891–27897.

[Hoober et al., 1999a] Hoober, K. L., Glynn, N. M., Burnside, J., Coppock, D. L., and Thorpe, C. (1999a). Homology between egg white sulfhydryl oxidase and quiescin q6 defines a new class of flavin-linked sulfhydryl oxidases. *Journal of Biological Chemistry*, 274(45):31759–31762.

[Hoober et al., 1996] Hoober, K. L., Joneja, B., White, H. B., and Thorpe, C. (1996). A sulfhydryl oxidase from chicken egg white. *Journal of Biological Chemistry*, 271(48):30510–30516.

[Hoober et al., 1999b] Hoober, K. L., Sheasley, S. L., Gilbert, H. F., and Thorpe, C. (1999b). Sulfhydryl oxidase from egg white a facile catalyst for disulfide bond formation in proteins and peptides. *Journal of Biological Chemistry*, 274(32):22147–22150.

[Horowitz et al., 2018] Horowitz, B., Javitt, G., Ilani, T., Gat, Y., Morgenstern, D., Bard, F. A., and Fass, D. (2018). Quiescin sulfhydryl oxidase 1 (qsox1) glycosite mutation perturbs secretion but not golgi localization. *Glycobiology*, 1:12.

[Hwang et al., 1992] Hwang, C., Sinskey, A. J., and Lodish, H. F. (1992). Oxidized redox state of glutathione in the endoplasmic reticulum. *Science*, 257(5076):1496–1502.

[Ilani et al., 2013] Ilani, T., Alon, A., Grossman, I., Horowitz, B., Kartvelishvily, E., Cohen, S. R., and Fass, D. (2013). A secreted disulfide catalyst controls extracellular matrix composition and function. *Science*, 341(6141):74–76.

[Ingles-Prieto et al., 2013] Ingles-Prieto, A., Ibarra-Molero, B., Delgado-Delgado, A., Perez-Jimenez, R., Fernandez, J. M., Gaucher, E. A., Sanchez-Ruiz, J. M., and Gavira, J. A. (2013). Conservation of protein structure over four billion years. *Structure*, 21(9):1690–1697.

[Isaacs et al., 1984] Isaacs, C. E., Pascal, T., Wright, C. E., and Gaull, G. E. (1984). Sulfhydryl oxidase in human milk: stability of milk enzymes in the gastrointestinal tract. *Pediatric research*, 18(6):532.

[Janolino and Swaisgood, 1975] Janolino, V. G. and Swaisgood, H. E. (1975). Isolation and characterization of sulfhydryl oxidase from bovine milk. *Journal of Biological Chemistry*, 250(7):2532–2538.

[Kamisawa et al., 1995] Kamisawa, T., Isawa, T., Koike, M., Tsuruta, K., and Okamoto, A. (1995). Hematogenous metastases of pancreatic ductal carcinoma. *Pancreas*, 11(4):345–349.

[Katchman et al., 2011] Katchman, B. A., Antwi, K., Hostetter, G., Demeure, M. J., Watanabe, A., Decker, G. A., Miller, L. J., Von Hoff, D. D., and Lake, D. F. (2011). Quiescin sulfhydryl oxidase 1 promotes invasion of pancreatic tumor cells mediated by matrix metalloproteinases. *Molecular Cancer Research*, 9(12):1621–1631.

[Katchman et al., 2013] Katchman, B. A., Ocal, I. T., Cunliffe, H. E., Chang, Y.-H., Hostetter, G., Watanabe, A., LoBello, J., and Lake, D. F. (2013). Expression of quiescin sulfhydryl oxidase 1 is associated with a highly invasive phenotype and correlates with a poor prognosis in luminal b breast cancer. *Breast Cancer Research*, 15(2):R28.

[Kiermeier and Petz, 1967] Kiermeier, F. and Petz, E. (1967). An enzyme in milk which oxidizes sulphydryl groups. i. isolation and characterization of the enzyme. *Z. Lebensm. Unters. Forsch*, 132:342–352.

[Knutsvik et al., 2016] Knutsvik, G., Collett, K., Arnes, J., Akslen, L. A., and Stefansson, I. M. (2016). Qsox1 expression is associated with aggressive tumor features and reduced survival in breast carcinomas. *Modern Pathology*, 29(12):1485–1491.

[Köhrmann et al., 2009] Köhrmann, A., Kammerer, U., Kapp, M., Dietl, J., and Anacker, J. (2009). Expression of matrix metalloproteinases (mmps) in primary human breast cancer and breast cancer cell lines: New findings and review of the literature. *BMC cancer*, 9(1):188.

[Kusakabe et al., 1982] Kusakabe, H., Kuninaka, A., and Yoshino, H. (1982). Purification and properties of a new enzyme, glutathione oxidase from penicillium sp. k-6-5. *Agricultural and Biological Chemistry*, 46(8):2057–2067.

[LaBrecque and Pesch, 1975] LaBrecque, D. R. and Pesch, L. A. (1975). Preparation and partial characterization of hepatic regenerative stimulator substance (ss) from rat liver. *The Journal of physiology*, 248(2):273–284.

[Lake et al., 2016] Lake, D., Katchman, B., and Fass, D. (2016). Qsox1 as an anti-neoplastic drug target. US Patent App. 14/849,013.

[Lake and Faigel, 2014] Lake, D. F. and Faigel, D. O. (2014). The emerging role of qsox1 in cancer. *Antioxidants & redox signaling*, 21(3):485–496.

[Larsson et al., 1983] Larsson, A., Orrenius, S., Holmgren, A., and Mannervik, B. (1983). Functions of glutathione. *Biochemical, Physiological, Toxicological and Clinical Aspects (Raven, New York)*.

[Lash and Jones, 1983] Lash, L. H. and Jones, D. P. (1983). Characterization of the membrane-associated thiol oxidase activity of rat small-intestinal epithelium. *Archives of biochemistry and biophysics*, 225(1):344–352.

[Lash and Jones, 1986] Lash, L. H. and Jones, D. P. (1986). Purification and properties of the membranal thiol oxidase from porcine kidney. *Archives of biochemistry and biophysics*, 247(1):120–130.

[Lemarechal et al., 2007] Lemarechal, H., Anract, P., Beaudeux, J.-L., Bonnefont-Rousselot, D., Ekindjian, O. G., and Borderie, D. (2007). Expression and extracellular release of trx80, the truncated form of thioredoxin, by tnf-α-and il-1β-stimulated human synoviocytes from patients with rheumatoid arthritis. *Clinical Science*, 113(3):149–155.

[Levine and Kroemer, 2008] Levine, B. and Kroemer, G. (2008). Autophagy in the pathogenesis of disease. *Cell*, 132(1):27–42.

[Li et al., 2002] Li, Y., Wei, K., Lu, C., Li, Y., Li, M., Xing, G., Wei, H., Wang, Q., Chen, J., Wu, C., et al. (2002). Identification of hepatopoietin dimerization, its interacting regions and alternative splicing of its transcription. *European journal of biochemistry*, 269(16):3888–3893.

[Lisowsky, 1992] Lisowsky, T. (1992). Dual function of a new nuclear gene for oxidative phosphorylation and vegetative growth in yeast. *Molecular and General Genetics MGG*, 232(1):58–64.

[Liu et al., 2004] Liu, Q., Yu, H.-F., Sun, H., and Ma, H.-F. (2004). Expression of human augmenter of liver regeneration in pichia pastoris yeast and its bioactivity in vitro. *World Journal of Gastroenterology: WJG*, 10(21):3188.

[Mahmood et al., 2013] Mahmood, D. F. D., Abderrazak, A., El Hadri, K., Simmet, T., and Rouis, M. (2013). The thioredoxin system as a therapeutic target in human health and disease. *Antioxidants & redox signaling*, 19(11):1266–1303.

[Marciniak et al., 2004] Marciniak, S. J., Yun, C. Y., Oyadomari, S., Novoa, I., Zhang, Y., Jungreis, R., Nagata, K., Harding, H. P., and Ron, D. (2004). Chop induces death by promoting protein synthesis and oxidation in the stressed endoplasmic reticulum. *Genes & development*, 18(24):3066–3077.

[May et al., 2005] May, D., Itin, A., Gal, O., Kalinski, H., Feinstein, E., and Keshet, E. (2005). Ero1-lα plays a key role in a hif-1-mediated pathway to improve disulfide bond formation and vegf secretion under hypoxia: implication for cancer. *Oncogene*, 24(6):1011.

[McMahon et al., 2005] McMahon, S., Grondin, F., McDonald, P. P., Richard, D. E., and Dubois, C. M. (2005). Hypoxia-enhanced expression of the proprotein convertase furin is mediated by hypoxia-inducible factor-1 impact on the bioactivation of proproteins. *Journal of Biological Chemistry*, 280(8):6561–6569.

[Miranda-Vizuete et al., 2001] Miranda-Vizuete, A., Ljung, J., Damdimopoulos, A. E., Gustafsson, J.-Å., Oko, R., Pelto-Huikko, M., and Spyrou, G. (2001). Characterization of sptrx, a novel member of the thioredoxin family specifically expressed in human spermatozoa. *Journal of Biological Chemistry*, 276(34):31567–31574.

[Mitchell and Marletta, 2005] Mitchell, D. A. and Marletta, M. A. (2005). Thioredoxin catalyzes the s-nitrosation of the caspase-3 active site cysteine. *Nature chemical biology*, 1(3):154.

[Mitsui et al., 2002] Mitsui, A., Hamuro, J., Nakamura, H., Kondo, N., Hirabayashi, Y., Ishizaki-Koizumi, S., Hirakawa, T., Inoue, T., and Yodoi, J. (2002). Overexpression of human thioredoxin in transgenic mice controls oxidative stress and life span. *Antioxidants and Redox Signaling*, 4(4):693–696.

[Moenner et al., 2007] Moenner, M., Pluquet, O., Bouchecareilh, M., and Chevet, E. (2007). Integrated endoplasmic reticulum stress responses in cancer. *Cancer research*, 67(22):10631–10634.

[Morel et al., 2007] Morel, C., Adami, P., Musard, J.-F., Duval, D., Radom, J., and Jouvenot, M. (2007). Involvement of sulfhydryl oxidase qsox1 in the protection of cells against oxidative stress-induced apoptosis. *Experimental cell research*, 313(19):3971–3982.

[Musard et al., 2001] Musard, J.-F., Sallot, M., Dulieu, P., Fraîchard, A., Ordener, C., Remy-Martin, J.-P., Jouvenot, M., and Adami, P. (2001). Identification and expression of a new sulfhydryl oxidase sox-3 during the cell cycle and the estrus cycle in uterine cells. *Biochemical and biophysical research communications*, 287(1):83–91.

[Nguyen et al., 2017] Nguyen, K. H., Nguyen, A. H., and Dabir, D. V. (2017). Clinical implications of augmenter of liver regeneration in cancer: A systematic review. *Anticancer research*, 37(7):3379–3383.

[Organization et al., 2014] Organization, W. H. et al. (2014). Global status report on noncommunicable diseases 2014. Technical report, World Health Organization.

[Ormstad et al., 1979] Ormstad, K., Moldéus, P., and Orrenius, S. (1979). Partial characterization of a glutathione oxidase present in rat kidney plasma membrane fraction. *Biochemical and biophysical research communications*, 89(2):497–503.

[Ostrowski and Kistler, 1980] Ostrowski, M. C. and Kistler, W. (1980). Properties of a flavoprotein sulfhydryl oxidase from rat seminal vesicle secretion. *Biochemistry*, 19(12):2639–2645.

[Otsu et al., 2006] Otsu, M., Bertoli, G., Fagioli, C., Guerini-Rocco, E., Nerini-Molteni, S., Ruffato, E., and Sitia, R. (2006). Dynamic retention of ero1α and ero1β in the endoplasmic reticulum by interactions with pdi and erp44. *Antioxidants & redox signaling*, 8(3-4):274–282.

[Pagani et al., 2000] Pagani, M., Fabbri, M., Benedetti, C., Fassio, A., Pilati, S., Bulleid, N. J., Cabibbo, A., and Sitia, R. (2000). Endoplasmic reticulum oxidoreductin 1-lβ (ero1-lβ), a human gene induced in the course of the unfolded protein response. *Journal of Biological Chemistry*, 275(31):23685–23692.

[Pagani et al., 2001] Pagani, M., Pilati, S., Bertoli, G., Valsasina, B., and Sitia, R. (2001). The c-terminal domain of yeast ero1p mediates membrane localization and is essential for function. *FEBS letters*, 508(1):117–120.

[Pani et al., 2010] Pani, G., Galeotti, T., and Chiarugi, P. (2010). Metastasis: cancer cell's escape from oxidative stress. *Cancer and Metastasis Reviews*, 29(2):351–378.

[Pernodet et al., 2012] Pernodet, N., Hermetet, F., Adami, P., Vejux, A., Descotes, F., Borg, C., Adams, M., Pallandre, J.-R., Viennet, G., Esnard, F., et al. (2012). High expression of qsox1 reduces tumorogenesis, and is associated with a better outcome for breast cancer patients. *Breast Cancer Research*, 14(5):R136.

[Pollard et al., 1998] Pollard, M. G., Travers, K. J., and Weissman, J. S. (1998). Ero1p: a novel and ubiquitous protein with an essential role in oxidative protein folding in the endoplasmic reticulum. *Molecular cell*, 1(2):171–182.

[Prat and Perou, 2011] Prat, A. and Perou, C. M. (2011). Deconstructing the molecular portraits of breast cancer. *Molecular oncology*, 5(1):5–23.

[Raffel et al., 2003] Raffel, J., Bhattacharyya, A. K., Gallegos, A., Cui, H., Einspahr, J. G., Alberts, D. S., and Powis, G. (2003). Increased expression of thioredoxin-1 in human colorectal cancer is associated with decreased patient survival. *Journal of Laboratory and Clinical Medicine*, 142(1):46–51.

[Rancy and Thorpe, 2008] Rancy, P. C. and Thorpe, C. (2008). Oxidative protein folding in vitro: a study of the cooperation between quiescin-sulfhydryl oxidase and protein disulfide isomerase. *Biochemistry*, 47(46):12047–12056.

[Ridge et al., 2008] Ridge, P. G., Zhang, Y., and Gladyshev, V. N. (2008). Comparative genomic analyses of copper transporters and cuproproteomes reveal evolutionary dynamics of copper utilization and its link to oxygen. *PLoS One*, 3(1):e1378.

[Rofstad et al., 2006] Rofstad, E. K., Mathiesen, B., Kindem, K., and Galappathi, K. (2006). Acidic extracellular ph promotes experimental metastasis of human melanoma cells in athymic nude mice. *Cancer research*, 66(13):6699–6707.

[Ron and Walter, 2007] Ron, D. and Walter, P. (2007). Signal integration in the endoplasmic reticulum unfolded protein response. *Nature reviews Molecular cell biology*, 8(7):519.

[Roth and Koshland, 1981] Roth, R. and Koshland, M. E. (1981). Identification of a lymphocyte enzyme that catalyzes pentamer immunoglobulin m assembly. *Journal of Biological Chemistry*, 256(9):4633–4639.

[Rouault, 2016] Rouault, T. A. (2016). Mitochondrial iron overload: causes and consequences. *Current opinion in genetics & development*, 38:31–37.

[Rudolf et al., 2013] Rudolf, J., Pringle, M. A., and Bulleid, N. J. (2013). Proteolytic processing of qsox1a ensures efficient secretion of a potent disulfide catalyst. *Biochemical Journal*, 454(2):181–190.

[Rychtarcikova et al., 2017] Rychtarcikova, Z., Lettlova, S., Tomkova, V., Korenkova, V., Langerova, L., Simonova, E., Zjablovskaja, P., Alberich-Jorda, M., Neuzil, J., and Truksa, J. (2017). Tumor-initiating cells of breast and prostate origin show alterations in the expression of genes related to iron metabolism. *Oncotarget*, 8(4):6376.

[Saitoh et al., 1998] Saitoh, M., Nishitoh, H., Fujii, M., Takeda, K., Tobiume, K., Sawada, Y., Kawabata, M., Miyazono, K., and Ichijo, H. (1998). Mammalian thioredoxin is a direct inhibitor of apoptosis signal-regulating kinase (ask) 1. *The EMBO journal*, 17(9):2596–2606.

[Sankar and Means, 2011] Sankar, U. and Means, A. R. (2011). Gfer is a critical regulator of hsc proliferation. *Cell Cycle*, 10(14):2263–2268.

[Schmelzer et al., 1982] Schmelzer, C. H., Swaisgood, H. E., and Horton, H. R. (1982). Resolution of renal sulfhydryl oxidase from γ-glutamyltransferase by covalent chromatography on cysteinylsuccinamidopropyl-glass. *Biochemical and biophysical research communications*, 107(1):196–201.

[Schroeder et al., 2007] Schroeder, P., Popp, R., Wiegand, B., Altschmied, J., and Haendeler, J. (2007). Nuclear redox-signaling is essential for apoptosis inhibition in endothelial cells—important role for nuclear thioredoxin-1. *Arteriosclerosis, thrombosis, and vascular biology*, 27(11):2325–2331.

[Sevier and Kaiser, 2002] Sevier, C. S. and Kaiser, C. A. (2002). Formation and transfer of disulphide bonds in living cells. *Nature reviews Molecular cell biology*, 3(11):836–847.

[Sevier and Kaiser, 2007] Sevier, C. S. and Kaiser, C. A. (2007). Ero1 and redox homeostasis in the endoplasmic reticulum. *Biochimica et Biophysica Acta (BBA)-Molecular Cell Research*, 1783(4):549–556.

[Sevier et al., 2007] Sevier, C. S., Qu, H., Heldman, N., Gross, E., Fass, D., and Kaiser, C. A. (2007). Modulation of cellular disulfide-bond formation and the er redox environment by feedback regulation of ero1. *Cell*, 129(2):333–344.

[Sherr and McCormick, 2002] Sherr, C. J. and McCormick, F. (2002). The rb and p53 pathways in cancer. *Cancer cell*, 2(2):103–112.

[Shi et al., 2013] Shi, C.-Y., Fan, Y., Liu, B., and Lou, W.-H. (2013). Hif1 contributes to hypoxia-induced pancreatic cancer cells invasion via promoting qsox1 expression. *Cellular Physiology and Biochemistry*, 32(3):561–568.

[Siegel et al., 2014] Siegel, R., Ma, J., Zou, Z., and Jemal, A. (2014). Cancer statistics, 2014. *CA: a cancer journal for clinicians*, 64(1):9–29.

[Simstein et al., 2003] Simstein, R., Burow, M., Parker, A., Weldon, C., and Beckman, B. (2003). Apoptosis, chemoresistance, and breast cancer: insights from the mcf-7 cell model system. *Experimental biology and medicine*, 228(9):995–1003.

[Skogastierna et al., 2012] Skogastierna, C., Johansson, M., Parini, P., Eriksson, M., Eriksson, L. C., Ekström, L., and Björkhem-Bergman, L. (2012). Statins inhibit expression of thioredoxin reductase 1 in rat and human liver and reduce tumour development. *Biochemical and biophysical research communications*, 417(3):1046–1051.

[Soloviev et al., 2013] Soloviev, M., Esteves, M. P., Amiri, F., Crompton, M. R., and Rider, C. C. (2013). Elevated transcription of the gene qsox1 encoding quiescin q6 sulfhydryl oxidase 1 in breast cancer. *PloS one*, 8(2):e57327.

[Sørlie et al., 2003] Sørlie, T., Tibshirani, R., Parker, J., Hastie, T., Marron, J. S., Nobel, A., Deng, S., Johnsen, H., Pesich, R., Geisler, S., et al. (2003). Repeated observation of breast tumor subtypes in independent gene expression data sets. *Proceedings of the national academy of sciences*, 100(14):8418–8423.

[Steeg, 2006] Steeg, P. S. (2006). Tumor metastasis: mechanistic insights and clinical challenges. *Nature medicine*, 12(8):895.

[Stewart et al., 2014] Stewart, B., Wild, C. P., et al. (2014). World cancer report 2014.

[Tang et al., 2009] Tang, L., Sun, H., Zhang, L., Deng, J. C., Guo, H., Zhang, L., and Liu, Q. (2009). Effects of the augmenter of liver regeneration on the biological behavior of hepatocellular carcinoma. *Saudi medical journal*, 30(8):1001–1009.

[Tavender and Bulleid, 2010] Tavender, T. J. and Bulleid, N. J. (2010). Molecular mechanisms regulating oxidative activity of the ero1 family in the endoplasmic reticulum. *Antioxidants & redox signaling*, 13(8):1177–1187.

[Tavender et al., 2008] Tavender, T. J., Sheppard, A. M., and Bulleid, N. J. (2008). Peroxiredoxin iv is an endoplasmic reticulum-localized enzyme forming oligomeric complexes in human cells. *Biochemical Journal*, 411(1):191–199.

[Teng et al., 2011] Teng, E. C., Todd, L. R., Ribar, T. J., Lento, W., Dimascio, L., Means, A. R., and Sankar, U. (2011). Gfer inhibits jab1-mediated degradation of p27kip1 to restrict proliferation of hematopoietic stem cells. *Molecular biology of the cell*, 22(8):1312–1320.

[Thorpe et al., 2002] Thorpe, C., Hoober, K. L., Raje, S., Glynn, N. M., Burnside, J., Turi, G. K., and Coppock, D. L. (2002). Sulfhydryl oxidases: emerging catalysts of protein disulfide bond formation in eukaryotes. *Archives of biochemistry and biophysics*, 405(1):1–12.

[Todd et al., 2010] Todd, L. R., Damin, M. N., Gomathinayagam, R., Horn, S. R., Means, A. R., and Sankar, U. (2010). Growth factor erv1-like modulates drp1 to preserve mitochondrial dynamics and function in mouse embryonic stem cells. *Molecular biology of the cell*, 21(7):1225–1236.

[Tu et al., 2000] Tu, B. P., Ho-Schleyer, S. C., Travers, K. J., and Weissman, J. S. (2000). Biochemical basis of oxidative protein folding in the endoplasmic reticulum. *Science*, 290(5496):1571–1574.

[Tu and Weissman, 2004] Tu, B. P. and Weissman, J. S. (2004). Oxidative protein folding in eukaryotes: mechanisms and consequences. *The Journal of cell biology*, 164(3):341–346.

[Turi et al., 2001] Turi, G., Harrison, G., Singh, S., and Coppock, D. (2001). The distribution and specificity of expression of quiescin q6 (q6) in human tissues is associated with both endocrine and non-endocrine protein secretion. 42:74.

[Tury et al., 2005] Tury, A., Mairet-Coello, G., Lisowsky, T., Griffond, B., and Fellmann, D. (2005). Expression of the sulfhydryl oxidase alr (augmenter of liver regeneration) in adult rat brain. *Brain research*, 1048(1-2):87–97.

[Tury et al., 2004] Tury, A., Mairet-Coello, G., Poncet, F., Jacquemard, C., Risold, P., Fellmann, D., and Griffond, B. (2004). Qsox sulfhydryl oxidase in rat adenohypophysis: localization and regulation by estrogens. *Journal of endocrinology*, 183(2):353–363.

[Ueno et al., 1999] Ueno, M., Masutani, H., Arai, R. J., Yamauchi, A., Hirota, K., Sakai, T., Inamoto, T., Yamaoka, Y., Yodoi, J., and Nikaido, T. (1999). Thioredoxin-dependent redox regulation of p53-mediated p21 activation. *Journal of Biological Chemistry*, 274(50):35809–35815.

[UniProt, 2019] UniProt (2019). UniProtKB - Q96HE7 (ERO1 - HUMAN). https://www.uniprot.org/uniprot/Q96HE7. [Online; accessed 24-April-2019].

[Vallejos et al., 2010] Vallejos, C. S., Gómez, H. L., Cruz, W. R., Pinto, J. A., Dyer, R. R., Velarde, R., Suazo, J. F., Neciosup, S. P., León, M., Miguel, A., et al. (2010). Breast cancer classification according to immunohistochemistry markers: subtypes and association with clinicopathologic variables in a peruvian hospital database. *Clinical breast cancer*, 10(4):294–300.

[Wang et al., 1999] Wang, G., Yang, X., Zhang, Y., Wang, Q., Chen, H., Wei, H., Xing, G., Xie, L., Hu, Z., Zhang, C., et al. (1999). Identification and characterization of receptor for mammalian hepatopoietin that is homologous to yeast erv1. *Journal of Biological Chemistry*, 274(17):11469–11472.

[Welsh et al., 2002] Welsh, S. J., Bellamy, W. T., Briehl, M. M., and Powis, G. (2002). The redox protein thioredoxin-1 (trx-1) increases hypoxia-inducible factor 1α protein expression: Trx-1 overexpression results in increased vascular endothelial growth factor production and enhanced tumor angiogenesis. *Cancer research*, 62(17):5089–5095.

[Witsch et al., 2010] Witsch, E., Sela, M., and Yarden, Y. (2010). Roles for growth factors in cancer progression. *Physiology*, 25(2):85–101.

[World Health Organisation, 2018] World Health Organisation (2018). Cancer key facts. https://www.who.int/en/news-room/fact-sheets/detail/cancer. [Online; accessed 24-April-2019].

[Zito, 2015] Zito, E. (2015). Ero1: A protein disulfide oxidase and h2o2 producer. *Free Radical Biology and Medicine*, 83:299–304.

[Zito et al., 2010] Zito, E., Melo, E. P., Yang, Y., Wahlander, Å., Neubert, T. A., and Ron, D. (2010). Oxidative protein folding by an endoplasmic reticulum-localized peroxiredoxin. *Molecular cell*, 40(5):787–797.

Appendices

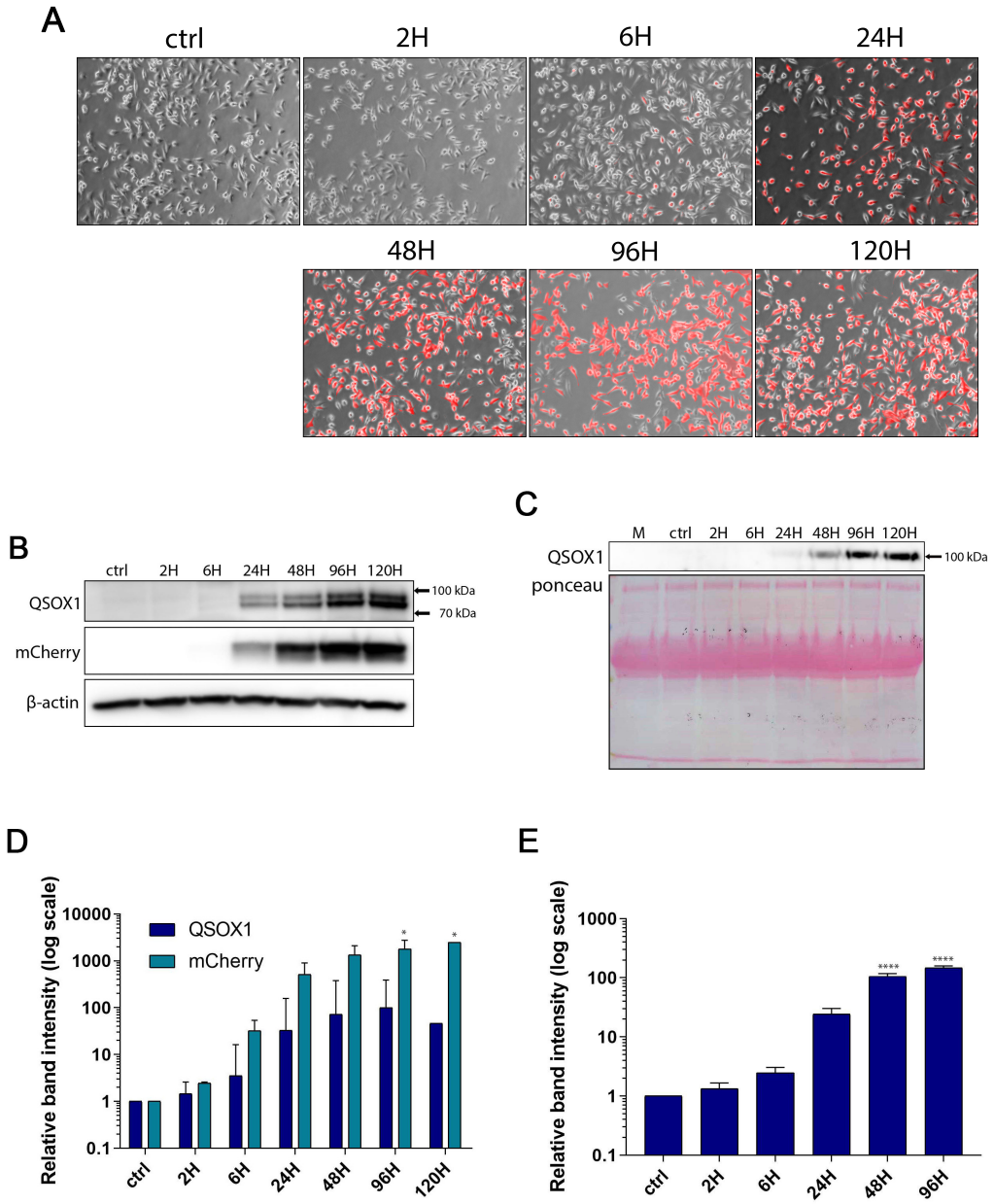

Figure S1: **QSOX1 induction in *QSOX1*-overexpressing clone Cl14. A** Merged images of fluorescent and brightfield pictures of mCherry expression in different time-points during DOX incubation as a substitute for QSOX1 protein induction. Pictures were taken with fluorescent microscope Leica400 after 120 hours of incubation with (2H-120H) or without (ctrl) 250 ng/ml of DOX, and modified in Photoshop software; **B** QSOX1 protein induction after DOX addition in cell lysate. 50 µg of total protein from cell lysate was separated by reducing SDS-PAGE followed by Western blotting, β-actin was used as a loading control; **C** QSOX1 protein induction after DOX addition in conditioned medium. 20 µl of centrifuged cell medium was separated by reducing SDS-PAGE followed by Western blotting, ponceau S was used as a loading control; densitometry of QSOX1 and mCherry protein induction after DOX addition in cell lysate **D** and conditioned media **E**. Cells were seeded with the same starting confluence ($3.33 \cdot 10^3$ cells/cm^2) on petri dishes and 250 ng/ml of DOX was added in appropriate time-points to appropriate dishes. **ctrl** refers to not treated MDA-MB-231 cells, **M** refers to free complete medium without cells. Statistical significance in D and E was assessed by two-way ANOVA test by means of GraphPad PRISM software. Ns: $p > 0.05$, *: ≤ 0.05, **: ≤ 0.01, *** ≤ 0.001 and **** < 0.0001. Data are shown as geomean $\pm$ SEM (n=3 for all samples except for 120 hours where n=1).

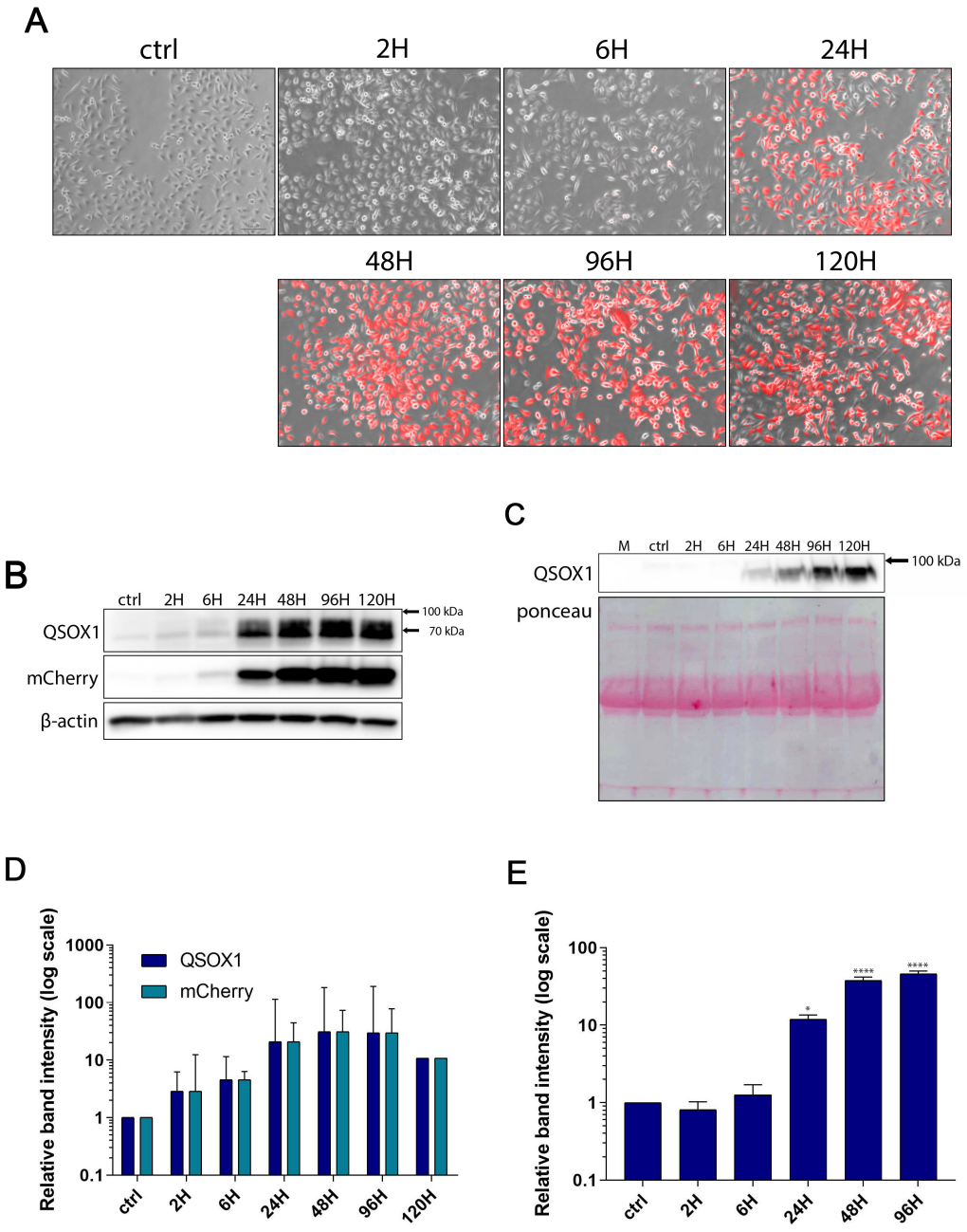

Figure S2: **QSOX1 induction in *QSOX1*-overexpressing clone Cl41. A** Merged images of fluorescent and brightfield pictures of mCherry expression in different time-points during DOX incubation as a substitute for QSOX1 protein induction. Pictures were taken with fluorescent microscope Leica400 after 120 hours of incubation with (2H-120H) or without (ctrl) 250 ng/ml of DOX, and modified in Photoshop software; **B** QSOX1 protein induction after DOX addition in cell lysate. 50 µg of total protein from cell lysate was separated by reducing SDS-PAGE followed by Western blotting, β-actin was used as a loading control; **C** QSOX1 protein induction after DOX addition in conditioned medium. 20 µl of centrifuged cell medium was separated by reducing SDS-PAGE followed by Western blotting, ponceau S was used as a loading control; densitometry of QSOX1 and mCherry protein induction after DOX addition in cell lysate **D** and conditioned media **E**. Cells were seeded with the same starting confluence ($3.33 \cdot 10^3$ cells/cm^2) on petri dishes and 250 ng/ml of DOX was added in appropriate time-points to appropriate dishes. **ctrl** refers to not treated MDA-MB-231 cells, **M** refers to free complete medium without cells. Statistical significance in d) and e) was assessed by two-way ANOVA test by means of GraphPad PRISM software. Ns: $p > 0.05$, *: ≤ 0.05, **: ≤ 0.01, *** ≤ 0.001 and **** < 0.0001. Data are shown as geomean $\pm$ SEM (n=3 for all samples except for 120 hours where n=1).

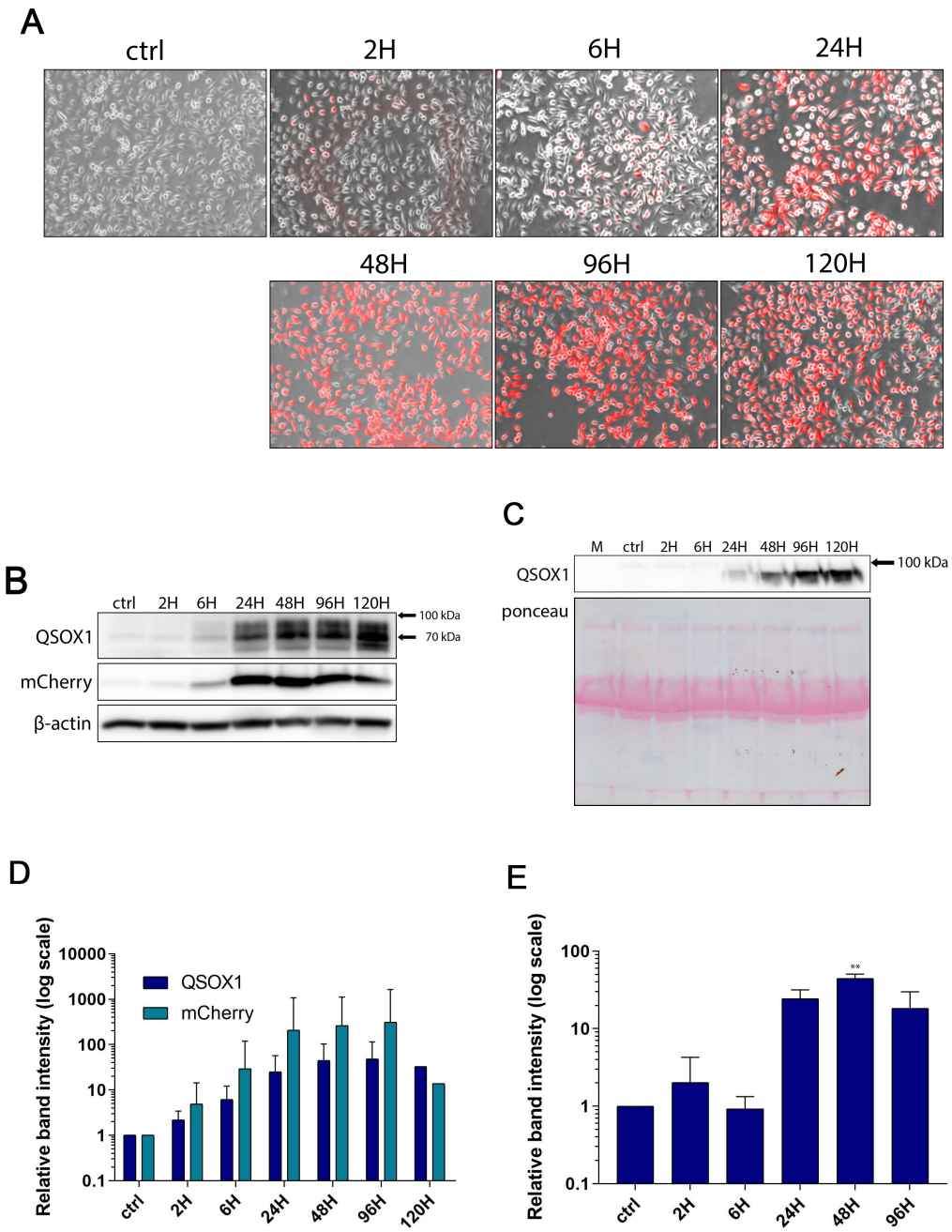

Figure S3: **QSOX1 induction in *QSOX1*-overexpressing clone Cl47. A** Merged images of fluorescent and brightfield pictures of mCherry expression in different time-points during DOX incubation as a substitute for QSOX1 protein induction. Pictures were taken with fluorescent microscope Leica400 after 120 hours of incubation with (2H-120H) or without (ctrl) 250 ng/ml of DOX, and modified in Photoshop software; **B** QSOX1 protein induction after DOX addition in cell lysate. 50 µg of total protein from cell lysate was separated by reducing SDS-PAGE followed by Western blotting, β-actin was used as a loading control; **C** QSOX1 protein induction after DOX addition in conditioned medium. 20 µl of centrifuged cell medium was separated by reducing SDS-PAGE followed by Western blotting, ponceau S was used as a loading control; densitometry of QSOX1 and mCherry protein induction after DOX addition in cell lysate **D** and conditioned media **E**. Cells were seeded with the same starting confluence ($3.33 \cdot 10^3$ cells/cm^2) on petri dishes and 250 ng/ml of DOX was added in appropriate time-points to appropriate dishes. **ctrl** refers to not treated MDA-MB-231 cells, **M** refers to free complete medium without cells. Statistical significance in d) and e) was assessed by two-way ANOVA test by means of GraphPad PRISM software. Ns: $p > 0.05$, *: ≤ 0.05, **: ≤ 0.01, *** ≤ 0.001 and **** < 0.0001. Data are shown as geomean $\pm$ SEM (n=3 for all samples except for 120 hours where n=1).

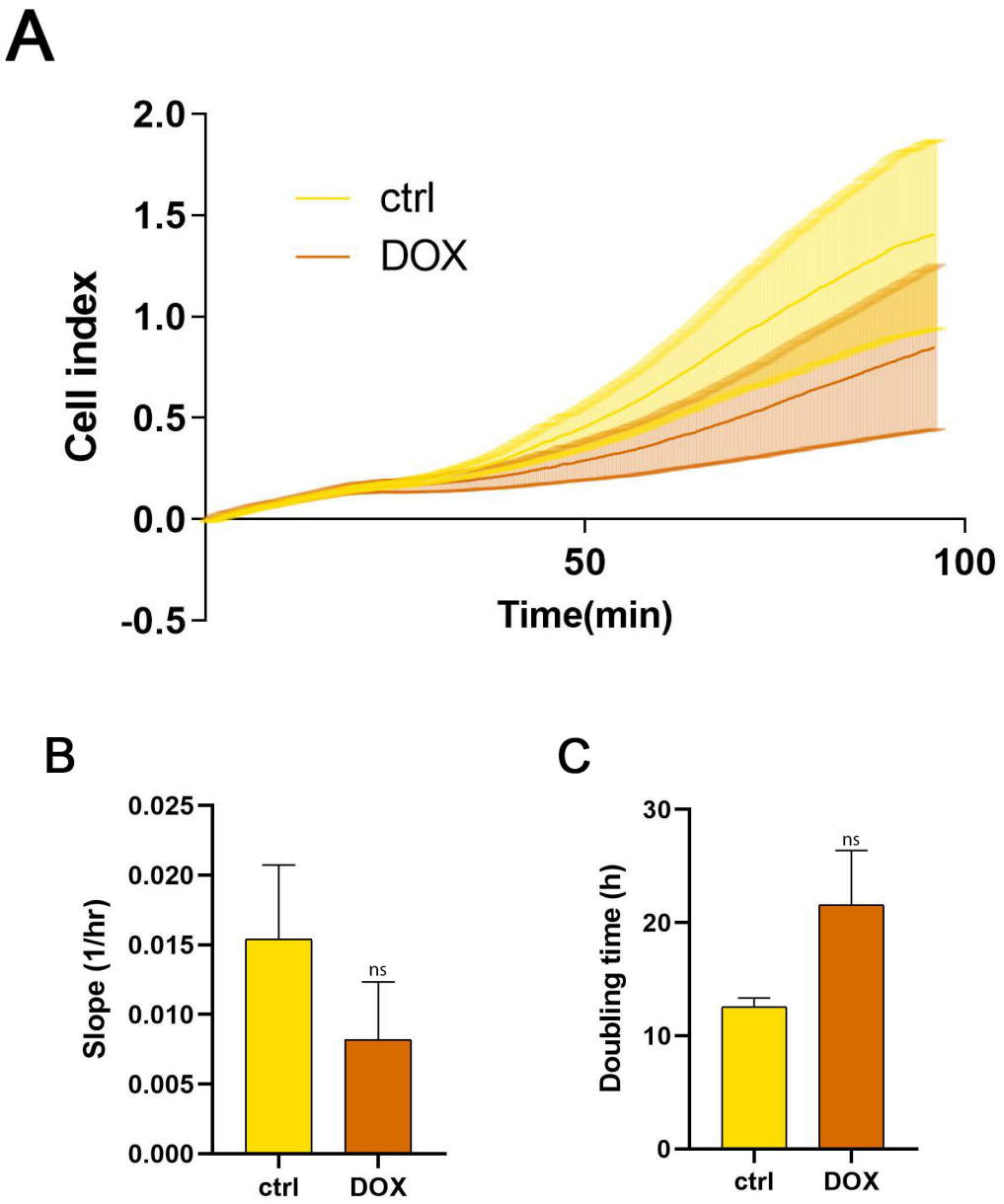

Figure S4: **Proliferation of Cl14 - xCelligence.** **A** growth curves comparison of Cl14 obtained from xCelligence; **B** slopes of shown curves representing their steepness, calculated by xCelligence software; **C** graph representing the time needed for the cell population to double,calculated by xCelligence software. Cells were incubated with or without 250 ng/ml of DOX for 120 hours. Statistical significance was assessed by t-test by means of GraphPad PRISM software. Ns: $p > 0.05$, *: ≤ 0.05, **: ≤ 0.01, *** ≤ 0.001 and **** < 0.0001. Data are shown as mean $\pm$ SEM (n=4).

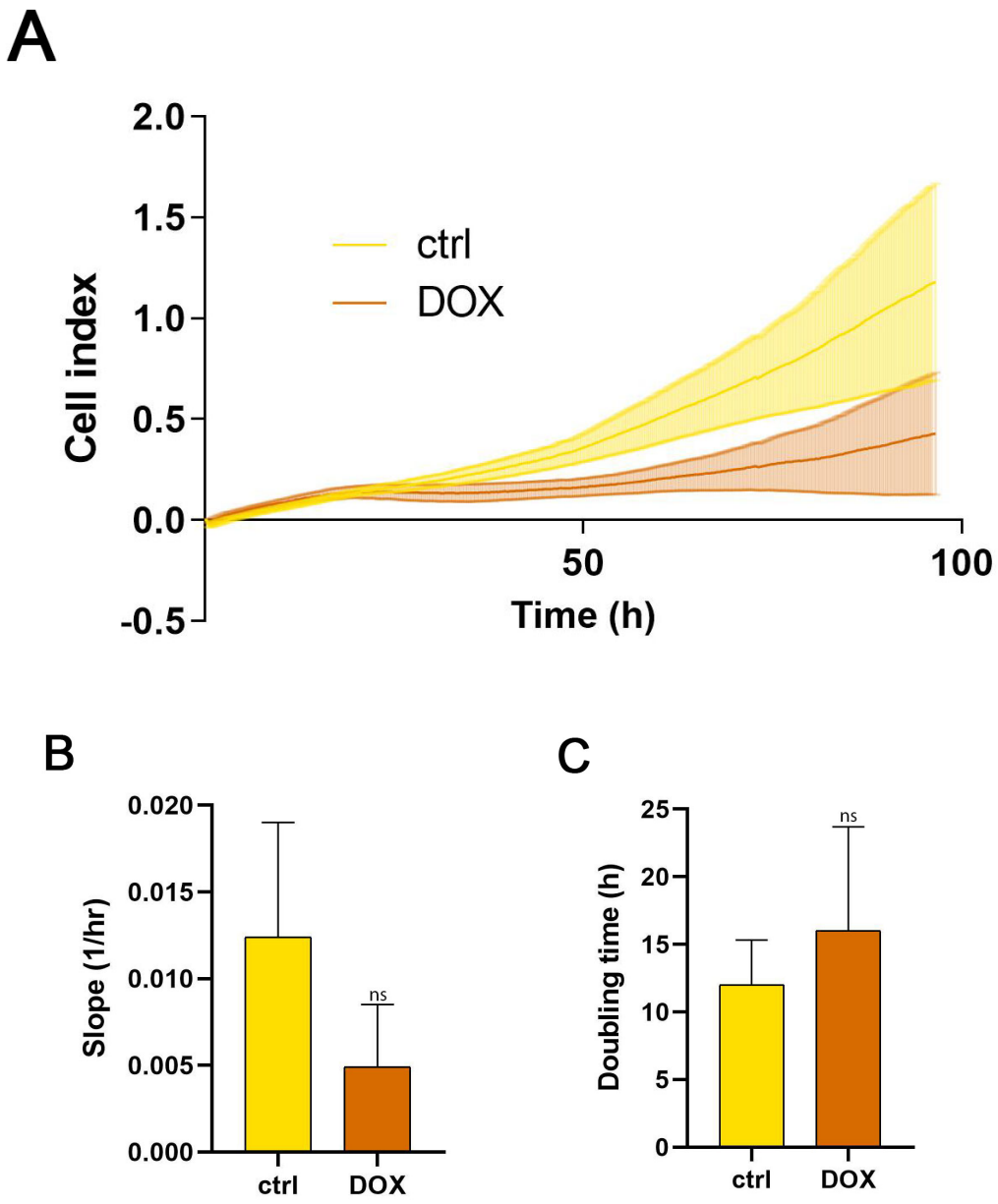

Figure S5: **Proliferation of Cl41 - xCelligence.** **A** growth curves comparison of Cl14 obtained from xCelligence; **B** slopes of shown curves representing their steepness, calculated by xCelligence software; **C** graph representing the time needed for the cell population to double, calculated by xCelligence software. Cells were incubated with or without 250 ng/ml of DOX for 120 hours. Statistical significance was assessed by t-test by means of GraphPad PRISM software. Ns: $p > 0.05$, *: ≤ 0.05, **: ≤ 0.01, *** ≤ 0.001 and **** < 0.0001. Data are shown as mean $\pm$ SEM (n=4).

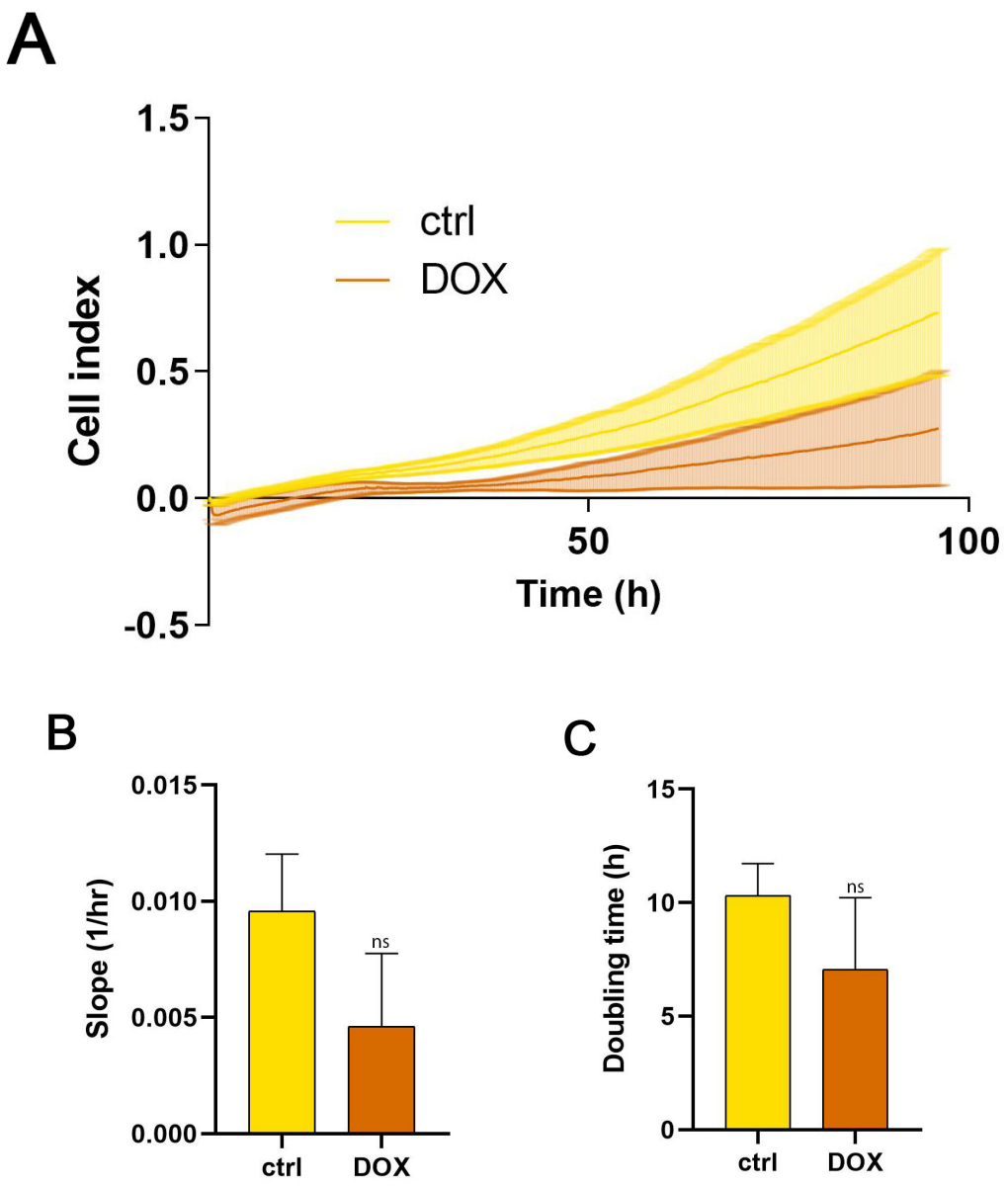

Figure S6: **Proliferation of Cl47 - xCelligence.** **A** growth curves comparison of Cl14 obtained from xCelligence; **B** slopes of shown curves representing their steepness, calculated by xCelligence software; **C** graph representing the time needed for the cell population to double, calculated by xCelligence software. Cells were incubated with or without 250 ng/ml of DOX for 120 hours. Statistical significance was assessed by t-test by means of GraphPad PRISM software. Ns: $p > 0.05$, *: ≤ 0.05, **: ≤ 0.01, *** ≤ 0.001 and **** < 0.0001. Data are shown as mean $\pm$ SEM (n=4).

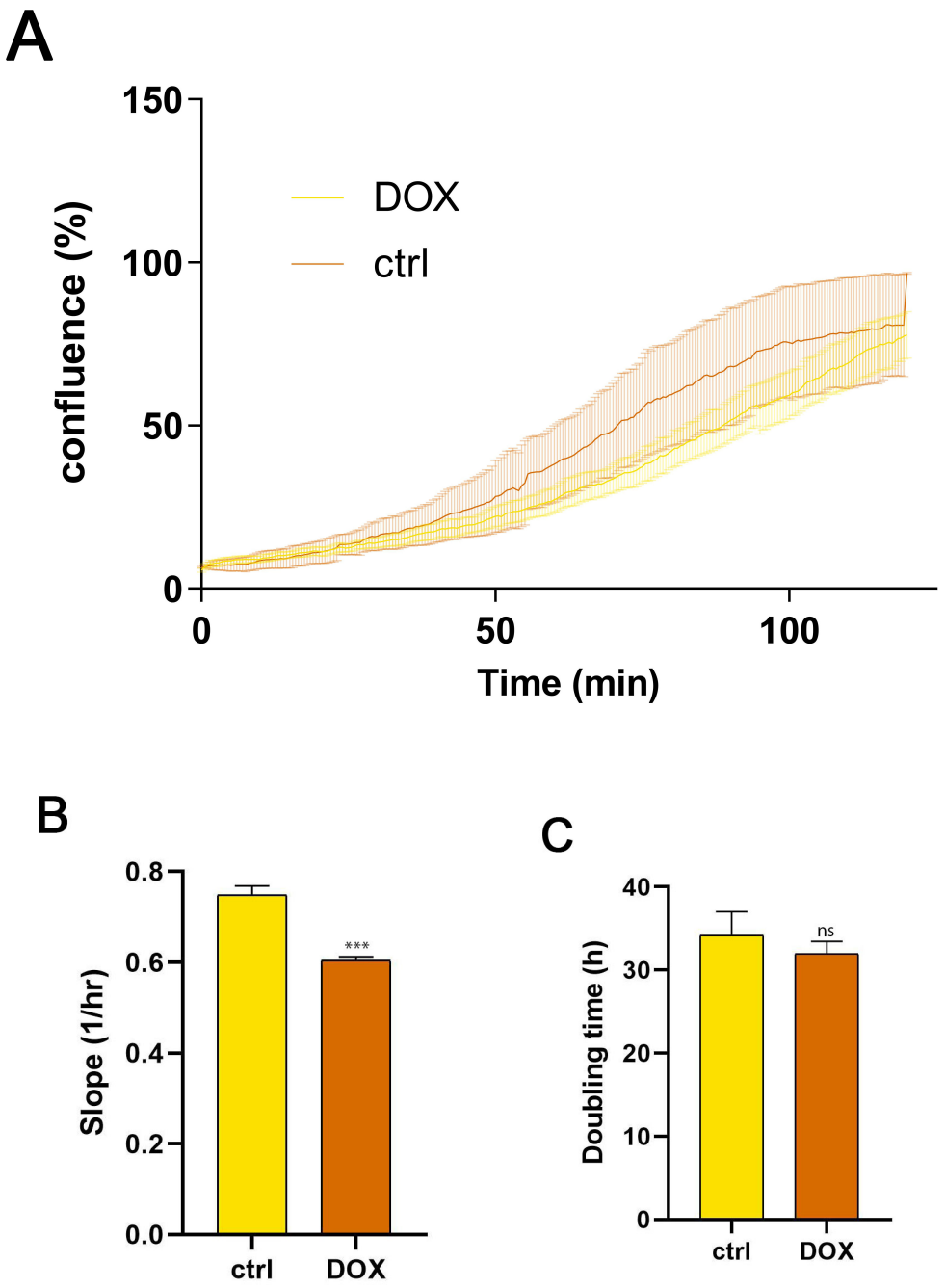

Figure S7: **Proliferation of Cl14 - JuLi.** **A** growth curves comparison of Cl14 obtained from JuLi; **B** slopes of shown curves representing their steepness, calculated in GraphPad PRISM; **C** graph representing the time needed for the cell population to double, calculated online (http://www.doubling-time.com/compute.php). Cells were incubated with or without 250 ng/ml of DOX for 120 hours. Statistical significance was assessed by t-test by means of GraphPad PRISM software. Ns: $p > 0.05$, *: ≤ 0.05, **: ≤ 0.01, *** ≤ 0.001 and **** < 0.0001. Data are shown as mean $\pm$ SEM (n=4).

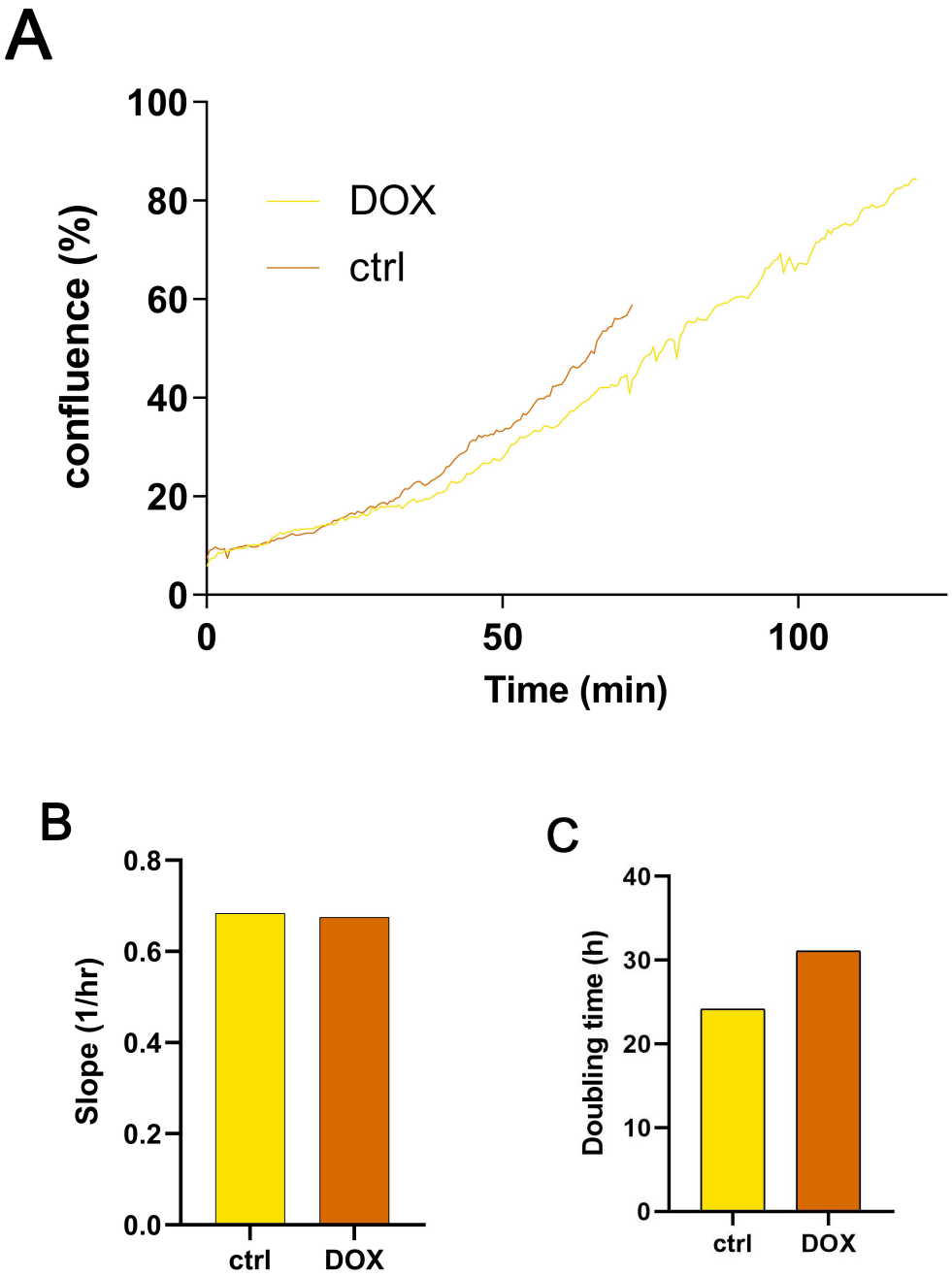

Figure S8: **Proliferation of Cl41 - JuLi. A** growth curves comparison of Cl41 obtained from JuLi; **B** slopes of shown curves representing their steepness, calculated in GraphPad PRISM; **C** graph representing the time needed for the cell population to double, calculated online (http://www.doubling-time.com/compute.php). Cells were incubated with or without 250 ng/ml of DOX for 120 hours. Statistical significance was assessed by t-test by means of GraphPad PRISM software. Ns: $p > 0.05$, *: ≤ 0.05, **: ≤ 0.01, *** ≤ 0.001 and **** < 0.0001. Data are shown as mean $\pm$ SEM (n=1).

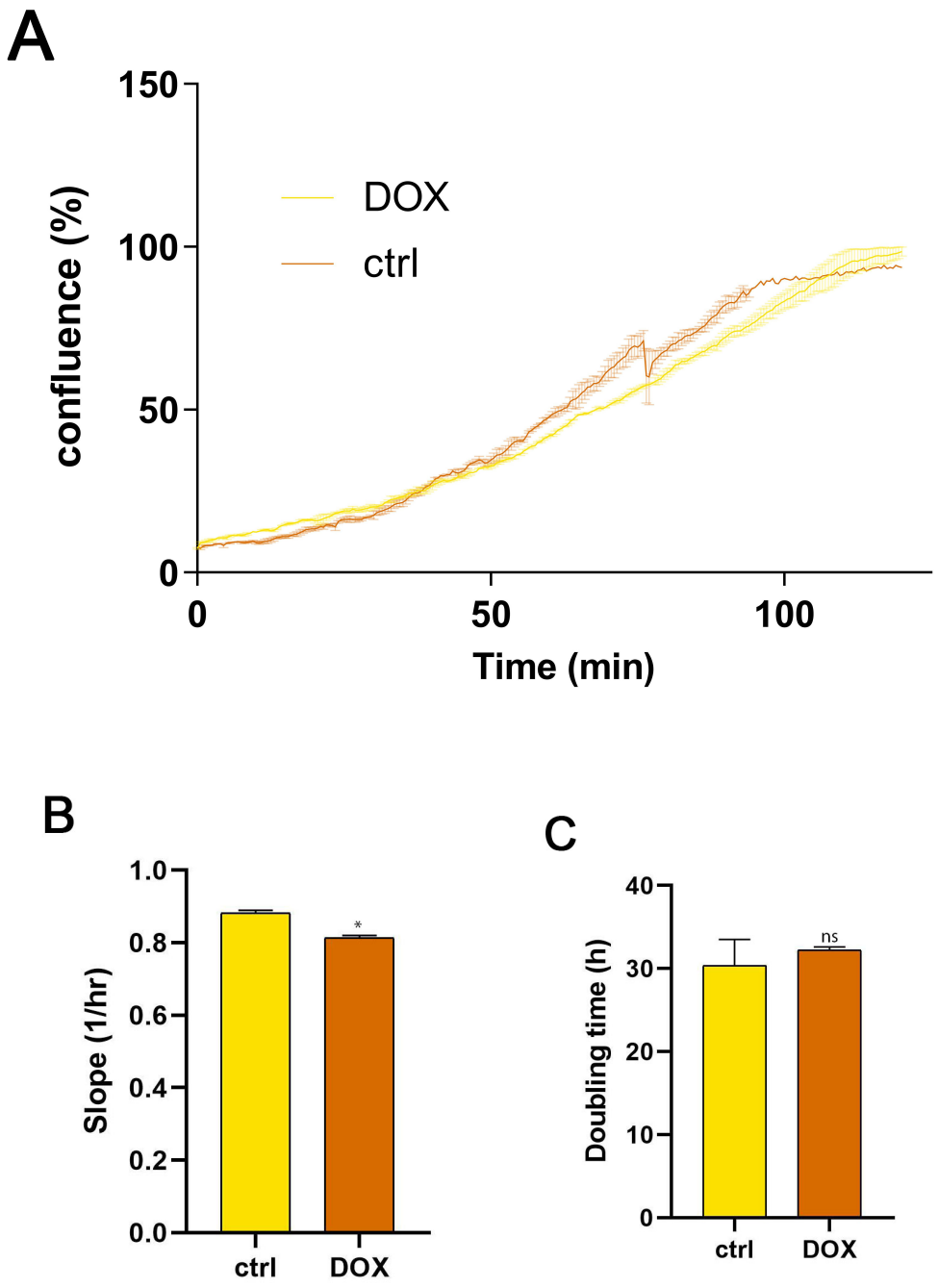

Figure S9: **Proliferation of Cl47 - JuLi.** **A** growth curves comparison of Cl47 obtained from JuLi; **B** slopes of shown curves representing their steepness, calculated in GraphPad PRISM; **C** graph representing the time needed for the cell population to double, calculated online (http://www.doubling-time.com/compute.php). Cells were incubated with or without 250 ng/ml of DOX for 120 hours. Statistical significance was assessed by t-test by means of GraphPad PRISM software. Ns: $p > 0.05$, *: ≤ 0.05, **: ≤ 0.01, *** ≤ 0.001 and **** < 0.0001. Data are shown as mean $\pm$ SEM (n=2).

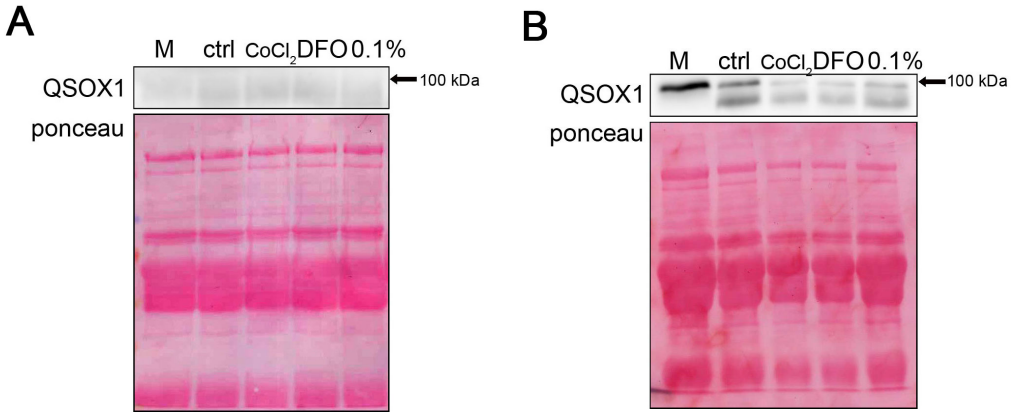

Figure S10: **QSOX1 protein level conditioned medium of MCF10A cells under different hypoxia-mimicking conditions.** **A** First western blot ;**B** Second western blot; figure showing the possible technical problem we have occured during the protein secretion measurement causing high standard deviations in Figure 4.20; 20 µl of centrifuged cell medium was separated by reducing SDS-PAGE followed by Western blotting, ponceau S was used as a loading control. Cells were incubated with the reagents or under different O_2 concentrations for 48 hours, then the medium was harvested.